UC Riverside

UC Riverside Electronic Theses and Dissertations

Title

Effect of Electrostatic Interactions on Performance of Electrically Conductive Ultrafiltration Membranes for Protein Fractionation

Permalink

https://escholarship.org/uc/item/79q015j9

Author

Yeung, Raymond Kai-yen

Publication Date

2017

Copyright Information

Peer reviewed|Thesis/dissertation

UNIVERSITY OF CALIFORNIA
RIVERSIDE

Effect of Electrostatic Interactions on Performance of Electrically Conductive
Ultrafiltration Membranes for Protein Fractionation

A Thesis submitted in partial satisfaction
of the requirements for the degree of

Master of Science

in

Bioengineering

by

Raymond Kai-yen Yeung

September 2017

Thesis Committee:
      Dr. Victor G. J. Rodgers, Chairperson
      Dr. David Jassby
      Dr. Boris Hyle Park

The Thesis of Raymond Kai-yen Yeung is approved:

Committee Chairperson

University of California, Riverside

ACKNOWLEDGEMENTS

ABSTRACT OF THE THESIS

Effect of Electrostatic Interactions on Performance of Electrically Conductive
Ultrafiltration Membranes for Protein Fractionation

by

Raymond Kai-yen Yeung

Master of Science, Graduate Program in Bioengineering
University of California, Riverside, September 2017
Dr. Victor G. J. Rodgers, Chairperson

Ultrafiltration is used extensively in downstream processing of biopharmaceuticals. Although recent studies have demonstrated the importance of electrostatic interactions in both traditional ultrafiltration and electroultrafiltration, electrically conductive ultrafiltration membranes have yet to be investigated for enhancement of protein fractionation. For the effective industrial usage of membrane ultrafiltration for protein separation, a thorough understanding of the effect of electrostatic contributions on throughput and fractionation characteristics is necessary. This thesis investigates the performance of electrically conductive ultrafiltration membranes for single and binary protein electroultrafiltration and studies the effect of electrostatic contributions on the separation characteristics.

Electrically conductive ultrafiltration membranes were fabricated by deposition of a poly(vinyl alcohol)-carbon nanotube (PVA-CNT) composite layer onto a polysulfone (PS-35) ultrafiltration membrane support followed by cross-linking of the carbon nanotube

network. The effects of an applied cathodic potential on the hydraulic permeability, permeate flux, sieving, and selectivity during single and binary protein crossflow electroultrafiltration were studied using the PVA-CNT/PS-35 ultrafiltration membranes. For the electroultrafiltration of BSA at an applied potential of -9 V, there was a marginal increase in permeate flux and no change in observed sieving behavior. The application of -9 V potential during electroultrafiltration of similarly sized but differently charged proteins of alpha-lactalbumin (αLA) and hen egg white lysozyme (HEL) at pH of 7.4 resulted in an enhancement in selectivity by a factor of 30 at the low transmembrane pressure of 1 psi and a factor of 4 at the moderate transmembrane pressure of 15 psi during the initial phase (< 16 minutes) of electroultrafiltration. For longer durations of electroultrafiltration (> 7.5 hours), the applied potential of -9 V had no effective improvement in selectivity. The decline in permeate flux during crossflow electroultrafiltration of single protein solutions of αLA and HEL at low and moderate transmembrane pressure indicate significant protein adsorption which contributes to the sieving behavior.

Contents

List of figures

List of tables

List of symbols

English Letters

A' Leveque solution constant for mass transfer coefficient correlation, [dimensionless]

B_v Constant for entrance length for velocity profile, [dimensionless]

C Mass concentration, [kg/L]

C_b Bulk concentration, [kg/L]

C_p Permeate concentration, [kg/L]

C_w Membrane wall concentration, [kg/L]

d_h Hydraulic diameter, [m]

D Protein diffusion coefficient, [m^2/s]

h Height of hydraulic flow channel, [m]

J_0 Initial permeate flux, [m/s]

J_v Permeate flux, [m/s]

k Solute mass transfer coefficient, [m/s]

l Length of hydraulic flow channel, [m]

L Characteristic length of flow channel, [m]

L_c Entrance length at which the concentration polarization is fully developed, [m]

L_v Entrance length at which the velocity profile is fully developed, [m]

L_p Hydraulic permeability, [m/(s·Pa)]

M_w Molecular weight, [g/mol]

ΔP Transmembrane hydraulic pressure, [Pa]

Re Reynolds number, [dimensionless]

S_i Intrinsic sieving coefficient, [dimensionless]

S_o Observed sieving coefficient, [dimensionless]

Sc   Schmidt number, [dimensionless]

Sh   Sherwood number, [dimensionless]

v Average crossflow velocity, [m/s]

W Width of hydraulic flow channel, [m]

Greek Letters

α Constant in mass transfer coefficient correlation, [dimensionless]

β Constant in mass transfer coefficient correlation, [dimensionless]

$\dot{\gamma}$ Crossflow shear rate, [s^{-1}]

δ Concentration polarization boundary layer thickness, [m]

ε_0 Permittivity of free space, 8.85419×10^{-12} [C^2/(J·m)]

ε_r Relative dielectric constant of the solvent, [dimensionless]

κ Debye length, [m]

Λ_0 Conductivity of the electrolyte solution, [m^2·S/mol]

μ Dynamic viscosity, [Pa·s]

v Kinematic viscosity, [m^2/s]

$\Delta\pi$ Osmotic pressure, [Pa]

ρ Fluid density, [kg/m^3]

σ Reflection coefficient, [dimensionless]

$\Delta\Psi$ Streaming potential, [V]

ζ Zeta potential, [V]

ψ Selectivity, [dimensionless]

ω Constant in mass transfer coefficient correlation, [dimensionless]

List of abbreviations

AMC	Anode-membrane-cathode (configuration for electroultrafiltration)
BSA	Bovine serum albumin
CNT-COOH	Carboxylated multiwalled carbon nanotubes
DDBS	Dodecylbenzensulfonic acid
EUF	Electroultrafiltration
HP	Hydraulic permeability
MW	Molecular weight
MWCO	Molecular weight cut off
pI	Isoelectric point
PS	Polysulfone
PVA	Poly(vinyl alcohol)
PVA-CNT	Poly(vinyl alcohol)-carbon nanotube composite
TMP	Transmembrane pressure
TFF	Tangential flow filtration
UF	Ultrafiltration

Chapter 1　　　　Introduction

1.1 Description and objectives of the current research

1.1.1 Introduction

In the late 1980s, only three commercial recombinant protein products were available on the United States market which included human insulin, tissue plasminogen activator, and Muromonab-CD3. However, in the span of 30 years, the number of approved protein-based products in the United States has grown to over 150 [1]. This growth in production of protein pharmaceuticals has demanded high-resolution, high-throughput, and cost-effective methods for separation and purification. Table 1.1 presents a list of the major clinically available therapeutic proteins [2-4].

The early recombinant therapeutic proteins, largely comprising of highly active hormones, thrombolytic agents, and clotting factors, required relatively low doses and had typical annual production levels below 1 kg. More recently, the introductions of protein-based pharmaceuticals have been in the form of monoclonal antibodies. The stoichiometric action of binding of these proteins to receptors necessitates higher dosage levels to ensure sufficient drug efficacy. Recent annual production requirements for these monoclonal antibodies are estimated to be around 1,000 kg [5]. Significant progress has been made in enhancing the yield of recombinant proteins from mammalian cell lines to meet such a demand. Currently, industrial recombinant protein product titers from mammalian cell cultures have reached about 5 g/L which is a 100-fold improvement in production over similar culture processes in the mid-1980s [6, 7].

Table 1.1 List of protein-based therapeutic products (adapted from Walsh and Headon, 1994 [2]; Dimitrov, 2012 [3]; Leader, 2008 [4])

Protein type	Applications	Examples of therapeutic proteins
Blood clotting factors	Hemophilia; blood disorders	Factor VIII
Colony stimulating factors	Multiple myeloma; low neutrophil and macrophage counts	Filgrastim; pegfilgrastim; sargramostim
Epidermal growth factor receptor inhibitors	Cancer; skin ulcers	Getfitinib
Erythropoietins	Anemia	Epoetin alfa
Human growth hormones	Cancer; AIDS; growth deficiency	Somatotropin; somatropin
Interferons	Cancer; asthma; arthritis; multiple sclerosis; infectious diseases	Interferon beta-1a
Interleukins	Cancer; AIDS; bone marrow failure; rheumatoid arthritis	Anakinra; tocilizumab
Monoclonal antibodies	Cancer; rheumatoid arthritis	Bevacizumab; cetuximab
Recombinant insulin	Diabetes	Insulin glargine
Superoxide dismutase	Oxygen toxicity	Orgotein
Tissue plasminogen activators	Stroke; heart attack	Alteplase; reteplase; tenecteplase
Vaccines	Influenza; Hepatitis B; malaria; meningococcal, streptococcal infections	Flublok; RTS,S

Protein-based biopharmaceuticals are manufactured from microbial, mammalian, or plant cell cultures. Regardless of the origin of production, the desired protein is present among mixtures of numerous impurities. Such impurities include those from the host cells (intact cells, DNA, viruses, residual substrates, and other proteins) or from the product itself (variants formed from physical or chemical alterations). Recombinant proteins are subject to many chemical instability pathways (deamidation, isomerization, oxidation, acetylation, dimerization, and glycosylation) and physical instability pathways

(denaturation, aggregation, precipitation, and surface adsorption) [8]. These physical and chemical variants typically differ in binding affinity, biological activity, and immunogenicity from the desired protein. Since the biotherapeutic proteins and peptides are typically administered to patients intravenously or subcutaneously, the Food and Drug Administration (FDA) and World Health Organization (WHO) have stringent purification requirements for all approved biotherapeutic products. The concentration of host cell protein (HCP) impurities in the final formulations must be 1 – 100 ppm. Bioprocessing of large, dilute volumes of precursory materials into highly purified products results in downstream purification accounting for 50 – 80% of the total manufacturing costs for therapeutic proteins [9, 10].

Current methods for purification and separation of proteins typically employ various chromatographic techniques including size-exclusion, ion-exchange, reverse-phase, and affinity chromatography. Size-exclusion chromatography involves preferentially trapping proteins based on the varying sizes of the loaded proteins and the size of the pores from the packed, porous polymeric beads. Ion-exchange chromatography utilizes charged resins to separate proteins based on their respective charge properties. Complementary to size-exclusion and ion-exchange chromatography, reverse-phase chromatography separates proteins based on their hydrophobicity. Affinity chromatography relies on selective binding interactions with ligands that are immobilized within the gel matrix. Although resin-based column chromatography can achieve high selectivity protein separations, the high costs and low throughput of the method are problematic for industrial-scale therapeutic protein separation. Furthermore,

chromatographic separations require substantial solution volumes due to the multiple

equilibration, wash, elution, regeneration, and sanitization steps [11].

1.2 Protein separation and purification using membranes

Membrane technologies are advantageous for protein separation and purification

due to their high throughput, cost efficiency, and mild processing conditions. These

membrane operations do not require phase changes or chemical additives which

minimizes the extent of denaturation and deactivation of the highly labile proteins. In

addition, membranes have fewer temperature and pressure restraints over

chromatographic separation processes and can better maintain the pH and ionic

environment. More importantly, membrane systems are significantly easier to scale for

industrial bioprocessing, thus making them viable options for meeting the challenges in

the downstream purification of therapeutic proteins [12-15].

Ultrafiltration (UF), a pressure-driven process using membranes, has become the

standard method for protein concentration and has been utilized for various stages of

protein fractionation. Ultrafiltration is primarily based on size-exclusion with the extent

of solute transmission determined by the relative size of the solutes and the membrane

pores. Commercial UF membranes are typically synthetic polymeric membranes prepared

using a phase inversion process involving removal of a solvent from a liquid polymer

solution. Aside from polymeric ultrafiltration membranes, inorganic UF membranes,

typically fabricated via anodization of zirconia, titania, or alumina, are also used

commercially. The choice of membranes is typically directed by its molecular weight cut

off (MWCO), which is defined as the equivalent molecular weight of the smallest protein

that would exhibit greater than 90% rejection. Ultrafiltration membranes have a pore size ranging between 1 and 100 nm corresponding to a MWCO of 3 – 1000 kDa. These membranes can separate proteins and viruses primarily based on size exclusion [5, 16, 17]. Traditional ultrafiltration, however, is a relatively low-resolution separation process which requires the particles of interest to be significantly different in size (typically an order-of-magnitude difference is required for effective separation).

There has been, however, increasing demonstrations of electrostatic interactions having a significant effect on ultrafiltration performance. Many researchers have examined the effects of solution pH and ionic strength on permeate flux, membrane fouling, and solute transmission during protein ultrafiltration. Fane *et al.* (1983) were among the first researchers to investigate the effects of electrostatic interactions in protein ultrafiltration. The researchers observed maximum BSA transmission, as well as adsorption, at its isoelectric point for low ionic strength solutions [18, 19]. More recently, there have been many studies on protein ultrafiltration for fractionation of various binary protein mixtures: bovine serum albumin and lysozyme [20]; bovine serum albumin and hemoglobin [21]; bovine serum and hemoglobin [22]; whey protein mixtures [23-25]; and select, binary and ternary combinations of lactoferrin, myoglobin, bovine serum albumin, ovalbumin, and lysozyme [26]. These reports indicate the maximal selectivity for protein fractionation with ultrafiltration membranes was achieved when the solution pH was around the isoelectric point of one protein whose transmission was desired, while the other protein(s) was/were further rejected. Additionally, the transmission of the protein at its isoelectric point was observed to substantially increase with decreasing ionic

5

strength. Van Eijndhoven *et al.* (1995), in their study of the fractionation of similarly

sized proteins with different charge properties (bovine serum albumin (BSA) with a

molecular weight of 69 kDa and isoelectric point of 4.7; and hemoglobin (Hgb) with

molecular weight of 67 kDa and isoelectric point of 6.85), observed an increase in

separation factor between BSA and Hgb from 2.5 to more than 70 by decreasing the ionic

strength from 0.10 M to 0.0023 M at a solution pH close to the isoelectric point of

hemoglobin [21].

These recent studies indicate that exploiting electrostatic interactions can render

ultrafiltration a highly selective process for protein purification. Many researchers have

attributed the significant effects of solution pH and ionic strength on protein transmission

to the effective protein size [18, 27-29]. Figure 1.1 displays a schematic of the selective

electrostatic exclusion of a negatively charged protein from a similarly charged

membrane pore.
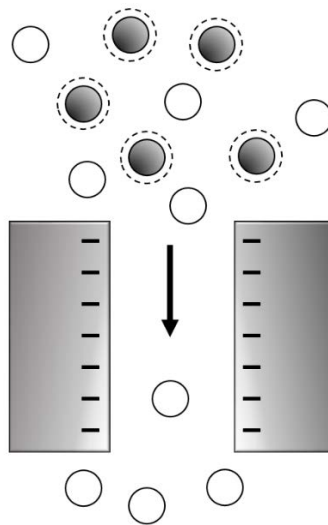
Figure 1.1 Schematic diagram of selective electrostatic exclusion and electrical double layer deformation in a charged membrane pore. Proteins that are electrically neutral are able to enter the charged pore more readily.

The charged protein and membrane are surrounded by a diffuse electrical double layer composed of an excess concentration of counter-ions to maintain electroneutrality. The entrance of the charged protein into the pore causes a distortion of the electrical double layers, resulting in an increase in the free energy of the system and reducing the partitioning of proteins into the pores of the like charged membrane. More complete analysis of the electrostatic interactions will be discussed in the later chapter.

1.3 Electrofiltration

1.3.1 Introduction

Flux decline remains a major problem in membrane processes due to concentration polarization (i.e. accumulation of retained solutes) and membrane fouling which includes pore-blocking, adsorption, and gel-layer formation (as will be discussed later). To reduce concentration polarization and membrane fouling, various techniques have been employed including transmembrane pressure pulsing [30-32], gas sparging [33], pulsatile flow [34], vortex mixing [35], ultrasound [36], membrane modification [37, 38], and electric field [39-45].

The approach of applying an external electric field is attractive for enhanced ultrafiltration due to the ability to be implemented independently of the velocity field. Electroultrafiltration (EUF), which involves application of an external electric field, has demonstrated effectiveness in enhancing permeate flux for protein concentration [39, 43, 44, 46-48], non-protein colloid concentration [40, 49], protein fractionation [42, 50-53], protein/cell suspension fractionation [54], arsenic removal [55, 56], and chromium removal [57].

1.3.2 Electroultrafiltration with anode-membrane-cathode (AMC) assembly

The typical configuration reported for electrofiltration is the anode-membrane-cathode (AMC) assembly which involves application of an electric field across the membrane with electrodes on the retentate and permeate sides. Figure 1.2 shows a schematic of the AMC configuration for crossflow electroultrafiltration.
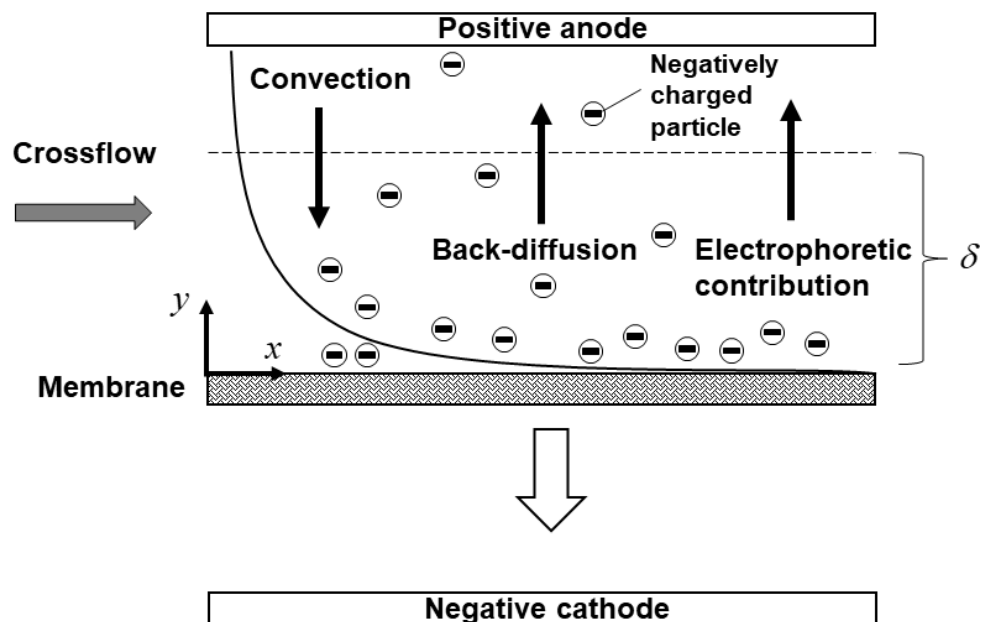
Figure 1.2 Schematic for crossflow electroultrafiltration with the anode-membrane-cathode configuration. Permeate flux is enhanced by the electrophoresis of the negatively charged solute when an external electric field is applied.

There have been demonstrations of effective electrofiltration in the AMC configuration for concentration of single protein solutions [43, 46, 48, 54]. Chuang *et al.* [54] and Song *et al.* [43] investigated the crossflow electroultrafiltration of BSA at a solution pH of 7 – 8 in the AMC configuration with the cathode on the permeate side. They reported an enhancement in permeate flux and BSA rejection with a constant

8

electric field due to the electrostatic force acting on the negatively charged BSA molecules in the direction away from the membrane surface.

Protein fractionation can also be enhanced using electrofiltration at a solution pH where one of the proteins is positively charged and the other negatively charged [42, 50, 58]. For example, Sarkar *et al.* [42] investigated the crossflow electroultrafiltration with external electrodes of dilute binary protein solutions (0.1 g/L BSA, 0.1 g/L lysozyme, 1 mM ionic strength, pH of 7.4 and 11). They noted at constant transmembrane pressure (TMP) and flow velocity (360 kPa and 0.12 m/s, respectively) that permeate flux increases nearly linearly with the applied electric field for both selected solution pH. It was also observed that the permeate flux increase was more significant at solution pH of 11 than at pH of 7.4 which the researchers attributed to electrostatic interactions. At pH 7.4, BSA is negatively charged and lysozyme is positively charged. Sarkar *et al.* proposed that the electrostatic association between the two oppositely charged protein molecules formed a compact layer that deposited onto the membrane surface resulting in a relative decrease in permeate flux. In contrast, at pH of 11 (which is close to the isoelectric point of lysozyme), the electrostatic interaction between BSA and lysozyme was minimized leading to higher permeate flux.

The studies of electric field enhanced ultrafiltration with the AMC assembly demonstrate the tremendous impact of an applied field can have on the permeate flux and protein transmission. The AMC configuration for electrofiltration, however, is not optimal because of the substantial reduction in electric field strength due to the large distance between the two electrodes [42, 59]. Furthermore, the use of counter electrodes

on each side of the membrane leads to high energy demands as the necessary electrical potential to impact the separation of charged solutes is greatly increased. In typical electrofiltration processes, a constant electric field is applied with subsequent high power consumption of around 10 kWh m^{-3} of permeate [60]. To reduce energy consumption, pulsed electric fields have been explored [39, 61-65]. Although application of pulsed electric fields resulted in enhancement of permeate flux for enzyme [39] and mineral [64] solutions compared to conventional ultrafiltration processes without an applied electric field, the improvement of permeate flux of these solutions were still greater when applying a constant electric field. For some other systems, the pulsed electric field resulted in an even higher flux compared to a constant electric field [64, 65]. Oussedik *et al.* reported a two- and four-fold increase in permeate flux for ultrafiltration of 10 g/L BSA with a pulsed electric field over constant electric field (electric field strength, E = 700 V/m) and no electric field, respectively [65].

1.3.3 Electroultrafiltration with electrically conductive membranes

Another configuration for electroultrafiltration involves application of an electric field between an electrically conductive membrane and another electrode. The membrane may be anodic or cathodic depending on the varying applications of the filtration processes. Figure 1.3 illustrates the crossflow electroultrafiltration configuration with the electrically conductive membrane acting as the cathode.

Utilization of electrically conductive membranes to improve membrane filtration performance would greatly simplify the construction of the electrofiltration systems while also reducing energy consumption of the process. Recent developments have allowed

polymeric membranes, including those commonly used for protein ultrafiltration, to be

made highly conductive thus presenting the opportunity to improve existing protein

filtration systems [49, 66-69]. Ultrafiltration studies using membranes that also act as

polarizable electrodes have mostly been limited to treatment of waste water [47, 49, 68,

70, 71]. Electroultrafiltration using an electrically conductive membrane has not yet been

investigated for protein fractionation. Guizard *et al.* investigated the electroultrafiltration

of a colloidal gelatin solution using a conductive metal alloy-coated α-alumina support,

but analysis of the permeate concentration and protein selectivity was not provided [47].
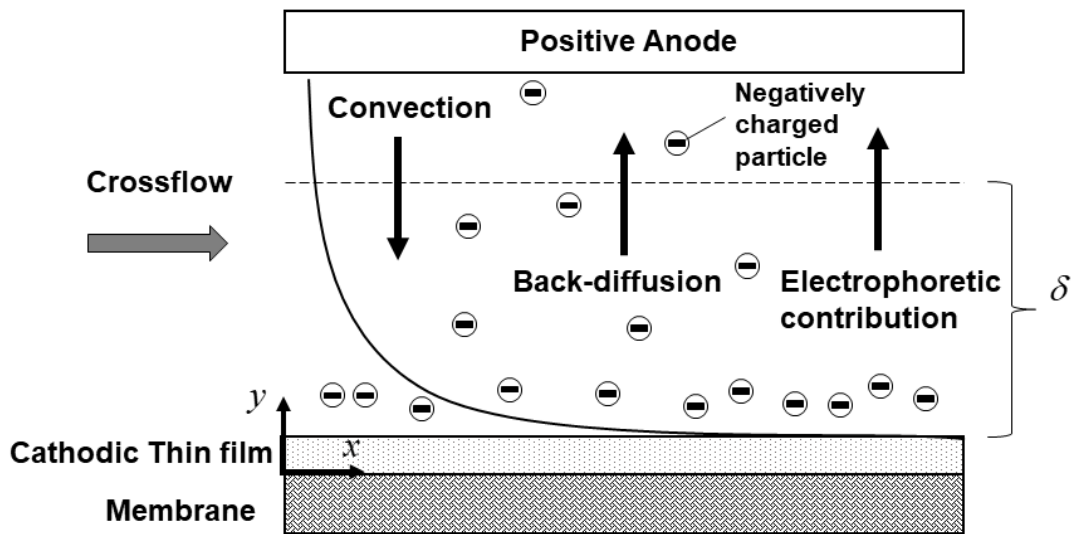
Figure 1.3 Schematic for crossflow electroultrafiltration with electrically conductive, cathodic membrane. The external electric field is applied above the membrane support.

1.4 Objectives of the current research

The overall objective of this thesis was to develop a fundamental understanding of the effects of electrostatic interactions on separation of charged proteins during electroultrafiltration using electrically conductive ultrafiltration membranes. The study is the first reported investigation of protein separation through electroultrafiltration using electrically conductive ultrafiltration membranes. Electroultrafiltration of single protein systems, consisting of alpha-lactalbumin (αLA), hen-egg white lysozyme (HEL), and bovine serum albumin (BSA), as well as binary protein systems, consisting of BSA-HEL and αLA-HEL, were analyzed. The separation performance of both single and binary protein electroultrafiltration was evaluated by determining the effect of an applied potential using a cathodic membrane on the permeate flux, membrane fouling, protein transmission, and protein selectivity during both single and binary protein electroultrafiltration. The contribution of protein fouling to the permeate flux, sieving, and selectivity was evaluated through analyzing the charge properties of membranes and the visualizations of the membrane surface following protein electroultrafiltration.

1.5 Scope of this thesis

In Chapter 2, a review of the theoretical analysis of the solute and solvent transport during protein ultrafiltration and electroultrafiltration is provided. Protein-protein and protein-membrane electrostatic interactions as well as electrophoresis of proteins during electroultrafiltration are described in detail.

In Chapter 3, the experimental materials, instrumentation, and methods for this thesis are outlined. The chapter covers the experimental setup and procedures for

membrane fabrication, protein electroultrafiltration, streaming potential measurements, and visualization of membrane surfaces.

In Chapter 4, the effects of an external applied electric field on the permeate flux, membrane fouling, protein sieving, and protein selectivity during single and binary protein electroultrafiltration with a cathodic membrane are reported.

In Chapter 5, the major findings of the thesis are summarized. Furthermore, recommendations for future work on the utilization of electrically conducting membranes for protein concentration and fractionation are proposed.

In Chapter 6, the protein electroultrafiltration data and complementary material from the characterization of the membranes following protein electroultrafiltration are provided.

Chapter 2 Theoretical background

In order to understand the characteristics of protein electroultrafiltration using an electrically conductive membrane, it is necessary to first understand the traditional ultrafiltration phenomena; the interactions between the proteins, solvent, and membrane; and the electrophoretic contribution of the applied electric field on the solutes. This chapter briefly provides background on the model protein of interest and reviews the general theoretical models used to describe solvent and solute transport through membranes during protein ultrafiltration and electroultrafiltration.

2.1 Protein characterization

Proteins are biomolecules consisting of one or more chains of amino acids. Proteins found in nature are typically made up of the common L-α-amino acids. The structure of the proteins is organized into four levels: primary, secondary, tertiary, quarternary. The primary structure specifies the sequence of amino acids in the polypeptide chain; the secondary structure describes the regular structural segments such as the common alpha helices and beta sheets; the tertiary structure refers to the three-dimensional structure of folded protein molecules; and the quaternary structure describes the aggregation of polypeptide subunits that operate as a single functional component [72]. Proteins have various biological functions and activity that are largely dictated by their three-dimensional structures. Globular proteins, such as bovine serum albumin, hen egg lysozyme, and alpha-lactalbumin utilized in this study, form native spherical structures whereas fibrous proteins possess linear structures.

2.1.1 Size

The most significant property of proteins in ultrafiltration is the size. The size of a protein is generally described by its molecular weight, M_w. As mentioned previously, an ultrafiltration membrane used for protein concentration or fractionation is characterized by its molecular weight cut off which represents the M_w of the protein at which 90% rejection is achieved. The MWCO, however, is not a sharply defined value since polymeric membranes have a broad pore size distribution. The protein M_w and membrane MWCO thus provide an estimation of how permeable a given ultrafiltration membrane is to a particular protein.

While M_w offers a simple parameter for assessing protein transport through membranes, the molecular weight does not provide three-dimensional information about the protein. The three-dimensional size of a protein may be obtained experimentally, *e.g.*, using x-ray diffraction [73]. Alternatively, the Stokes-Einstein radius, which is the radius of a solid sphere that has the same hydrodynamic properties as the protein, can provide an estimation of the size of globular proteins. The hydrodynamic radii can be determined using the gel filtration process [74, 75].

2.1.2 Charge properties and electrostatic interaction

The protein surface charge density can be determined by considering the dissociation of the ionizable amino acids residues on the protein surface in an aqueous environment. The net charge of a protein at a given solution pH and ionic strength is provided from the difference between the maximum number of positive charges on the protein and the sum of all the dissociated groups,

$$z = z_{\max}^+ - z^- \sum_{i=1}^{n} r_i \qquad (2.1)$$

where $z_{\max}^+$ is the maximum possible positive charge on the protein; n is the total number of titratable amino acid residues; subscript i denotes the particular ionizable group; z^- is the charge of the dissociated group, i; and r_i is the number of dissociated groups of i. The dissociation equilibrium of an ionizable amino acid residue is described by its intrinsic dissociation constant:

$$K_a = \frac{[A^-][H^+]}{[AH]} \qquad (2.2)$$

where $[AH]$ represents the concentration of the acid; $[A^-]$ represents the concentration of the dissociated counterpart or conjugate base of the acid; and $[H^+]$ represents the local concentration of charged hydrogen ions at the surface of the protein, which is different from the bulk H^+ concentration due the electrostatic interaction between the protein and the charged hydrogen ion. Equation (2.2) can be rewritten in terms of the logarithmic acid dissociation constant to provide a relationship to pH:

$$pK_a = -\log K_a = -\log \frac{[A^-][H^+]}{[AH]} = pH - \log \frac{[A^-]}{[AH]} \qquad (2.3)$$

The isoelectric point (pI) is defined as the pH value at which the protein has a zero net charge.

2.2 Classical theories in ultrafiltration

2.2.1 Membrane filtration key parameters

The main parameters used to characterize membrane performance are the permeate flux, hydraulic permeability, sieving coefficient, and selectivity. Permeate flux, J_v, is the volumetric flow rate of solution through the membrane divided by the effective membrane surface area. The permeate flux is primarily used to indicate the throughput of the ultrafiltration process and is directly related to the overall pressure driving force across the membrane. Hydraulic permeability, L_p, is related to the permeate flux as described in Eqn. (2.4) and is inversely related to the resistance to flow.

$$L_p = \frac{J_v}{\Delta P} \tag{2.4}$$

Hydraulic permeability is a useful parameter to quickly assess membrane fouling, which causes an increase in hydraulic resistance. The permeability of a membrane to a particular solute species is described by the intrinsic sieving coefficient, S_i, and is defined as,

$$S_i = \frac{C_p}{C_w} \tag{2.5}$$

where C_p is the concentration in the permeate and C_w is the concentration at the membrane surface. The intrinsic sieving coefficient is a fundamental membrane-solute property. The concentration at membrane surface, however, is not a simple constant, but rather a complex parameter that is a function of the mass transfer characteristics of the membrane and the operating conditions. Another parameter that can be more easily resolved experimentally is the observed sieving coefficient, S_0, which is defined as,

$$S_0 = \frac{C_p}{C_b} \qquad (2.6)$$

where C_b is the bulk concentration of the solute species (more details are provided in the next section). For feed solutions containing two or more species, another parameter known as the selectivity, ψ, is used to characterize the capability of a membrane to separate the solute species, and is defined as the ratio of the observed sieving coefficients of the two solute species,

$$\psi = \frac{S_{o,1}}{S_{o,2}} \qquad (2.7)$$

where the subscripts 1 and 2 represent the solute species.

2.2.2 Concentration polarization and film theory

In any type of membrane filtration process, the convective flow towards the selective membrane results in an accumulation of retained protein above the surface of the membrane until the diffusion away from the membrane is in balance with the convection toward the membrane. This phenomenon, known as concentration polarization, is illustrated in Figure 2.1. As evident in the schematic, the concentration of the solute C, increases from the bulk concentration, C_b, to a much higher concentration at the membrane surface, C_w, over a layer referred to as the concentration polarization boundary layer with a given thickness, δ. The solute is transported through the membrane and leaves at a rate defined by the permeate flux, J_v, and the permeate concentration, C_p.
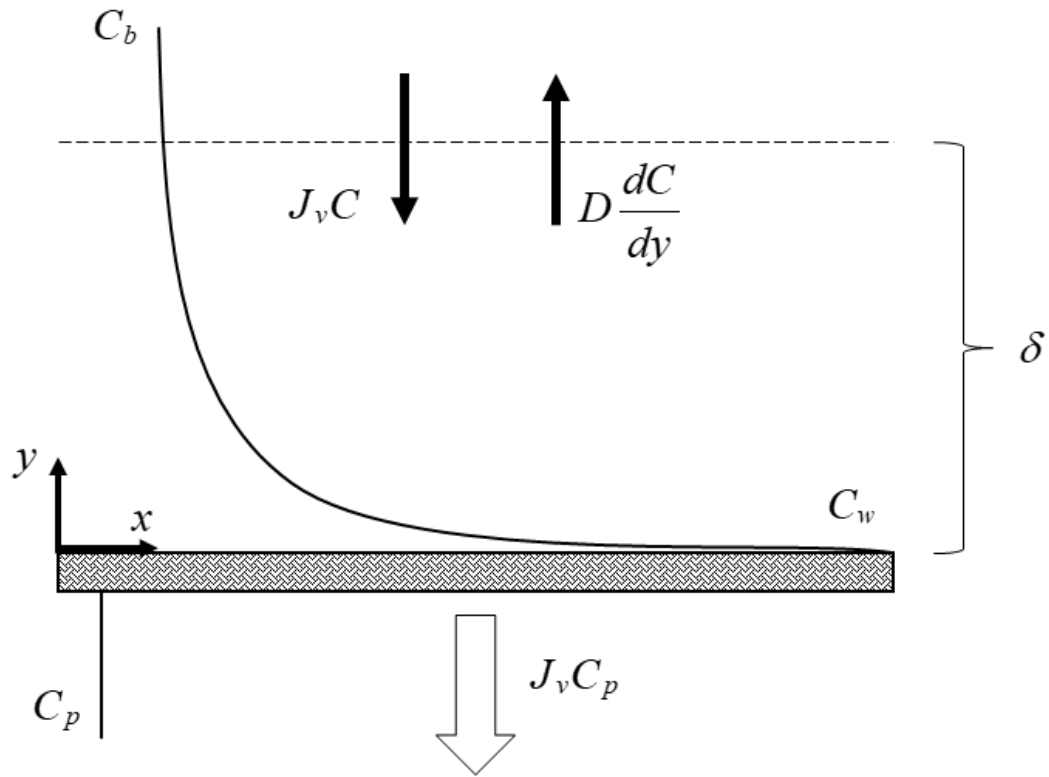
Figure 2.1 Schematic for concentration polarization in membrane processes.

2.2.3 Film theory model

In film theory, the concentration gradients parallel to the membrane surface are assumed to be negligible compared with the concentration gradients orthogonal to the membrane surface. A one-dimensional solute mass balance above the membrane equates the rate of convective transport of the solute toward the membrane to the rate of solute transmission through the membrane plus the rate of diffusion of the solute away from the membrane.

$$-J_v C_p = -J_v C + D \frac{dC}{dy} \tag{2.8}$$

Integration of Eqn. (2.8) over the boundary layer thickness (which is defined as being negative due to the way the axis was defined) with the boundary conditions

$$C(y = -\delta) = C_b$$
$$C(y = 0) = C_w$$

(2.9)

gives the widely used film theory model:

$$J_v = k \ln\left(\frac{C_w - C_p}{C_b - C_p}\right)$$

(2.10)

where $k = D/\delta$ refers to the solute mass transfer coefficient which can be obtained by Schmidt number correlations that are further discussed in Section (3.3.6 Experimental parameters).

2.2.4 Flux model

During ultrafiltration, the rejection of solutes by the membrane affects the flux through introduction of additional resistances to flow which alters the hydraulic permeability. Moreover, the high concentration of retained solutes upstream of the surface of the membrane generates an osmotic pressure, $\Delta\pi$. The equation for the volumetric flux through the membrane can be expressed by the Kedem-Katchalsky model [76] as described by:

$$J_v = L_p\left(\Delta P - \sigma\Delta\pi\right)$$

(2.11)

where σ is the reflection coefficient that is a corrective factor for the effect of the osmotic pressure on the flux ($\sigma=1$ for a fully retentive membrane and σ for a non-retentive membrane).

2.3 Electrostatic properties in ultrafiltration

2.3.1 pH

As discussed previously, the net charge of proteins in solution and the corresponding electrostatic interactions strongly depend on the solution pH. As a result, pH is a critical factor in protein ultrafiltration studies. At a given pH, the net surface charge of the protein can be estimated from its pI; a protein in solution is negatively charged at a pH above its pI and positively charged at a pH below its pI.

2.3.2 Ionic strength

Ionic strength strongly influences protein transmission during ultrafiltration. The ionic strength of salt solutions was evaluated using Eqn. (2.12)

$$ I = \frac{1}{2} \sum_i z_i^2 c_i $$

(2.12)

where z_i and c_i is the net charge of the ion and total concentration, respectively, of the ion species, i. Electrostatic interactions of colloidal particles are screened by the presence of mobile ions in the solvent. Relatively low ionic strengths were considered in the present study in order to investigate the electrostatic effects in electroultrafiltration.

2.3.3 Zeta potential

At any charged interface between two phases, there is an affinity for charges (electrons or ions) to accumulate. The surface charge (positive or negative) generates an electrostatic field and attracts counterions which screen the electric surface charge. These counterion are also subject to thermal motion which distributes them uniformly through the surrounding medium. The interfacial charge arrangement thus comprises of strongly

bound counterions to the particle surface with the concentration of the remainder

counterions gradually decreasing until it approaches the bulk concentration. This charge

arrangement is known as the diffuse electrical double layer, which is characterized by the

Debye length, κ^{-1}. Within the electrostatic double layer, there exists a Stern surface and a

surface of shear. The Stern surface is a hypothetical surface that passes through the

counterions absorbed on the charged surface. The surface of shear, located further from

the Stern surface, is a defined boundary where the relative velocity between the particle

and its surrounding mobile fluid is zero. A schematic of the charged interface and the

potential gradient is provided in Figure 2.2.

Although properties of colloidal systems are determined directly or indirectly by

the surface potential, Ψ_0, it is fundamentally difficult to measure. As Hunter (1981) points

out, the test charge (electron) used to measure the potential as it moves from the interior

of one phase to the second has a dramatic effect on the electrical structure of the

surroundings and thus influences the measurement [77]. As a result, the zeta potential,

which is defined as the electrostatic potential at the surface of shear and denoted by ζ, is

typically used to characterize the charge density of steady interfacial layers. The zeta

potential can be evaluated experimentally and provides a magnitude approximation of the

surface potential and is a practical parameter for comparing different interfaces.
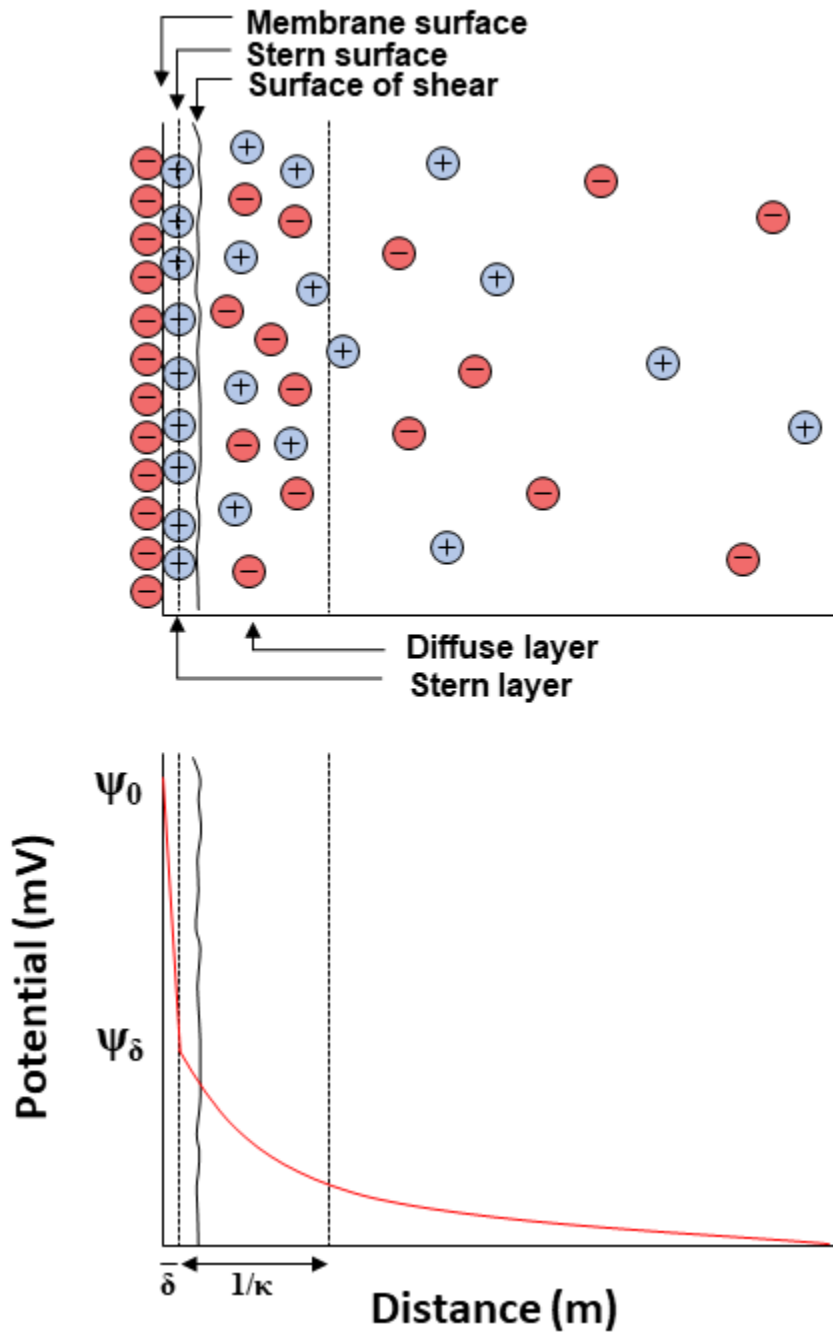
Figure 2.2 Schematic of the electric double layer in the vicinity of a charged membrane surface. The potential changes dramatically with small changes in distance near the surface. Zeta potential at the surface of shear may be used to provide an estimate of the charge properties of the surface.

2.3.4 Streaming potential

A modification of the Helmholtz-Smoluchowski equation [78] was given by Hunter (1981) which provides a relationship between the streaming potential and the zeta potential [77, 79] as given by

$$\frac{\Delta\Psi}{\Delta P} = \frac{\varepsilon_0 \varepsilon_r \zeta}{\mu \Lambda_0} \tag{2.13}$$

where $\Delta\Psi$ is the change in streaming potential; ΔP is the change in transmembrane hydraulic pressure; ε_0 is the permittivity of free space (8.85419×10^{-12} C^2/(J·m) [80]); ε_r is the relative dielectric constant of the solvent; μ is the viscosity; and Λ_0 is the conductivity of the electrolyte solution. When an electrolyte is driven by a pressure gradient through the membrane pores, the movement of ions generates a current denoted as the streaming current. The corresponding streaming potential, which is correlated to the streaming current, can be used to evaluate the zeta potential using Eqn. (2.13).

Chapter 3   Experimental methods

This chapter describes the materials, instruments, and experimental methods used for the studies. Additional details on the specific experimental procedures are provided in the subsequent chapter.

3.1 Poly(vinyl alcohol)-carbon nanotube ultrafiltration membrane

3.1.1 Support membrane

Axisymmetric membranes are widely used for various commercial applications of ultrafiltration including wastewater treatment and bioprocessing [5, 16, 81, 82]. These anisotropic membranes have a thin skin on the surface of the membrane which dictates the rejection property of the membrane, and a significantly thicker, more porous support layer underneath. The relatively small thickness of the skin allows for higher fluxes during ultrafiltration operation compared to symmetric, microporous membranes. Moreover, the axisymmetric membrane structure mitigates significant pore plugging that may be present during use of microporous membranes [13].

From the variety of polymeric membranes, the most common include polysulfone, polyethersulfone, polyvinylidene fluoride, and composite regenerated cellulose. Polysulfone ultrafiltration membranes are favored due to their relatively high thermal stability, high glass transition temperatures, and chemical cleaning resistance [83]. Compared to polyethersulfone membranes, polysulfone membranes are more hydrophobic and thus are subject to more significant protein adsorption due to the presence of alkyl groups. Polysulfone membranes remain widely used due to

aforementioned advantages although researchers have performed surface modification to render the membranes more hydrophilic to reduce protein adsorption [37, 38, 84, 85].
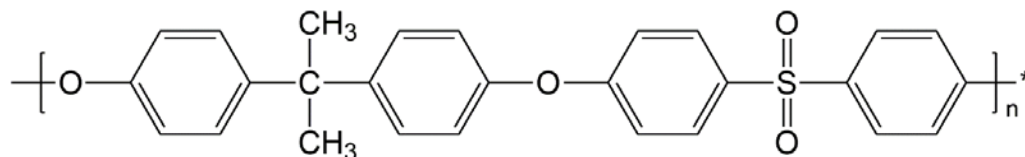
Figure 3.1 Chemical structure of polysulfone.

3.1.2 Electrically conductive ultrafiltration membrane fabrication

All filtration experiments performed in this work were carried out using a thin film composite ultrafiltration membrane comprised of a PVA-CNT film on a porous polysulfone (PS) support UF membrane. The PVA-CNT/PS-35 membrane fabrication method, which was first developed by Dudchenko *et al.* [49], was adapted from procedures reported by Duan *et al.* consisting of modifications to the cross-linking procedure [57]. Covalent cross-links were introduced into PVA-CNT composites with glutaraldehyde through an acetalization reaction [49, 86-88]. From studies on the rejection of various polymers of different sizes, Duan *et al.* determined the molecular weight cut-off to range from 100 to 150 kDa (corresponding to 18 to 21 nm in spherical particle diameter). Furthermore, the typical pore diameter of the CNT network (assuming circular pores) was determined to be 125 nm from analysis of the images of the membrane surface from scanning electron microscopy [57, 89].

Commercial PS-35 polysulfone ultrafiltration membrane, with a thickness of 0.165 mm and a reported MWCO of 35 kDa, was used as the support membrane (Sepro Membranes Inc.; Oceanside, CA). These membranes were provided in the form of large, flat sheets which were cut into appropriately sized disks. Similar polysulfone

ultrafiltration membranes have been reported to have an isoelectric point of around 4.0 [20]. Multi-walled, carboxyl-functionalized carbon nanotubes (CNT-COOH) with a reported outer diameter of 13 – 18 nm, length of 3 – 30 μm, functional group content of 7.0%, and purity of >99 wt % (Cheaptubes Inc.; Brattleboro, VT) was used for preparation of the CNT solution. 146,000 – 186,000 MW poly(vinyl alcohol) and dodecylbenezenesulfonic acid (DDBS) from Sigma-Aldrich, Corp. (St. Louis, MO) were used. 50 wt% glutaraldehyde solution (G151-1; Fisher Scientific; Waltham, MA) was used for cross-linking of the PVA-CNT composites with 40 wt% hydrochloric acid (Fisher Scientific, Pittsburg, PA) as a catalyst for the cross-linking reaction.

For preparation of the carbon nanotube solution suspension, 0.01 wt% CNT-COOH powder and 0.1 wt% DDBS were suspended in an aqueous solution of DI water by horn sonication (Branson; Danbury, CT). The solution was centrifuged at 11,000 ×g relative centrifugal force for 10 minutes at 4 °C and decanted to remove non-dispersed agglomerated carbon nanotube particles. The centrifugation procedure was repeated two additional times to acquire a homogeneous solution ready for deposition onto the support ultrafiltration membrane.

Modification of the ultrafiltration membranes were performed using a pressure filtration deposition system (Millipore; Billerica, MA) connected to a nitrogen tank. A schematic of the pressure filtration system is provided in Figure 3.2. The PS-35 ultrafiltration membranes were thoroughly rinsed and subsequently flushed with DI water at 30 psi prior to modification. A 3:1 ratio of 1 wt% PVA to CNT-COOH solution was pressure-deposited onto the PS-35 UF membrane support at 50 psi, yielding a CNT-

COOH concentration of 0.57 g/m^2. The membranes were then flushed again with

deionized water at 30 psi. The coated membranes were then immersed in a crosslinking

solution consisting of 1 g/L glutaraldehyde and 0.37 g/L of hydrochloric acid at 90 °C for

1 hr. The membranes were then dried at the same temperature for 5 min, cooled to room

temperature, and used without any additional modification.
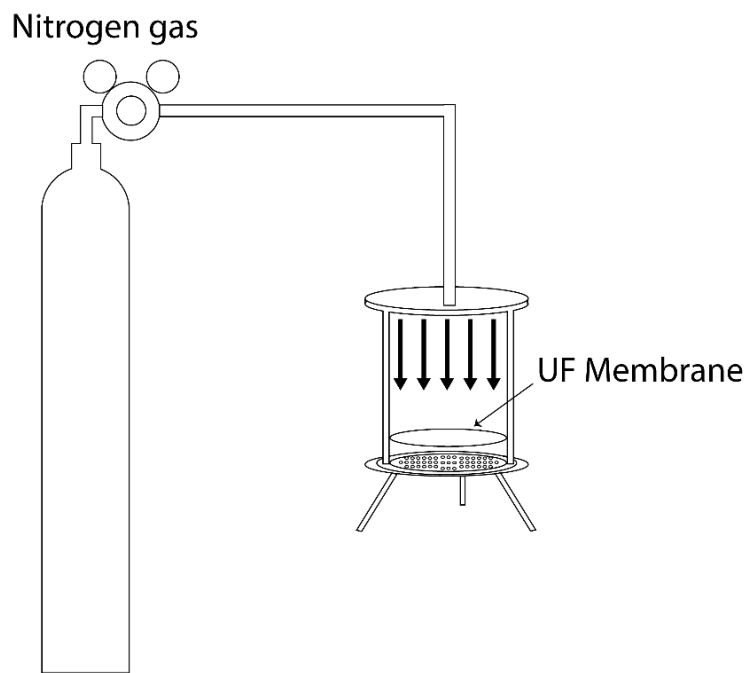
Figure 3.2 Schematic of pressure filtration deposition system
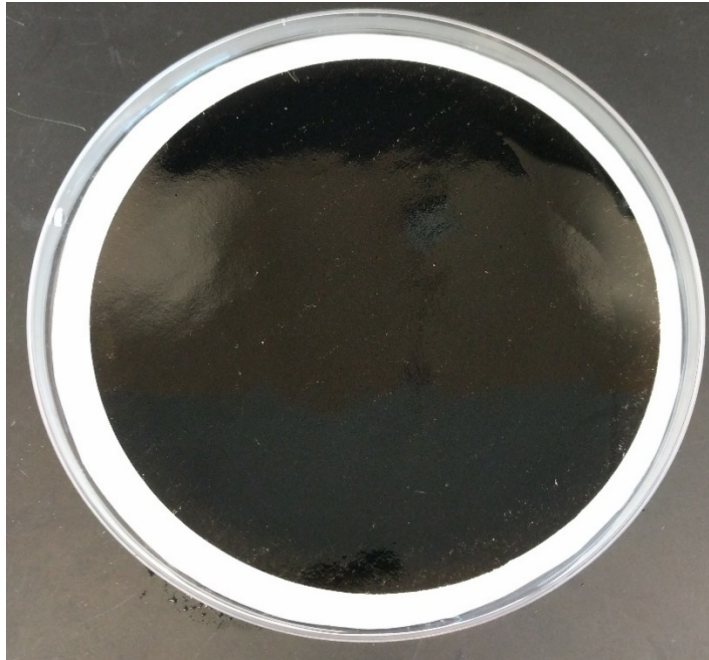
Figure 3.3 Image of a poly(vinyl alcohol)-carbon nanotube (PVA-CNT) composite membrane. A polysulfone UF membrane (PS-35) was used as the support.

3.1.3 Membrane properties

Images of the membrane surfaces were collected using scanning electron

microscopy (SEM; Nova NanoSEM 450 – UCR Center Facility for Advanced

Microscopy and Microanalysis; FEI; Hillsboro, OR) at 20 keV. Membrane samples were

affixed to carbon conductive tapes on SEM stubs (Prod. 16111; Ted Pella, Inc.; Redding,

CA) and sputter-coated with a Pt/Pd target for 60 s (Sputter Coater 108 Auto; Cressington

Scientific Instruments Ltd.; Watford, England, UK). For cross-sectional images, sample

slices from razor sectioning were affixed onto SEM stubs with 90° copper tape mounts.

From the acquired SEM images of the membranes, the porosity was calculated

using the ImageJ image processing program (NIH). The porosity was acquired by

calibrating the scale; adjusting the threshold to create a binary image; and utilizing the

software to outline the particles and compute the total pore area. The porosity was calculated from the ratio of the total pore area and the total image area. In the porosity calculation, the total image area was corrected to remove the area of the information bar.

3.1.4 Membrane charge characterization

For relative comparison of the charge characteristics of the membrane surfaces, zeta potential measurements were performed using the streaming potential method as described in Chapter 2. The measurements were made using a streaming potential device made by our group [90]. The device features an industrial grade, transparent polycarbonate flow cell with a test bed that allows the usage of standard 24 mM diameter Transwell® inserts (CLS3414; Corning; Corning, NY). A 1 mM diameter cylindrical pore structure limits the flow of the electrolyte solution.

The polycarbonate membrane was removed from the 24 mm Transwell inserts. Following application of epoxy (Low Viscosity Epoxy Resin and Non-Blushing Slow Hardener; Mas Epoxies; St. Paul, MN) onto the bottom rim of the insert, the Transwell insert was pressed onto the ultrafiltration membranes being tested and allowed to cure for 8 hours before use. The protruding edges of the membrane were removed using a scalpel and the insert with the sealed membrane was then put into our streaming potential device.
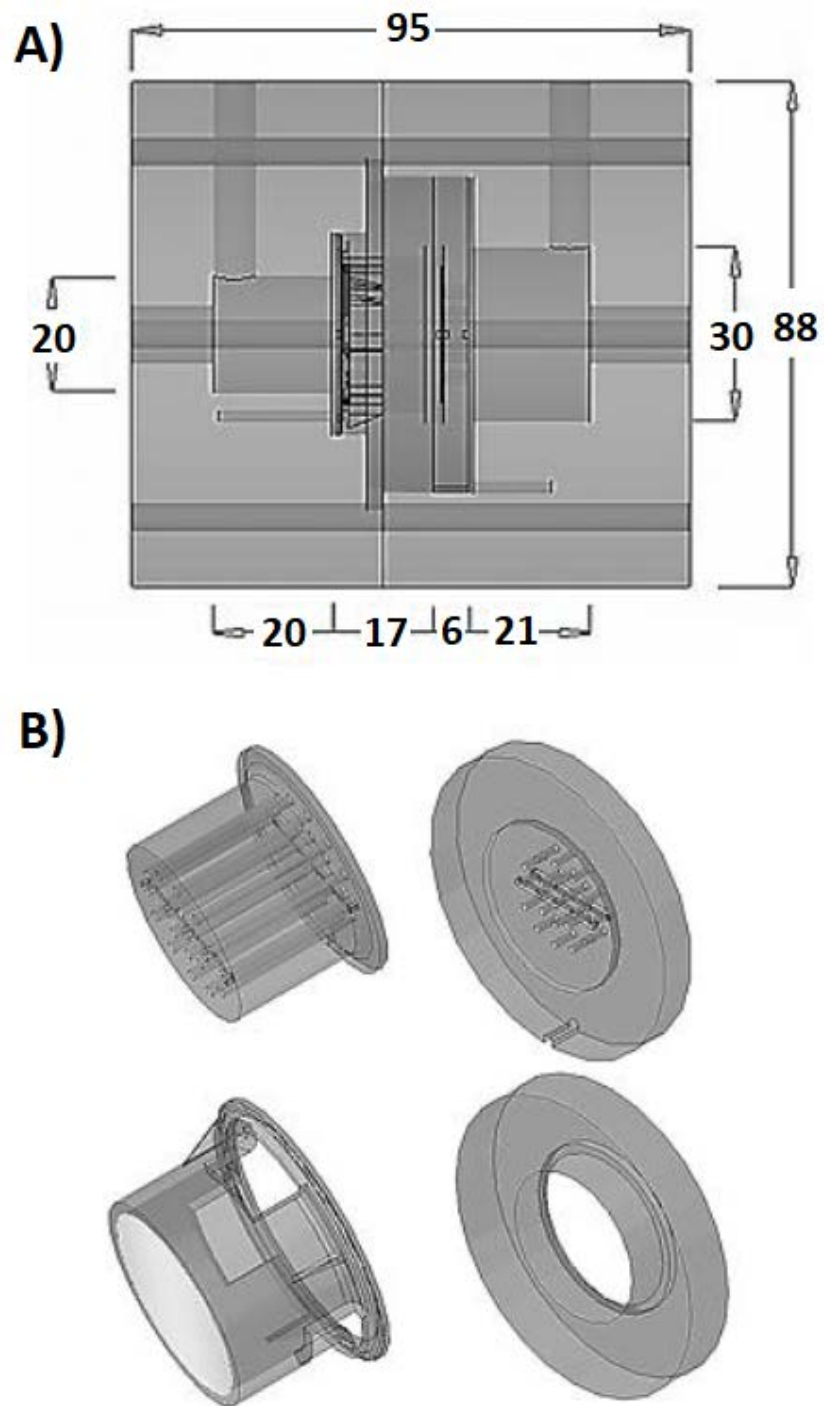
Figure 3.4 CAD images of the streaming potential device: A) Side view; B) Inner components of the device. All units are in mm. Adapted from Vandrangi et al. [91].

The device was filled with 10 mM NaCl solution at pH 7.4 with Ag/AgCl electrodes (Sigma Aldrich; St. Louis, MO) attached to each side of the membrane and symmetrically aligned with one another. These Ag/AgCl electrodes are 1.0 mm in diameter with a resistivity of 1.59 $\mu\Omega$-cm at 20 °C, density of 10.49 g/cm^3, and 99.9% trace metal composition. The changes in streaming potential ($\Delta\Psi$) upon alterations in the hydraulic pressure (ΔP) were detected using a voltmeter (77 Series II Multimeter; Fluke, Corp.; Everett, WA) connected to the electrodes. To eliminate potential experimental errors, the transmembrane pressure was varied in both ascending and descending phases. The streaming potential measurements were plotted with respect to the transmembrane hydraulic pressure and the slope of the line, representing the calculated zeta potential (ζ), was determined from the simple linear regression on the data points.
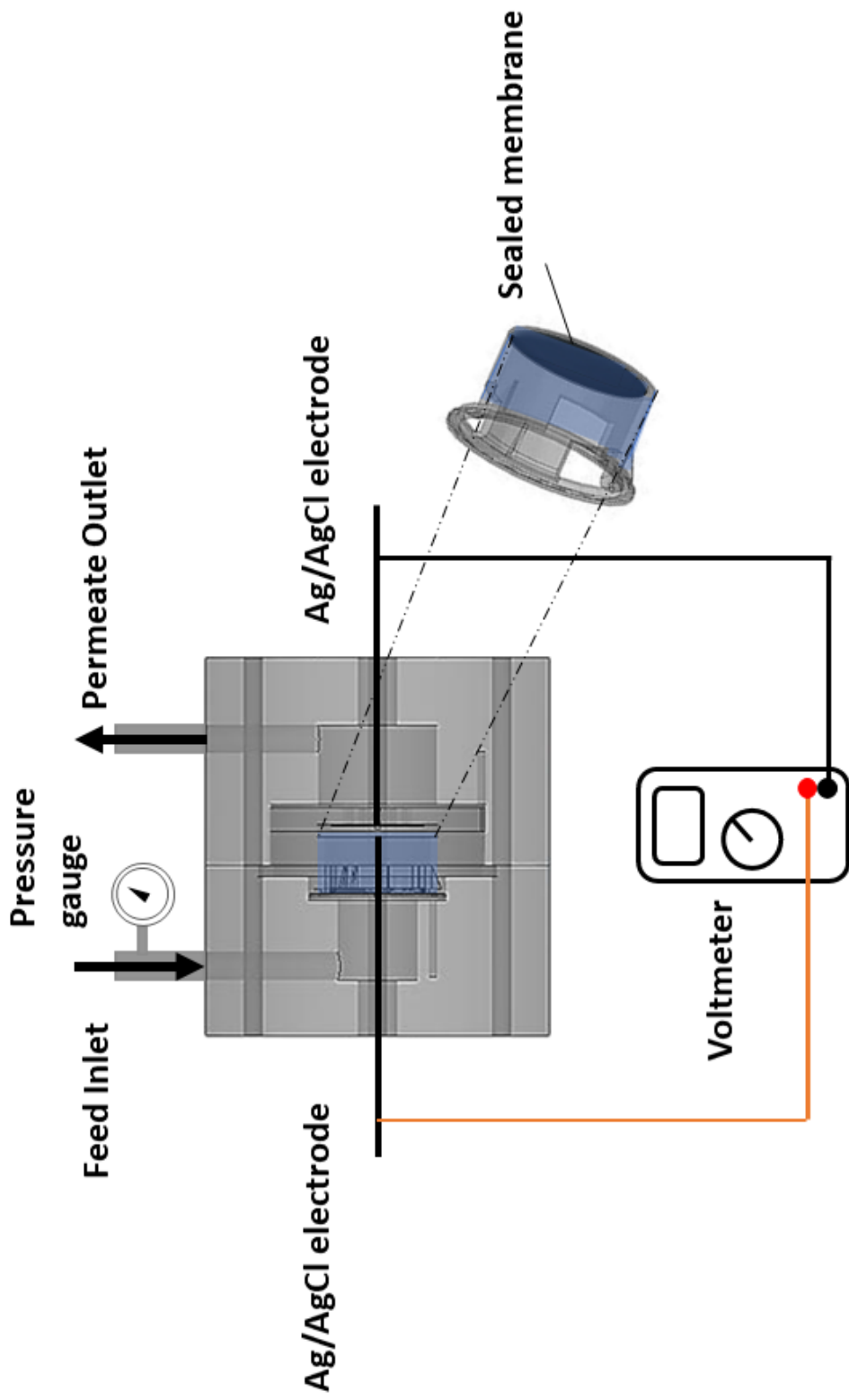
Figure 3.5 Schematic of streaming potential device. The membranes were sealed to the Transwell® inserts using epoxy. 10 mM NaCl was used as the electrolyte solution and the transmembrane pressure was monitored using a pressure gauge at the feed inlet side. Adapted from Vandrangi et al. [90].

3.2 Protein solutions

3.2.1 Protein solution preparation

Three globular proteins were used in this work which include bovine serum albumin (BSA; A30075; RPI, Corp.; Mount Prospect, IL), hen egg lysozyme (HEL; L-6876; Sigma-Aldrich, Corp.; St. Louis, MO), and alpha-lactalbumin (Davisco Foods International, Inc., Eden Prairie, MN). For single protein electroultrafiltration experiments, the feed solutions of 0.1 g/L protein concentration were made by dissolving the required mass of protein powder (AG204 DeltaRange; Mettler-Toledo, Inc; Columbus, OH) in the appropriate volume of water. For binary protein electroultrafiltration experiments, the feed solutions contained 0.1 g/L protein concentration of each protein component. All solutions were prepared using deionized water with resistivity of 18.2 MΩ cm at 25 °C (Barnstead Micropure UV/UF; Thermo Fisher Scientific; Waltham, MA). The ionic strength of the feed solutions was adjusted by adding the appropriate amount of NaCl into the feed solution to achieve 1 mM salt concentration. Besides NaCl, 1 mM of Na_2HPO_4 was added to act as a buffer to maintain the system pH values, thus the final solution ionic strength was 4 mM. The solution pH was adjusted by dropwise additions of 0.1 M HCl or NaOH solution and measured with a pH meter (Thermo Orion 720+; Thermo Electron, Corp.; Beverly, MA). All of the protein ultrafiltration experiments were conducted with protein feed solutions at room temperature (25 °C).

3.3 Electroultrafiltration setup and operation

3.3.1 Experimental setup

All electroultrafiltration experiments were conducted in a tangential flow system (Labscale Tangential Flow Filtration (TFF) System; Millipore; Billerica, MA) with a flow cell unit designed by our group. Figure 3.6 is a schematic illustration of the crossflow electroultrafiltration setup. Due to the limited capacity of the retentate tank in the tangential flow system, the experiments were operated in a fed batch crossflow filtration configuration in which the feed solution was siphoned into the retentate tank from a feed reservoir via vacuum as the permeate was leaving the system. The feed volume was therefore maintained constant. The feed solution was pumped into the flow cell and flowed tangentially to the membrane. The permeate solution was collected while the retentate was recycled back to the primary feed tank with a total solution volume of 500 mL. The crossflow flow rates were adjusted using the built-in TFF diaphragm pump and the transmembrane pressure was controlled using a retentate backpressure valve.

The custom-built flow cell features a carbon fiber mesh electrode in the top chamber with an attached carbon fiber mesh wire extending out of the top compartment for electrical connectivity. The membrane was stabilized between the two chambers of the flow cell with a thin, porous plastic mesh placed inside each chamber to provide mechanical support and prevent electrical contact with the counter electrode. The top and bottom compartments of the flow cell are each 8.62 cm in length (l), 5.00 cm in width (w), and 0.03 cm, in height (h) with an effective membrane surface area of 43.10 cm^2 and cross-sectional chamber area of 0.26 cm^2. All of the electroultrafiltration experiments

were conducted using a cathodic membrane (negatively charged) and anodic carbon fiber

mesh electrode. Electrical contacts were made at the carbon fiber mesh wire and the two

sides of the ultrafiltration membrane in close proximity to the feed inlet and retentate

outlet using alligator clips. For better electrical connection, carbon fiber meshes were

folded over the membrane edges and the alligator clips were clamped to the meshes. An

external electric field was applied between the electrically conductive ultrafiltration

membrane and the carbon fiber mesh electrode using a direct current output power supply

(LLS-4040; Lambda Electronics, Inc.; Melville, NY) under constant voltage operation.

The potential difference between the carbon fiber mesh electrode and the PVA-CNT

membrane (at the potential monitoring points: M1, E1, M2, M2; see Figure 3.7) was

monitored during the beginning and end of the protein electroultrafiltration experiments

using a digital multimeter (77 Series II; Fluke, Corp.; Everett, WA, USA).
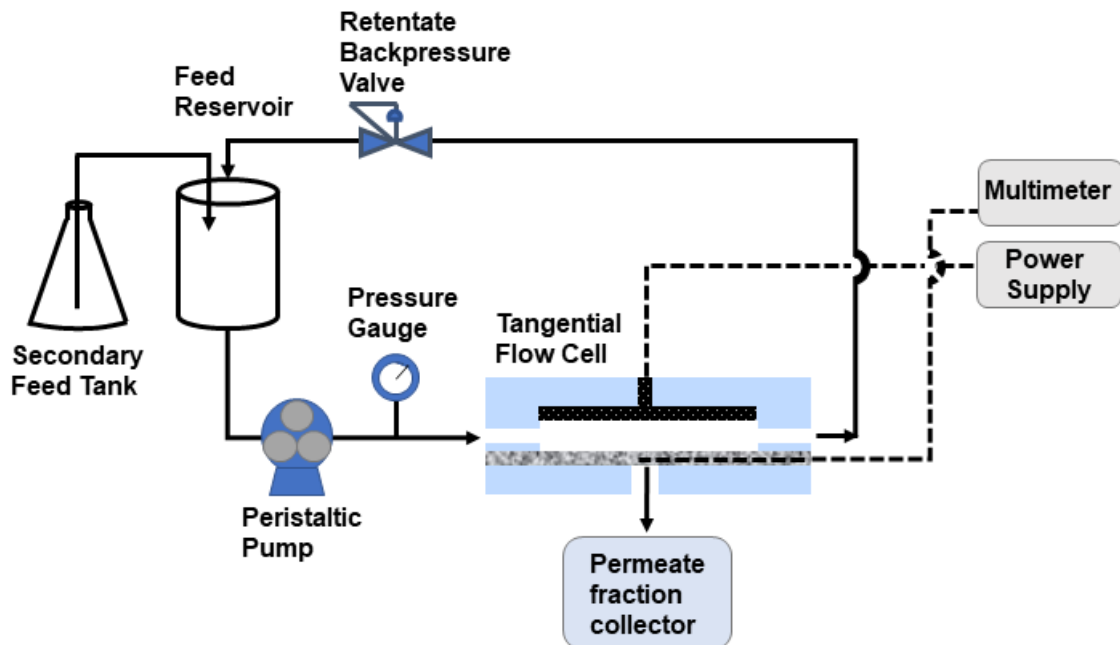
Figure 3.6 Schematic diagram of the crossflow electroultrafiltration setup.

A) Membrane flow cell side-view

Carbon fiber mesh wire

Top chamber

Carbon fiber mesh electrode

Plastic mesh spacers

Membrane

Bottom chamber

Permeate outlet

PVA-CNT

PS-35
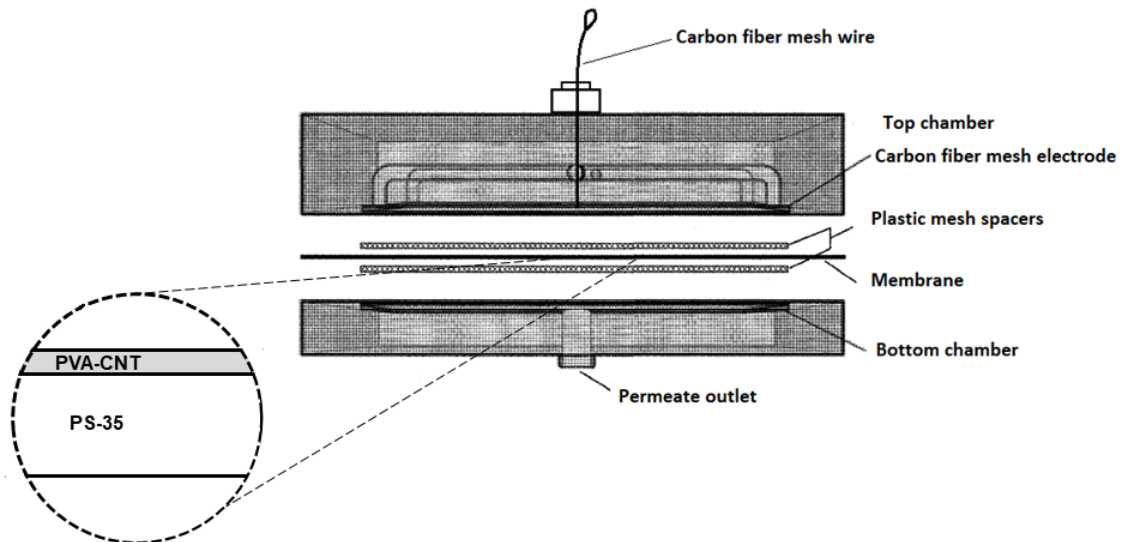
B) Membrane flow cell top-view

Potential monitoring point, M1

Retentate outlet

Potential monitoring point, E1

Membrane

8.62 cm

5.00 cm

0.03 cm

Potential monitoring point, E2

Feed inlet

Potential monitoring point, M2
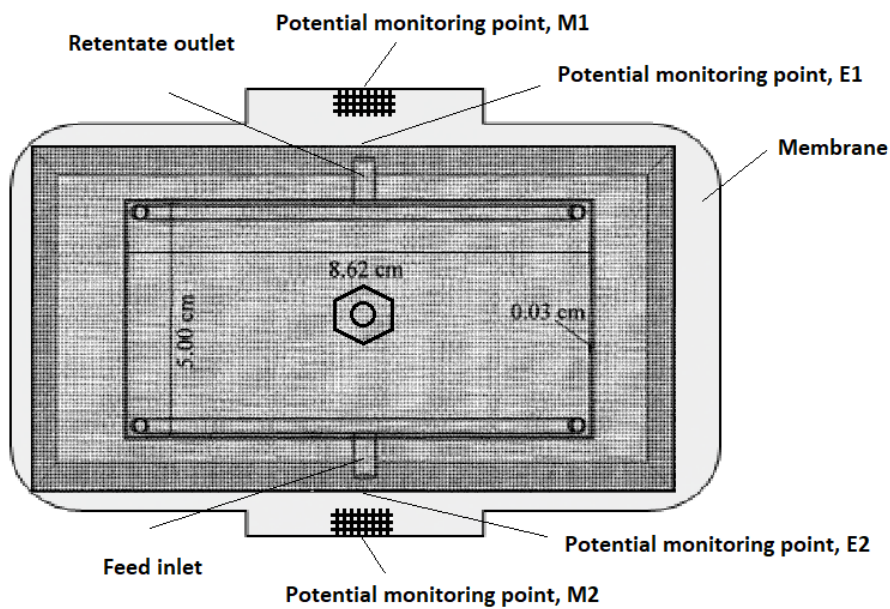
Figure 3.7 Schematic of the crossflow electroultrafiltration flow cell unit: A) side-view, B) top-view. Adapted from Wang 2008, D.Sc. Thesis [92].

3.3.2 Experimental operation

When pressure is applied to a polymeric membrane, the polymers are reorganized and the structure is altered, resulting in a decrease in the volume porosity, increase in the membrane resistance, and an eventual decrease in the permeate flux [93]. To eliminate the influence of membrane compaction on the flux, it is necessary to compact the membranes at a higher transmembrane pressure than the maximum experimental operating pressure. Prior to conducting the protein electroultrafiltration experiments, the PVA-CNT membranes were placed into the crossflow electroultrafiltration flow cell unit and compacted at 30 psi using deionized water with resistivity of 18.2 MΩ cm (Barnstead Micropure UV/UF; Thermo Fisher Scientific; Waltham, MA).

The protein electroultrafiltration experiments were performed using the tangential electroultrafiltration setup in a fed batch crossflow filtration configuration. The membranes were rinsed with deionized water, placed into the flow cell, and sealed. Before each protein filtration experiment, the hydraulic permeability of the membrane was measured using pure deionized water (Barnstead Micropure UV/UF; Thermo Fisher Scientific; Waltham, MA). The system was then purged and the protein solution was added to the primary and secondary feed reservoirs. The protein filtration experiments were performed at 1 and 15 psi transmembrane pressures; 440 s^{-1} and 555 s^{-1} crossflow shear rates; varied applied voltages (0 V to -9 V); and short and long durations (12 minutes to 9.33 hours). Samples of the permeate were collected during the entire filtration runs. For the protein electroultrafiltration experiments, the electric field was applied before the protein solution was fed into the system. After the protein filtration

experiments, the system was purged and the membrane hydraulic permeability was measured using pure deionized water. The current supplied by the power supply operating in the constant voltage configuration was monitored from the power supply digital output at the beginning and end of the filtration experiments. The potential difference was also measured at the beginning and end of the filtration experiments using the voltmeter. After each protein electroultrafiltration experiment, the membrane was removed, rinsed with deionized water, immersed in 0.4 wt% Terg-a-zyme enzymatic detergent solution at 40 °C for 1 hr, rinsed thoroughly with DI water, and stored in DI water for at least 8 hours before the next experiment. The cleaning procedure followed an optimal enzymatic cleaning procedure for polysulfone membranes [94]. The TFF system was cleaned with 0.4 wt% Terg-a-zyme detergent followed by a rinse with deionized water.

3.3.3 Hydraulic permeability

The membrane hydraulic permeability (HP) was measured before and after the protein filtration experiments to determine the extent of membrane fouling. All of the HP measurements were performed using pure deionized water with resistivity of 18.2 MΩ cm at 25 °C (Barnstead Micropure UV/UF; Thermo Fisher Scientific; Waltham, MA) without an applied electric field. The fluid flux was measured as a function of the transmembrane pressure and the slope, representing the value for the membrane hydraulic permeability, was determined following a simple linear regression. The applied transmembrane pressures were typically varied from 1 – 15 psi to prevent any additional compaction at higher pressures.

3.3.4 Permeate flux

The permeate solution was collected from the permeate outlet into glass test tubes of predetermined mass (AG204 DeltaRange; Mettler-Toledo, Inc; Columbus, OH) during the entire protein electroultrafiltration experiments using a fraction collector (Retriever 500 and Retriever II; Teledyne Isco, Inc.; Lincoln, NE). The mass of the permeate samples were measured using the analytical balance and the values for the permeate flux were subsequently determined.

3.3.5 Protein sieving and diagnostics

Various solution samples were collected for protein concentration analysis: the solution from the retentate reservoir after measurement of the pre-experimental hydraulic permeability; the prepared stock protein solution; the protein solutions from the feed and retentate reservoirs before and after the protein electroultrafiltration experiments; and the permeate fractions at different timepoints of UF. The solution from the retentate reservoir after measurement of the pre-experimental HP was sampled and its protein concentration analyzed to ensure that the crossflow filtration system was sufficiently cleaned and that there was no residual protein from previous UF runs.

All of the photometric measurements for evaluation of protein concentration were acquired using a spectrophotometer (Cary 50 Bio UV-VIS; Varian; Palo Alto, CA). For samples with a single protein, the protein concentration was determined using a bicinchoninic acid assay (#23225, Thermo Scientific, Waltham, MA, USA) which is used for determining the total protein concentration in a solution. For binary studies (BSA and HEL; αLA and HEL), the total protein concentration was determined first using the

bicinchoninic acid assay; the lysozyme concentration was evaluated using a lysozyme

activity assay (LY0100, Sigma-Aldrich, Corp., St. Louis, MO, USA); and the

concentration of either the BSA or αLA was determined from the difference in the

evaluated total protein concentration and lysozyme concentration. The observed sieving

coefficients and selectivity were then calculated.

3.3.6 Experimental parameters

The volumetric crossflow flow rates used in the experiments were 34.4 ml/min

and 43.3 ml/min corresponding to average crossflow velocities of 2.20 cm/s and 2.77

cm/s. The crossflow shear rate, $\dot{\gamma}$, was calculated to be 440 s^{-1} and 555 s^{-1} for the

respective cases using Eqn. (3.1).

$$\dot{\gamma} = \frac{6v}{h} \qquad (3.1)$$

The Reynolds number, Re, was calculated to be approximately 4.0 and 16.6 for

the respective flow rates mentioned earlier using Eqn. (3.2):

$$\mathrm{Re} = \frac{\rho v L}{\mu} \qquad (3.2)$$

where ρ is the fluid density, v is the characteristic velocity, L is the characteristic length

of the flow channel, and μ is the fluid dynamic viscosity. While the mesh spacers within

the flow cell induced eddies and possible turbulence, it can be assumed that the flow

contribution to the mass transfer behavior is the same for each set of experiments since

the same experimental setup and procedures were utilized. The Schimidt number, Sc,

used to characterize fluid flows with both momentum and mass diffusion-convection

processes, can be calculated using Eqn. (3.3) where v is the kinematic viscosity and D is the protein diffusion coefficient.

$$Sc = \frac{v}{D} \tag{3.3}$$

As such, the mass transfer coefficient, k, can be calculated for each set of experiments based on the mass transfer correlation (Eqn. (3.4)) for laminar flow systems [13]:

$$Sh = \frac{kd_h}{D} = A'(Re)^{\alpha}(Sc)^{\beta}\left(\frac{d_h}{l}\right)^{\omega} \tag{3.4}$$

where d_h is the hydraulic diameter; l is the length of the flow channel; and A', α, β, and ω are the system-specific constants. For the current system in which the velocity profile is fully developed while the concentration boundary layer is developing along the whole length of the flow channel, the Graetz-Léveque equation can be used with $A' = 1.86$, $\alpha = 1/3$, $\beta = 1/3$, and $\omega = 1/3$ [95].

$$Sh = \frac{kd_h}{D} = 1.86(Re)^{0.33}(Sc)^{0.33}\left(\frac{d_h}{l}\right)^{0.33} \tag{3.5}$$

This mass transfer correlation is valid for laminar flow systems when the Re value is greater than 1800; the entrance length at which the velocity profile is fully developed, L_v, is less than l; and the entrance length at which the concentration polarization layer is fully developed, L_c, is greater than l. The values for L_v and L_c for tangential flow ultrafiltration were calculated by the following equations [13]:

$$L_v = B_v \, Re \, d_h \tag{3.6}$$

$$L_c = \frac{0.1\dot{\gamma}d_h^3}{D} \tag{3.7}$$

42

where B_v is a coefficient from 0.029 to 0.05 (assumed to be 0.05 in calculations for validation of laminar flow system) and D is the diffusion coefficient of the protein. For our system with a channel length, l, of 5.0 cm, the entrance lengths were calculated as $L_v = 1.21 \times 10^{-4}$ m and 4.99×10^{-4} m, and $L_c = 49.1$ m and 203.1 m, for the respective cases assuming the absence of the mesh spacers. Consequently, the requirements for laminar flow are met and the Sherwood number correlation for the solute mass transfer coefficient, Eqn. (3.4), is valid for our study.

Chapter 4 Electrostatic contributions in single protein and binary protein electroultrafiltration

4.1 Introduction

As introduced in Chapter 1, electrostatic interactions have significant effects on both the permeate flux and protein transmission during protein ultrafiltration and electroultrafiltration. Researchers have investigated various methods to utilize electrostatic interactions to enhance the separation and throughput of protein ultrafiltration including altering solution pH and ionic strength, manipulating the membrane charge by surface modification, and applying an electric field with electrodes on opposite sides of the membrane. There have been, however, no reported studies on the separation characteristics of protein electroultrafiltration using an electrically conducting membrane.

In this chapter, the effects of electrostatic interactions on separation performance of charged proteins during single and binary protein electroultrafiltration using electrically conductive ultrafiltration membranes are presented. In particular, the effects of the applied external electric field during protein electroultrafiltration on the permeate flux, protein sieving, and protein selectivity were evaluated through a series of crossflow electroultrafiltration experiments using a cathodic thin film-ultrafiltration membrane composite (PVA-CNT) developed by Dudchenko *et al.* [49]. Crossflow protein electroultrafiltration experiments using the PVA-CNT membranes were performed for single protein feed of BSA, αLA, and HEL, and binary protein feed of BSA-HEL and αLA-HEL at pH 7.4, ionic strength of 4 mM, and various applied potentials (0 V to -9 V).

The two binary protein systems were chosen due to the different charge properties of the investigated proteins. The αLA-HEL binary system allowed for a focused study of the electrostatic contributions since the two small globular proteins have similar sizes but different charge characteristics.

4.2 Experimental materials and methods

The experimental setup and methods were described in Chapter 3. Briefly, crossflow electroultrafiltration experiments were conducted for single protein solutions (BSA, HEL, and αLA) and binary protein solutions (BSA-HEL and αLA-HEL) using a cathodic PVA-CNT membrane. All of the crossflow protein EUF experiments were conducted at constant transmembrane pressure. The type of membrane used in all of the experiments was a PVA-CNT membrane with a PS-35 ultrafiltration support. The membranes were compacted prior to use. Following each protein EUF experiment, the membranes were chemically cleaned using an enzymatic detergent solution to restore the permeability of the membranes. Permeate flux, hydraulic permeability, and protein concentration were evaluated for all the protein EUF studies. Moreover, zeta potential measurements and SEM images of the membranes were acquired post-protein electroultrafiltration for both single (αLA and HEL) and binary studies (αLA-HEL) operating at 1 psi transmembrane pressure, system pH of 7.4, and duration of 9.33 hrs.

Table 4.1 Properties of proteins investigated in the study.

Characteristics	BSA	αLA	HEL
Molecular weight (kDa)	69 [96]	14 [97]	14 [97]
Hydrodynamic radius (10^{-9} m)	3.13 [96]	2.02 [98]	2.09 [99]
Isoelectric point	4.7 [100]	5.2 [101]	11.0 [100]
Diffusion coefficient (m^2/s)	6.76×10^{-11} [102]	1.06×10^{-10} [103]	1.18×10^{-10} [104]

Table 4.2 Summary of experimental parameters for single protein crossflow electroultrafiltration studies.

Experimental parameters: Single protein EUF experiments			
	Single protein EUF with BSA	Single protein EUF with HEL		Single protein EUF with αLA
Membrane	PVA-CNT/PS-35	PVA-CNT/PS-35	PVA-CNT/PS-35	PVA-CNT PS-35
Applied potential	0 V, - 3 V, -6 V, -9 V	0 V, -9 V	0 V, -9 V	0 V, - 9 V
Transmembrane pressure	15 psi	15 psi	1 psi	1 psi
Crossflow flowrate	440 s^{-1}	555 s^{-1}	555 s^{-1}	555 s^{-1}
Feed solution	0.1 g/L BSA	0.1 g/L HEL	0.1 g/L HEL	0.1 g/L αLA
System pH	7.4	7.4	7.4	7.4
Ionic strength	4 mM	4 mM	4 mM	4 mM
Observed output	Permeate flux, hydraulic permeability, protein concentration	Permeate flux, hydraulic permeability, protein concentration	Permeate flux, hydraulic permeability, protein concentration, zeta potential, surface image	Permeate flux, hydraulic permeability, protein concentration, zeta potential, surface image

Table 4.3 Summary of experimental parameters for binary protein crossflow electroultrafiltration studies.

Experimental parameters: Binary protein EUF experiments		
	Binary protein EUF with BSA-HEL	Binary protein EUF with αLA-HEL
Membrane	PVA-CNT/PS-35	PVA-CNT/PS-35	PVA-CNT/PS-35
Applied potential	0 V, - 9 V	0 V, -9 V	0 V, -9 V
Transmembrane pressure	15 psi	15 psi	1 psi
Crossflow flowrate	440 s^{-1}	555 s^{-1}	555 s^{-1}
Feed solution	0.1 g/L BSA, 0.1 g/L HEL	0.1 g/L αLA, 0.1 g/L HEL	0.1 g/L αLA, 0.1 g/L HEL
System pH	7.4	7.4	7.4
Ionic strength	4 mM	4 mM	4 mM
Observed output	Permeate flux, hydraulic permeability, protein concentration	Permeate flux, hydraulic permeability, protein concentration	Permeate flux, hydraulic permeability, protein concentration, zeta potential, surface image

4.3 Results and analysis

4.3.1 Pre- and post-experimental hydraulic permeability data

The pre- and post-experimental hydraulic permeability, L_p, of the membranes used in the single protein and binary protein electroultrafiltration experiments are summarized in Table 6.1 and Table 6.2, respectively. The post-experimental hydraulic permeability all decreased to various extent, but the change in pre- and post-experimental L_p, exceeded 25% for all studies. This indicated membrane fouling was a significant factor in the transient flux behavior during protein ultrafiltration with and without an applied electric field. A greater decrease in hydraulic permeability was observed for filtration of a single protein HEL feed than for filtration of a single protein αLA feed when a potential of -9 V was applied. This suggested HEL, which has a net positive surface charge at the system pH of 7.4 for the studies, was fouling the negatively-charged PVA-CNT membrane. This observed significant hydraulic permeability decrease following electroultrafiltration of the single protein HEL solution indicated that the fouling was not due to complex formation which may be present in the binary protein systems (HEL-BSA and HEL-αLA).

The variation in pre-experimental hydraulic permeability between subsequent protein EUF experiments indicated the need for introducing another parameter for comparing the permeate flux data among the set of experiments. The membrane cleaning procedure, involving immersion in 0.4 wt% Terg-a-zyme enzymatic detergent at 1 hr, was effective for cleaning membrane after single protein EUF (HP % recovery around 90% following each experiment). The initial hydraulic permeability of the membrane,

however, does not fully recover and the decline in HP was even more substantial for binary protein systems. Therefore, for each experiment, the permeate flux of the protein solution, J_v, was normalized to the initial flux of the protein solution, J_0. The normalized permeate flux, J_v/J_0, will be used for the discussion and analysis in this thesis.

4.3.2 Permeate flux behavior for single protein electroultrafiltration

The normalized permeate flux during electroultrafiltration of single protein feed solutions of BSA and HEL at 15 psi transmembrane pressure are shown in Figure 4.1 and Figure 4.2, respectively. The application of a cathodic potential resulted in marginally better membrane fouling prevention during single protein crossflow electroultrafiltration of BSA at 15 psi as exhibited by the greater normalized permeate flux at increasing higher applied potentials. In contrast, a decrease in permeate flux was observed when applying the cathodic potential during single protein crossflow EUF at 15 psi of the smaller, positively charged HEL.
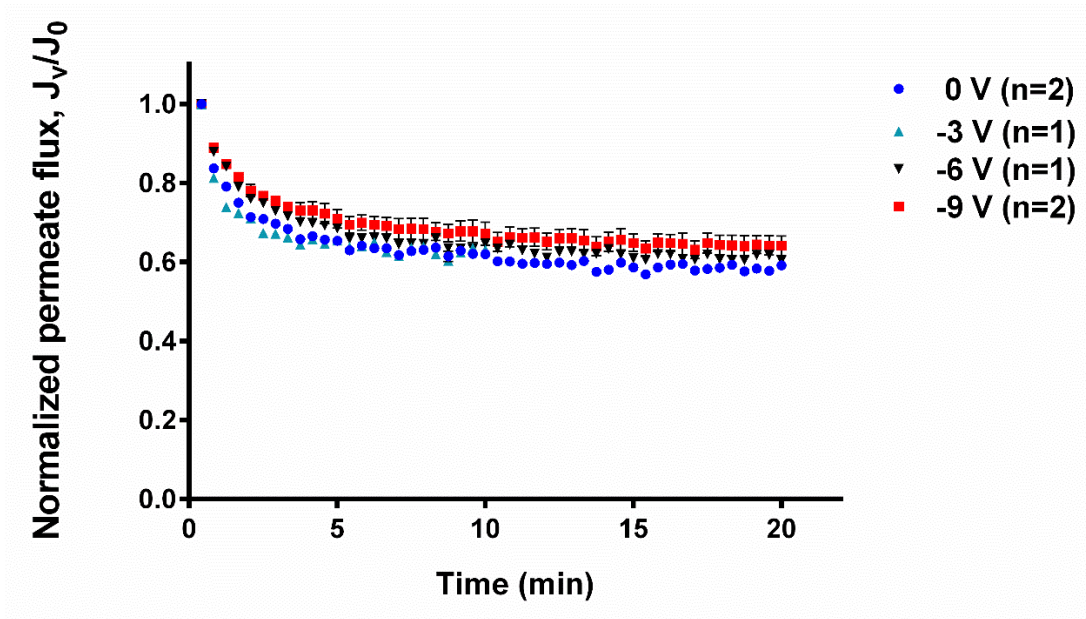
Figure 4.1 Change in permeate flux during single protein electroultrafiltration: 0.1 g/L BSA, 4 mM ionic strength, pH 7.4, 15 psi.
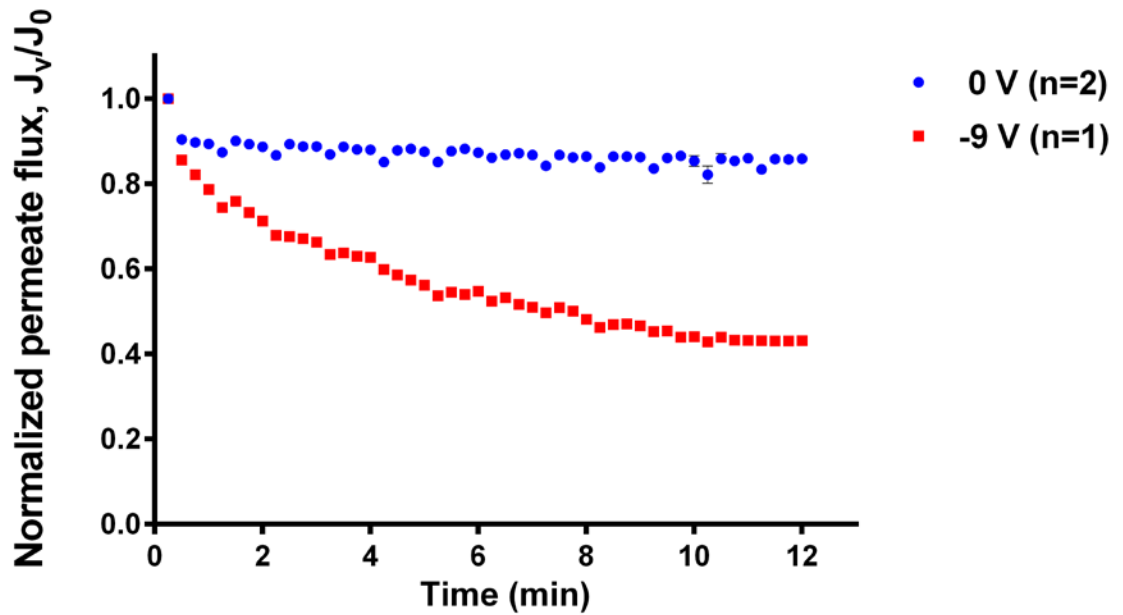
Figure 4.2 Change in permeate flux during single protein electroultrafiltration: 0.1 g/L HEL, 4 mM ionic strength, pH 7.4, 15 psi.

The normalized permeate flux data of single protein electroultrafiltration of αLA and HEL at 0.1 g/L feed, 4 mM ionic strength, pH 7.4, 1 psi transmembrane pressure, and with and without an applied cathodic potential are plotted in Figure 4.3 and Figure 4.4, respectively. In both cases of crossflow EUF of single protein feed solutions, the initial normalized permeate flux is similar with and without an applied potential, but the flux decreases following around 2 to 3 hours with good replicability amongst the set of experiments. This unusual flux behavior requires further investigation, but the abrupt change in flux suggests formation of protein aggregates blocking the membrane pores (as demonstrated by Figure 4.14).
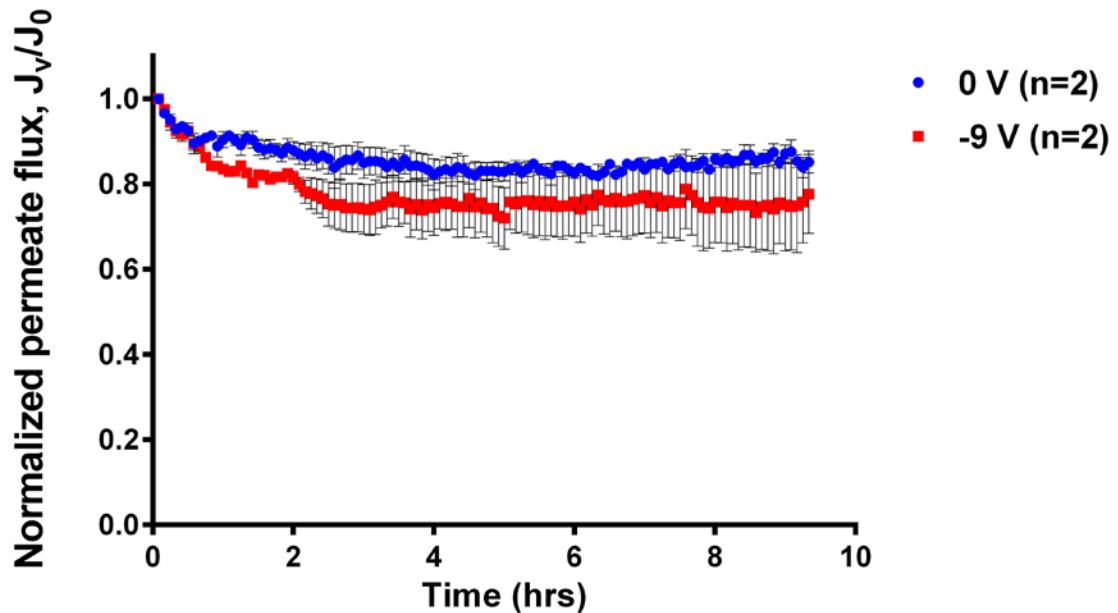
Figure 4.3 Change in permeate flux during single protein electroultrafiltration: 0.1 g/L αLA, 4 mM ionic strength, pH 7.4, 1 psi.
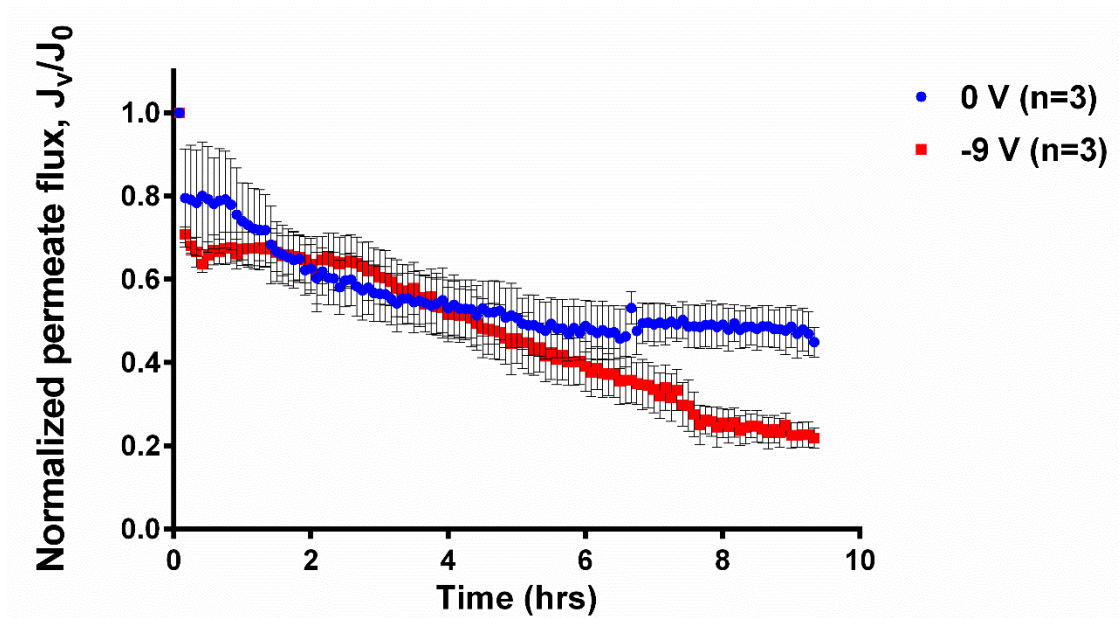
Figure 4.4 Change in permeate flux during single protein electroultrafiltration: 0.1 g/L HEL, 4 mM ionic strength, pH 7.4, 1 psi.

4.3.3 Permeate flux behavior for binary protein electroultrafiltration

The normalized permeate flux behavior during binary protein electroultrafiltration at 15 psi and 1 psi transmembrane pressures are displayed in Figure 4.5, Figure 4.6, Figure 4.7; and Figure 4.8, respectively. As previously for single BSA protein electroultrafiltration (Figure 4.1), the applied cathodic potential during EUF at 15 psi of the binary protein solution containing BSA (BSA-HEL) resulted in a minor increase in permeate flux (Figure 4.5). In contrast, the -9 V applied potential at the same TMP for the two small globular proteins (αLA-HEL) led to a reduction in normalized permeate flux during the entire duration of EUF (Figure 4.6 and Figure 4.7). Application of the cathodic potential had no effect on the EUF of the αLA-HEL binary protein solution (Figure 4.8).

It is important to note that the size of the globular proteins being filtered influenced the effect that the external applied electric field during EUF had on the

permeate flux. Although BSA and αLA have similar negative surface charge densities (pI: 4.7 and 5.2, respectively), BSA has a larger hydrodynamic radius of 3.13 nm than αLA with a hydrodynamic radius of 2.02 nm. Consequently, BSA experienced a greater electrophoretic force from the electrically conductive layer above the membrane due to the increased particle diameter. However, further investigation is required to determine whether proteins interactions within the porous polysulfone membrane structure also played a significant role in the permeate flux behavior. Comparison of the flux behavior of the binary protein EUF of αLA-HEL at 15 psi (Figure 4.6, Figure 4.7) and 1 psi (Figure 4.8) indicated fouling was more prominent with a greater pressure driving force and seems to suggest protein adsorption within the membrane pores.
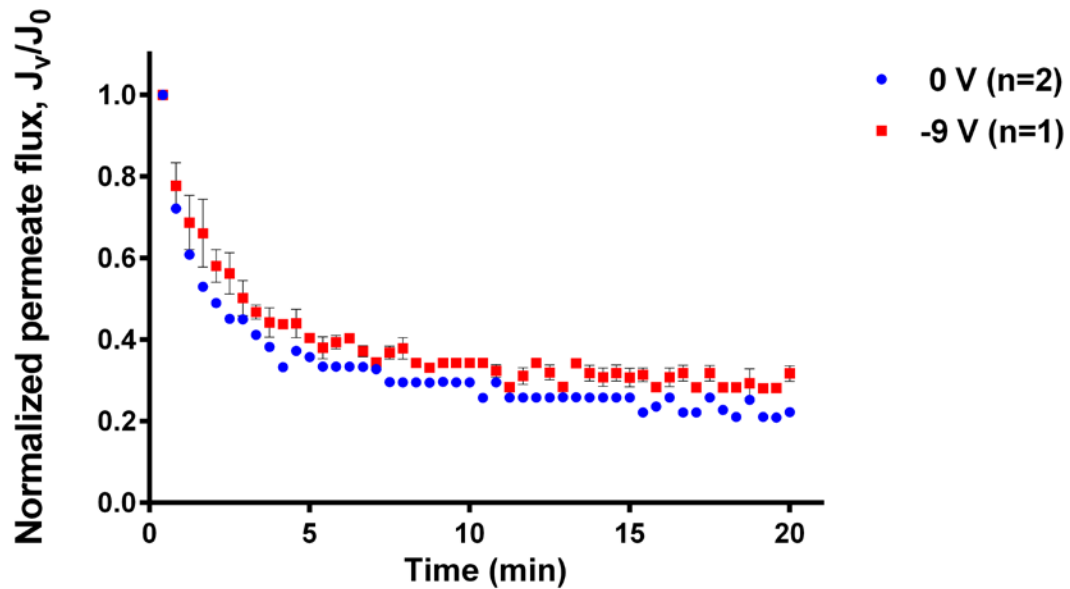
Figure 4.5 Change in permeate flux during binary protein electroultrafiltration: 0.1 g/L BSA, 0.1 g/L HEL, 4 mM ionic strength, pH 7.4, 15 psi.
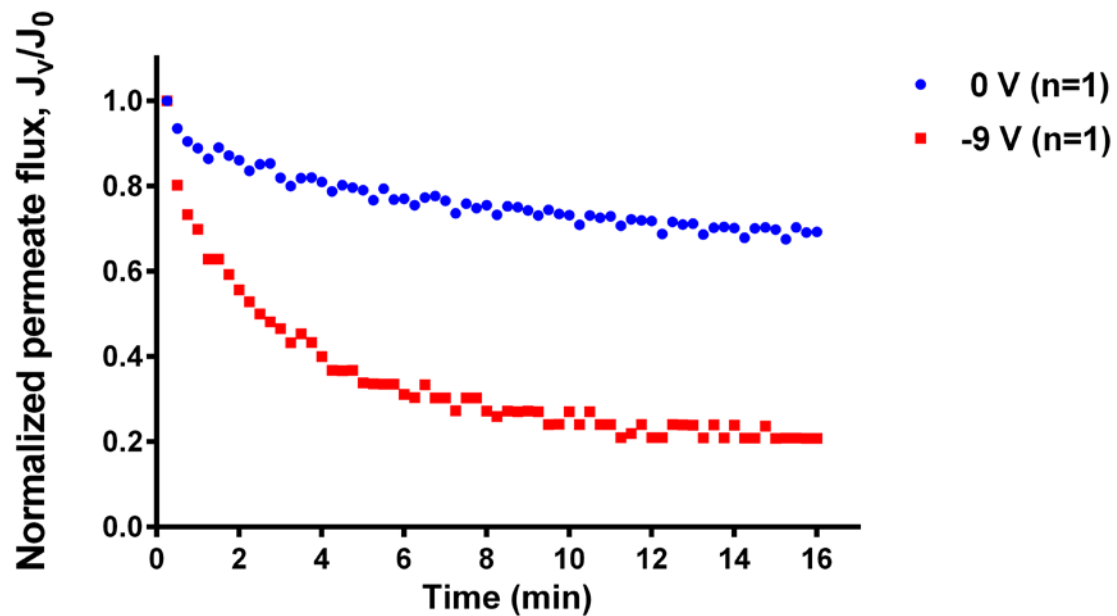
Figure 4.6 Change in permeate flux during binary protein electroultrafiltration: 0.1 g/L αLA, 0.1 g/L HEL, 4 mM ionic strength, pH 7.4, 15 psi, Membrane 24.
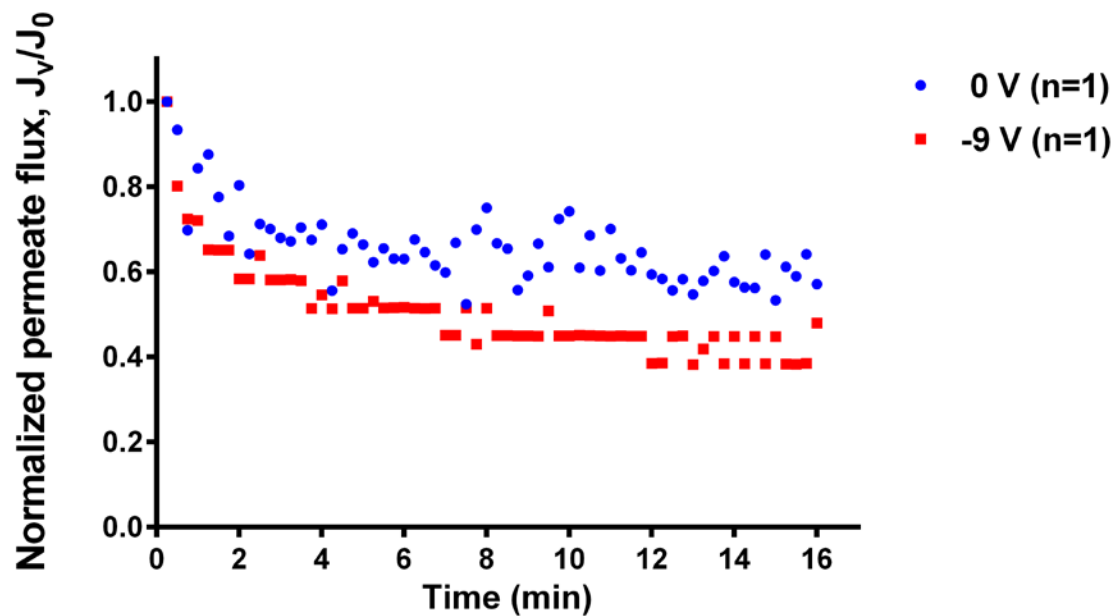
Figure 4.7 Change in permeate flux during binary protein electroultrafiltration: 0.1 g/L αLA, 0.1 g/L HEL, 4 mM ionic strength, pH 7.4, 15 psi, Membrane 31.
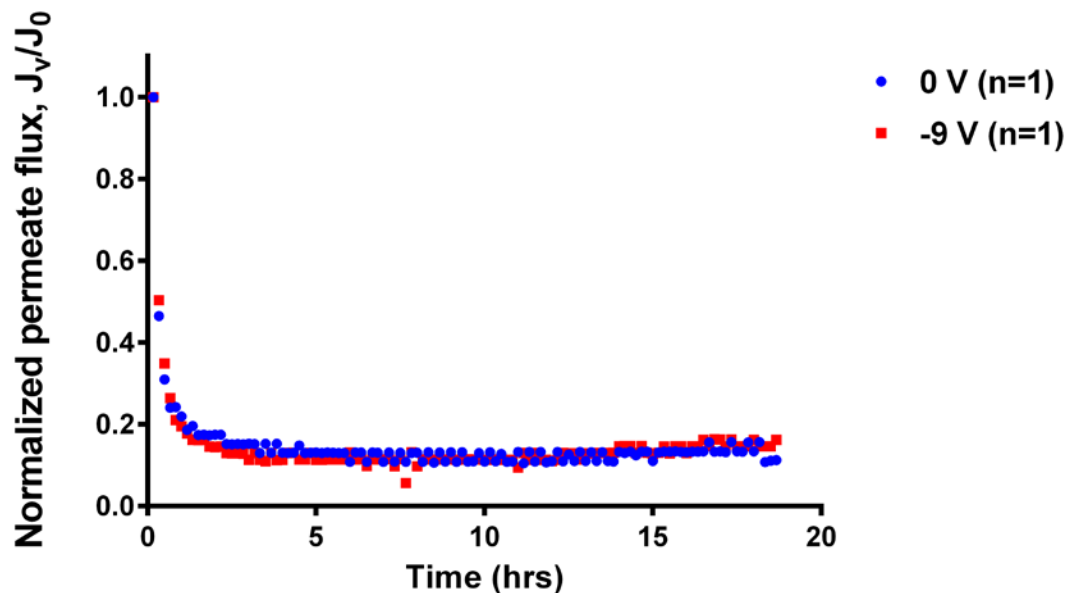
Figure 4.8 Change in permeate flux during binary protein electroultrafiltration: 0.1 g/L αLA, 0.1 g/L HEL, 4 mM ionic strength, pH 7.4, 1 psi.

4.3.4 Observed protein transmission for electroultrafiltration of single protein solutions

The change in observed sieving coefficients of single protein solutions of BSA and HEL during EUF (15 psi, system pH of 7.4) are presented in Figure 4.9 and Figure 4.10, respectively. The observed sieving coefficient data for αLA and HEL during single protein EUF at 1 psi and system pH of 7.4 are provided in Figure 4.11 and Figure 4.12.

All solutes, even the larger BSA protein, were not fully rejected as evident from the protein transmission data. Even though the unmodified PS-35 polysulfone ultrafiltration membrane support had a reported 20 kDa – 35 kDa MWCO, Duan *et al.* evaluated the rejection of various sized polymers using the same type of PVA-CNT/PS-35 membranes from the current thesis study and determined the approximate MWCO for the membranes to be between 100 and 150 kDa [89].

Application of various cathodic potentials during EUF (15 psi TMP) of a single

protein feed of BSA at 15 psi resulted in no effective change in the observed sieving of

BSA. For the UF and EUF (15 psi TMP) of a single protein feed of HEL at pH 7.4, the

observed sieving of lysozyme was maintained at steady values through the duration of the

filtration but was less when cathodic potential was applied. However, at a lower

operating pressure of 1 psi during EUF of the small globular proteins, significant

transient behavior was observed. A sharp increase in observed sieving of αLA was

exhibited in the EUF case over the UF case during the initial couple hours of filtration,

but the observed sieving coefficient gradually converged following around four hours

into the filtration process. For the studies on filtration of HEL at 1 psi, EUF at -9 V

exhibited a dramatic increase in observed sieving (around protein 90% transmission)

compared to the UF without an applied potential, but the observed sieving coefficients for

the two cases also converged following longer durations of filtration. Both set of

observed sieving data for the single protein filtration of αLA and HEL suggests that the

applied cathodic potential may be effective during the initial stage of EUF, but protein

adsorption dominates the solute transport resistance in the later stages of EUF. For single

protein electroultrafiltration of αLA and HEL the transient observed sieving coefficient

data with application and no application of an external potential begin to converge

following around 3 hours (Figure 4.11 and Figure 4.12).
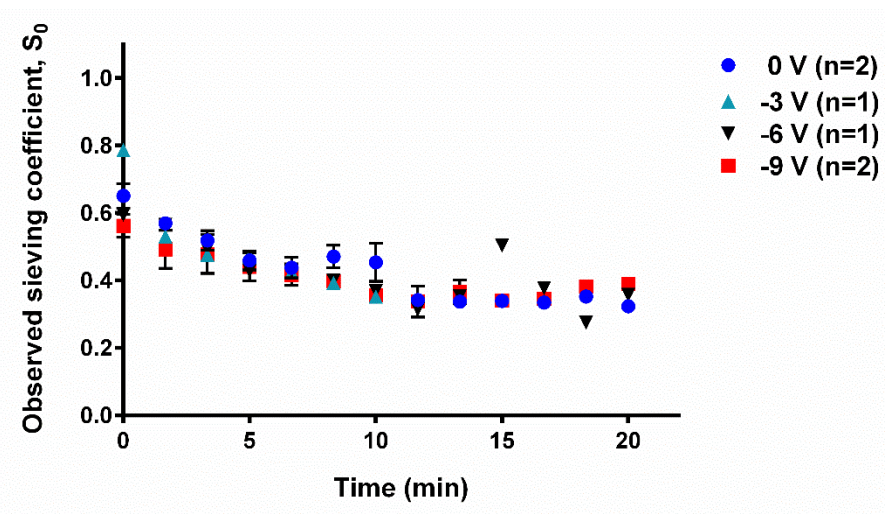
Figure 4.9 Change in observed sieving coefficient of BSA during single protein electroultrafiltration: 0.1 g/L BSA, 4 mM ionic strength, pH 7.4, 15 psi.
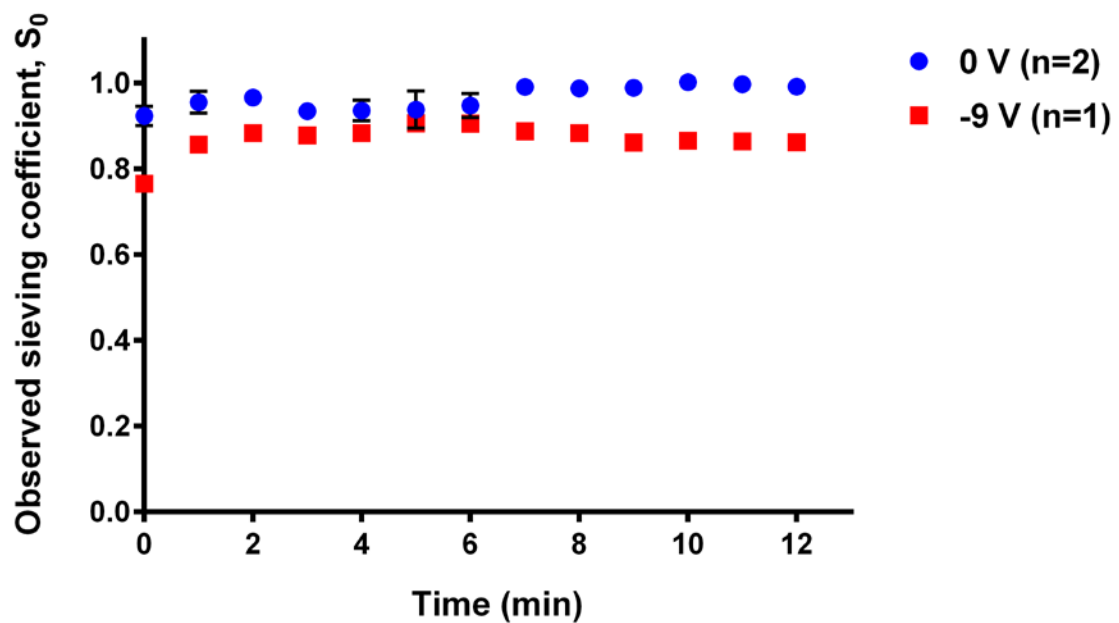
Figure 4.10 Change in observed sieving coefficient of HEL during single protein electroultrafiltration: 0.1 g/L HEL, 4 mM ionic strength, pH 7.4, 15 psi.
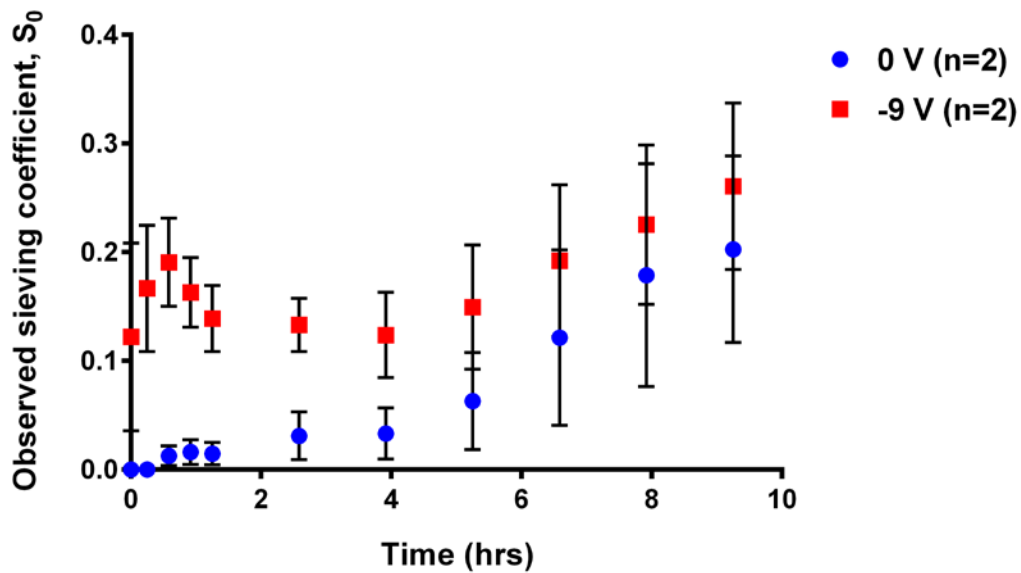
Figure 4.11 Change in observed sieving coefficient of αLA during single protein electroultrafiltration: 0.1 g/L αLA, 4 mM ionic strength, pH 7.4, 1 psi.
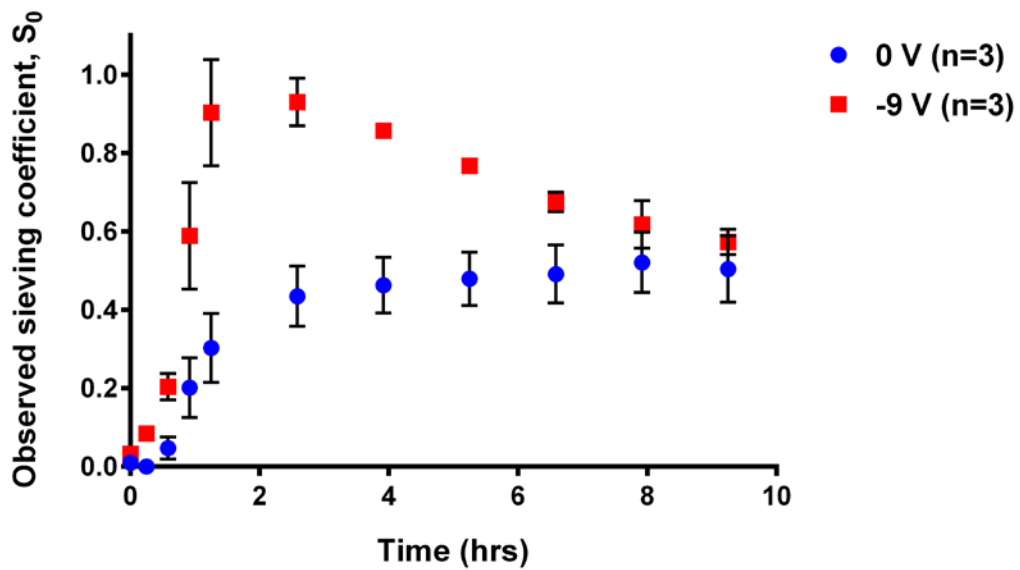
Figure 4.12 Change in observed sieving coefficient of HEL during single protein electroultrafiltration: 0.1 g/L HEL, 4 mM ionic strength, pH 7.4, 1 psi.

4.3.5 Observed protein transmission for electroultrafiltration of binary protein solutions

The observed sieving coefficient and selectivity data for short duration (< 20 minutes) crossflow EUF at 15 psi TMP of the binary protein systems, BSA-HEL and αLA-HEL, are provided in Table 4.4and Table 4.5, respectively. The change in selectivity over an extended duration of binary protein αLA-HEL EUF at 1 psi TMP is displayed in Figure 4.13. Application of a cathodic potential across the PVA-CNT membrane during binary protein BSA-HEL EUF at 15 psi resulted in permeate concentrations of both proteins below the detection limit of the assays following 16 minutes of filtration which suggests significant membrane fouling. This observation can be attributed to the attractive interactions of the positively charged HEL to the negatively charged UF membrane combined with the fouling from formation of HEL-BSA complexes at the system pH of 7.4 and low to moderate ionic strength (0.0015 M – 0.015 M) as reported by Wang *et al.* [92]. For the EUF of αLA-HEL at 15 psi, however, the selectivity ($S_{0,\alpha LA}/S_{0,HEL}$) at 20 minutes of filtration increased by a factor of around 4 when a cathodic potential was applied during the electroultrafiltration process. However, from the transient selectivity data for a protracted period of EUF at 1 psi (Figure 4.13), the improvement in selectivity may be effective only during the initial phase of EUF after which the selectivity reverted to values without an applied potential due to protein adsorption.

Table 4.4 Observed sieving coefficients for BSA and HEL, and selectivity after 20 min of electroultrafiltration: 0.1 g/L BSA, 0.1g/L HEL, 4 mM ionic strength, pH 7.4, 15 psi.

Observed sieving and selectivity for EUF of BSA-HEL			
Applied voltage (V)	Observed sieving coefficient of BSA, $S_{0,BSA}$	Observed sieving coefficient of HEL, $S_{0,HEL}$	Selectivity $(S_{0,HEL}/S_{0,BSA})$
0	0.006 ± 0.004	0.210 ± 0.003	3.5 ± 0.7
-9	0*	0*	0*

*At an applied potential of -9 V, the permeate concentration of both BSA and HEL were below the detection limit of the assays.

Table 4.5 Observed sieving coefficients for αLA and HEL, and selectivity after 16 min of electroultrafiltration: 0.1 g/L αLA, 0.1g/L HEL, 4 mM ionic strength, pH 7.4, 15 psi, Membrane 24 and 31.

Observed sieving and selectivity for EUF of BSA-HEL				
Membrane	Applied voltage (V)	Observed sieving coefficient of αLA, $S_{0,αLA}$	Observed sieving coefficient of HEL, $S_{0,HEL}$	Selectivity $(S_{0,αLA}/S_{0,HEL})$
24	0	0.83 ± 0.06	1.20 ± 0.04	0.69 ± 0.08
	-9	0.92 ± 0.03	0.29 ± 0.04	3.2 ± 0.1
31	0	0.72 ± 0.08	0.95 ± 0.01	0.8 ± 0.1
	-9	0.83 ± 0.07	0.32 ± 0.01	2.6 ± 0.09
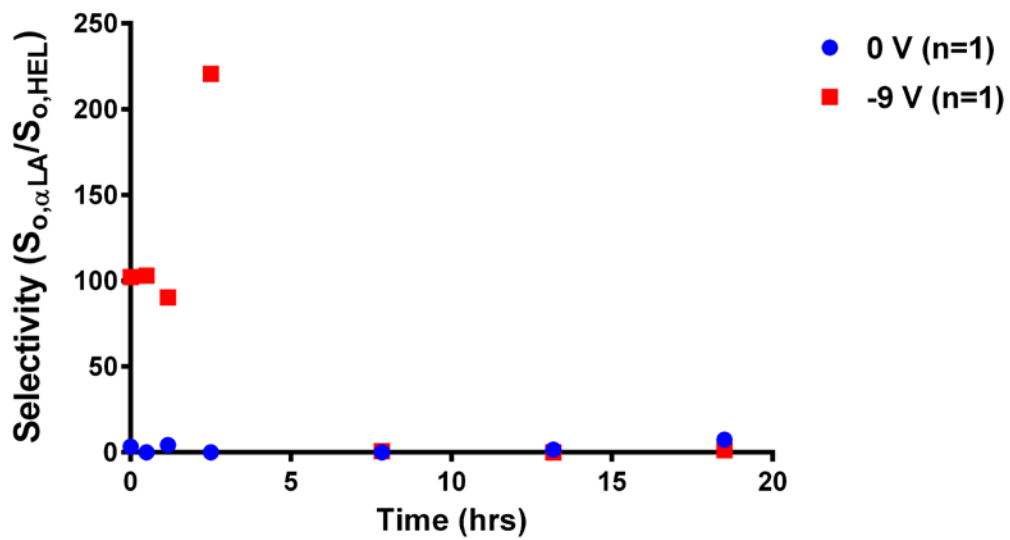
Figure 4.13 Change in protein selectivity during binary protein electroultrafiltration: 0.1 g/L αLA, 0.1 g/L HEL, 4 mM ionic strength, pH 7.4, 1 psi.

4.3.6 Zeta potential measurements

The evaluation of the zeta potential of the PVA-CNT membranes after protein electroultrafiltration (at 555 s^{-1} crossflow shear rate and 1 psi transmembrane pressure) is provided in Table 4.6. The zeta potential measurements of the original 3.0 μm pore size polycarbonate membrane from the Transwell insert and the virgin, unmodified PS-35 UF membrane and PVA-CNT UF membrane are also included in the table. The measured value for the zeta potential of the polycarbonate membrane was in good agreement with the previously reported literature value [90]. As expected for the hydrophobic polysulfone membrane with an isoelectric point of around 4.0 [20], its measured zeta potential was negative (-17.7 ± 0.2 mV) at the experimental system pH of 7.4. The measured zeta potential of the membrane following modification from the deposition of the PVA-CNT composite layer remained relatively unchanged (-17.4± 0.1 mV). The PVA-CNT thin film layer, at about 6 μm in thickness (Figure 6.43) compared to the 165 μm thick polysulfone support, has an intrinsic negative charge resulting from the protonation/deprotonation of the carboxylic acid groups on the CNT surface [105]. Since the streaming potential device used in the study measures the zeta potential of the membrane pores (due to the arrangement of the electrodes on opposite sides of the membrane), it is unsurprising that the zeta potential values were similar for the unmodified PS-35 membrane and PVA-CNT/PS-35 membrane.

From comparison of the measured zeta potential of the PVA-CNT membranes following single protein EUF of HEL with and without an applied potential of -9 V at the solution pH of 7.4, it is apparent that more significant HEL adsorption occurred when an

external potential was applied. HEL has a positive surface charge at the system pH for the study, thus it is reasonable to expect the attraction of the protein to the cathodic, negatively charged PVA-CNT membrane. The magnitude of the negative zeta potential of the PVA-CNT membrane was reduced after filtration of αLA. This observation was likely due to the UF membrane assuming the charge of the adsorbed solutes of alpha-lactalbumin which has a higher isoelectric point than the membrane. Application of -9V across the membrane during αLA electroultrafiltration resulted in a lesser decrease in negative zeta potential of the membrane which indicated less protein adsorption likely attributed to the electrostatic repulsive force arising from the surface potential present on the solutes and the membrane surface. Electroultrafiltration of a binary protein feed of αLA and HEL at -9 V resulted in the membrane zeta potential becoming slightly positive, suggesting protein-membrane interactions leading to deposition and adsorption of HEL and/or αLA-HEL complexes.

Table 4.6 Zeta potential measurements of the virgin, unmodified PS-35 membrane and PVA-CNT membrane, and PVA-CNT membrane after protein electroultrafiltration.

Membrane	Feed solution* for EUF**	Applied potential (V) for EUF	Zeta potential (mV)
Polycarbonate membrane (virgin)	-	-	-7.6 ± 0.3
PS-35 only (virgin)	-	-	-17.7 ± 0.2
PVA-CNT PS-35 (virgin) [Membrane 42]	-	-	-17.4 ± 0.1
PVA-CNT PS-35 [Membrane 37]	Binary protein feed: 0.1 g/L HEL & 0.1 g/L αLA	0	-5.7 ± 0.1
PVA-CNT PS-35 [Membrane 36]	Binary protein feed: 0.1 g/L HEL & 0.1 g/L αLA	-9	1.5 ± 0.1
PVA-CNT PS-35 [Membrane 38]	Single protein feed: 0.1 g/L αLA	0	-4.3 ± 0.2
PVA-CNT PS-35 [Membrane 41]	Single protein feed: 0.1 g/L αLA	-9	-9.9 ± 0.3
PVA-CNT PS-35 [Membrane 40]	Single protein feed: 0.1 g/L HEL	0	-15.9 ± 0.2
PVA-CNT PS-35 [Membrane 39]	Single protein feed: 0.1 g/L HEL	-9	-3.0 ± 0.1

* Feed solution at 4 mM ionic strength, pH 7.4

**Operating conditions for EUF: 555 s^{-1} crossflow shear rate, 1 psi transmembrane pressure

4.3.7 SEM image of membrane surface and porosity calculations

For visualization of the fouling at the PVA-CNT membranes surfaces following the extended duration of EUF (feed: 0.1 g/L of each protein component, 4 mM ionic strength, pH 7.4; operating conditions: 555 s^{-1} crossflow shear rate, 1 psi TMP, 9.33 hours), images of the membrane surfaces were obtained by scanning electron microscopy and are displayed in Figure 4.14. From the cross-sectional image of the PVA-CNT/PS-35 composite membrane, the thickness of the PVA-CNT thin film was determined to be around 6 μm which agrees with previously reported measurements [57, 89]. Porosity calculations from analysis of the membrane surface images are provided in Table 4.7. It is evident from the SEM images of the surfaces post-EUF that protein adsorption and aggregation are significant factors in protein electrofiltration with an electrically conductive membrane.

Large complexes of protein on the surface of the PVA-CNT membranes were observed following both single protein HEL and binary protein αLA-HEL EUF at 1 psi. Reduced surface fouling was observed when applying a cathodic potential during EUF of αLA. The significant differences in fouling above the PVA-CNT layer can largely explain the permeate flux behavior described previously. The evident protein fouling and aggregation above the PVA-CNT thin film for EUF at -9 V of binary protein αLA-HEL and single protein HEL reduced the effective membrane surface area and thus resulted in a decrease in permeate flux for those systems. Although the observed protein fouling above the PVA-CNT membrane following EUF was different in the cases of no applied potential and -9 V cathodic potential, it is worth noting that the observed protein sieving

still converged for the two cases at extended durations of EUF. This suggested protein transmission at the extended time periods of EUF was still predominantly influenced by the protein adsorption within the membrane pores as demonstrated by the zeta potential measurements.
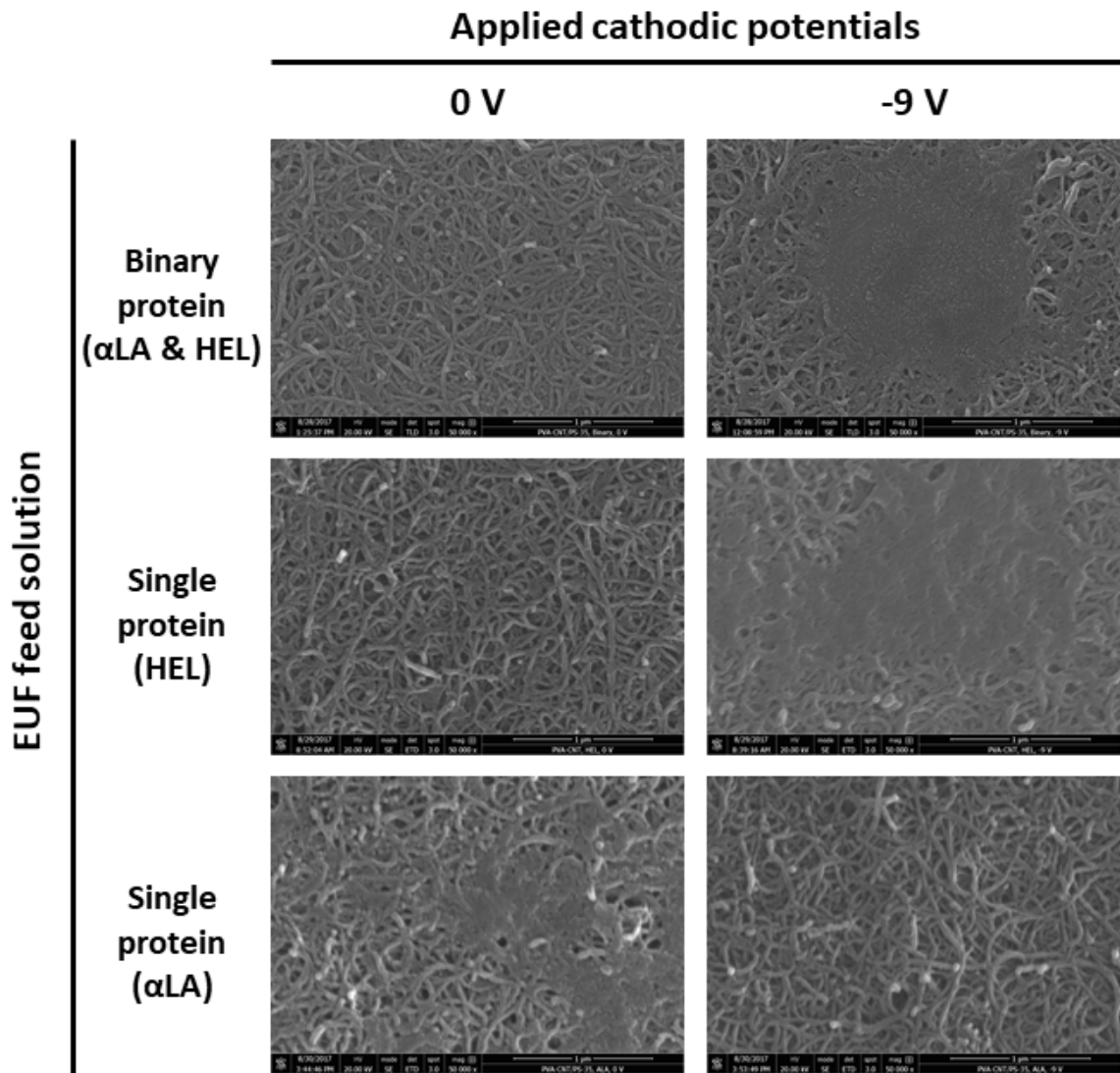
Figure 4.14 Fouling of PVA-CNT membrane surfaces following protein electroultrafiltration (0.1 g/L of each protein component, 4 mM ionic strength, pH 7.4, 555 s^{-1} crossflow shear rate; 1 psi TMP; 9.33 hours duration). Images were obtained by SEM.

Table 4.7 Membrane percent porosity following protein EUF (4 mM ionic strength, pH 7.4, 555 s^{-1}, 1 psi) as determined using ImageJ.

Protein EUF study	Average membrane % porosity post-protein EUF
- (Unfouled membrane)	11.8
Binary protein (0.1 g/L αLA & 0.1 g/L HEL) at 0 V	9.1
Binary protein (0.1 g/L αLA & 0.1 g/L HEL) at -9 V	6.9
Single protein (0.1 g/L HEL) at 0 V	10.6
Single protein (0.1 g/L HEL) at -9 V	5.0
Single protein (0.1 g/L αLA) at 0 V	3.7
Single protein (0.1 g/L αLA) at -9 V	10.7

4.4 Conclusions

In this chapter, the effects of electrostatic interactions on the permeate flux and protein transmission during single and binary protein electrultrafiltration using electrically conductive PVA-CNT/PS-35 ultrafiltration membranes were studied through various EUF experiments at low ionic strength (4 mM) and pH of 7.4. Further characterizations of the charge within the membrane pores and the protein fouling above the PVA-CNT/PS-35 UF membrane provided insight into the separation characteristics of protein crossflow EUF with a cathodic membrane. For the EUF of BSA at moderate TMP (15 psi), the application of cathodic potentials (-3 V, -6 V, and -9 V) resulted in minor improvements in permeate flux with no change to the protein sieving. For the EUF of HEL at moderate TMP (15 psi), the application of -9 V across the membrane resulted in a

significant decrease in permeate flux and slight decrease in protein transmission. At low

TMP (1 psi) and -9 V potential, however, the EUF of single protein αLA and HEL

resulted in an unusual decrease in permeate flux at different phases and enhancement in

sieving during the initial phase of filtration. For EUF of BSA-HEL at moderate TMP, an

applied potential of -9 V led to a minor enhancement in permeate flux but a significant

reduction in sieving of both proteins. Application of -9 V during EUF of binary αLA at

15 psi resulted in a decrease in the permeate flux. The binary αLA-HEL EUF studies at

both low and moderate TMP indicate improvements in selectivity during the initial phase

of filtration (< 16 minutes) with an application of -9 V. However, for the αLA-HEL

electroultrafiltration study at low TMP, no enhancement in selectivity was observed for

extended durations (> 7.5 hours) of EUF at -9 V. The significance of protein adsorption

and aggregation above and within the PVA-CNT/PS-35 membrane on the permeate flux

and protein transmission behavior during single and binary protein EUF were clearly

demonstrated by zeta potential measurements and surface visualization via SEM.

Chapter 5   Conclusion and recommendations

This thesis aimed to study the effects of electrostatic interactions on filtration performance during crossflow electroultrafiltration of single and binary protein solutions with an electrically conductive ultrafiltration membrane. To this end, protein crossflow electroultrafiltration experiments were conducted using a cathodic membrane at a system pH of 7.4, low ionic strength of 4 mM, and various applied potentials for protein system with different charge and/or size properties. The performance of protein EUF was evaluated by measurements of the hydraulic permeability, permeate flux, sieving, and selectivity. The contributions of the applied cathodic potential to the membrane performance were assessed.

Application of a cathodic potential across the electrically conductive PVA-CNT/PS-35 membrane resulted in a decrease in permeate flux for electroultrafiltration of single and binary protein systems of αLA and HEL. For the crossflow EUF of BSA, the increase in permeate flux with an applied cathodic potential was marginal and no change in sieving behavior was observed. However, the binary protein EUF experiments of the similarly sized but different charged αLA and HEL at the system pH of 7.4 demonstrate significant enhancement in protein selectivity when an external electric field was applied but only during the early phase of EUF. The SEM membrane surface images and zeta potential measurements indicated protein adsorption played a critical factor in the permeate flux, sieving, and selectivity behavior.

From the study, it was determined that electrically conductive composite ultrafiltration membranes have the potential to separate proteins of similar sizes with

different charge properties. The electroultrafiltration process, however, would require

additional methods to clear deposited proteins. Combination of protein

electroultrafiltration with the electrically conductive membrane and periodic back

washing should thus be explored. To develop a fundamental understanding of the EUF

mechanism and extend the electroultrafiltration process with an electrically conductive

membrane to other protein systems, a flux model and protein transport model should be

researched.

Chapter 6 Complementary material

This chapter provides data for the protein electroultrafiltration studies, zeta potential measurements, and SEM analysis.

6.1 Data

6.1.1 Protein electroultrafiltration data

Table 6.1 Summary of hydraulic permeability data for single protein EUF experiments.

Study	Membrane	Applied Potential (V)	Run	Pre-exp. HP ($\times 10^{-10}$ m s^{-1} Pa^{-1})	Post-exp. HP ($\times 10^{-10}$ m s^{-1} Pa^{-1})	% Change in pre- & post-exp. HP
Single protein EUF (BSA), 440 s^{-1}, 15 psi	20	-3	1	20.4 ± 0.5	11.2 ± 0.4	-55%
	20	0	2	21.1 ± 0.8	11.9 ± 0.2	-56%
	20	-9	3	12.8 ± 0.3	5.0 ± 0.1	-61%
	20	-6	4	9.0 ± 0.5	5.7 ± 0.2	-37%
	20	0	5	8.1 ± 0.3	5.6 ± 0.1	-31%
	20	-9	6	6.7 ± 0.2	4.3 ± 0.1	-36%
Single protein EUF (HEL), 555 s^{-1}, 15 psi	25	0	1	14.6 ± 0.3	10.5 ± 0.1	- 28%
	25	0	2	21.1 ± 0.5	13.0 ± 0.1	- 38%
	25	-9	3	18.8 ± 0.2	5.2 ± 0.1	- 72%
Single protein EUF (αLA), 555 s^{-1}, 1 psi	33	0	1	10.5 ± 0.2	7.7 ± 0.2	-27%
	33	-9	2	11.0 ± 0.1	7.8 ± 0.2	-29%
	33	0	3	14.2 ± 0.3	10.8 ± 0.3	-27%
	33	-9	4	12.2 ± 0.7	7.5 ± 0.3	-39%
Single protein EUF (HEL), 555 s^{-1}, 1 psi	34	0	1	11.7 ± 0.1	2.1 ± 0.1	-82%
	34	-9	2	10.5 ± 0.2	2.7 ± 0.1	-74%
	34	0	3	9.6 ± 0.1	3.2 ± 0.1	-66%
	34	-9	4	9.9 ± 0.3	2.1 ± 0.1	-79%
	34	0	5	7.0 ± 0.1	1.5 ± 0.1	-79%
	34	-9	6	7.1 ± 0.1	1.1 ± 0.1	-85%

Table 6.2 Summary of hydraulic permeability data for binary protein EUF experiments.

Study	Membrane	Applied Potential (V)	Run	Pre-exp. HP ($\times 10^{-10}$ m s^{-1} Pa^{-1})	Post-exp. HP ($\times 10^{-10}$ m s^{-1} Pa^{-1})	% Change in pre- & post-exp. HP
Binary protein EUF (BSA-HEL), 440 s^{-1}, 15 psi	26	0	1	18 ± 1	1.1 ± 0.2	-94%
	26	-9	2	12.9 ± 0.5	0.9 ± 0.4	-93%
	26	-9	3	2.8 ± 0.4	0.4 ± 0.2	-86%
Binary protein EUF (αLA - HEL), 555 s^{-1}, 15 psi	24	0	1	14.9 ± 0.6	10.9 ± 0.2	- 27%
	24	-9	2	21.7 ± 0.2	1.3 ± 0.1	- 94%
	31	0	1	4.0 ± 0.5	2.4 ± 0.1	-40%
	31	-9	2	9.3 ± 0.3	2.0 ± 0.1	-78%
Binary protein EUF (αLA - HEL), 555 s^{-1}, 1 psi	32	0	1	14.5 ± 0.1	0.3 ± 0.1	-98%
	32	-9	2	7.9 ± 0.1	0.6 ± 0.1	-92%
	32	-9	3	12.5 ± 0.4	2.9 ± 0.1	-77%

Table 6.3 Data for single protein (BSA) EUF at -3 V [Run 170122].

				Run 170122				
			Exp: 0.1 g/L BSA, 1 mM NaCl, 1 mM Na$_2$HPO$_4$, pH 7.4, -3 V					

Power supply current (A), start	0.02
Power supply current (A), end	0.02
Membrane	20 [01-20-17_1]
Operating pressure	15 psi
Crossflow shear rate	440 s^{-1}

ΔP (psi)	$J_v \times 10^6$ (m/s)	Pre-HP $\times 10^{10}$ m/(s·Pa)		ΔP (psi)	$J_v \times 10^6$ (m/s)	Post-HP $\times 10^{10}$ m/(s·Pa)
0.6	7.1			1	8.6	
1.2	16.2			2	17.0	
1.7	22.4	20.4 ± 0.5		3	25.1	11.2 ± 0.4
2.3	31.2			4	31.7	

ΔV (V) at M1, start	ΔV (V) at E1, start	ΔV (V) at E2, start	ΔV (V) at M2, start	ΔV (V) at M1, end	ΔV (V) at E1, end	ΔV (V) at E2, end	ΔV (V) at M2, end	Avg. start ΔV (V)
-2.882	-1.534	-1.012	-2.904	-2.886	-1.615	-0.971	-2.899	-1.273

Fraction sample	Sample time (s)	C_p (g/L)	pH			C (g/L)	pH	Λ_0 (µS/cm)
1	0	0.091681	-		Pre-sample	0	-	-
4	100	0.061935	-		Stock solution	0.122162	-	-
8	200	0.055577	-		Retentate(start)	0.116571	-	-
12	300	0.054969	-		Feed, (start)	0.116682	-	-
16	400	0.049442	-		Retentate(end)	-	-	-
20	500	0.045863	-		Feed (end)	-	-	-
24	600	0.041103	-					
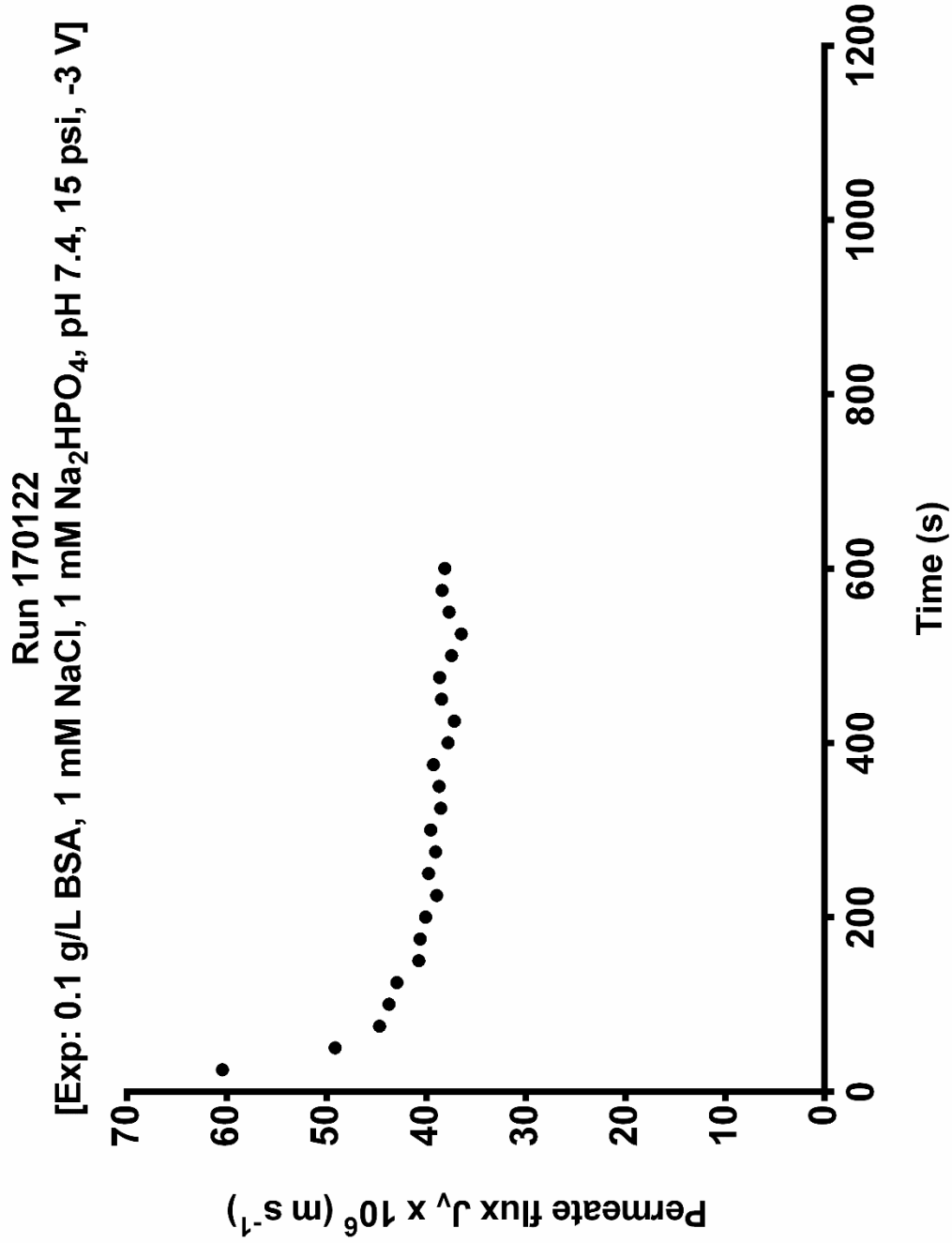
Figure 6.1 Permeate flux for single protein (BSA) EUF at -3 V [Run 170122].

Table 6.4 Data for single protein (BSA) EUF at 0 V [Run 170124].

Run 170124
Exp: 0.1 g/L BSA, 1 mM NaCl, 1 mM Na$_2$HPO$_4$, pH 7.4, 0 V

Power supply current (A), start	-	
Power supply current (A), end	-	
Membrane	20 [01-20-17_1]	
Operating pressure	15 psi	
Crossflow shear rate	440 s^{-1}	

ΔP (psi)	$J_v \times 10^6$ (m/s)	Pre-HP $\times 10^{10}$ m/(s·Pa)		ΔP (psi)	$J_v \times 10^6$ (m/s)	Post-HP $\times 10^{10}$ m/(s·Pa)
0.6	7.5			1	8.2	
1.2	17.6			2	16.9	
1.9	27.2	21.1 ± 0.8		3	24.6	11.9 ± 0.2
2.5	35.4			4	33.0	

ΔV (V) at M1, start	ΔV (V) at E1, start	ΔV (V) at E2, start	ΔV (V) at M2, start	ΔV (V) at M1, end	ΔV (V) at E1, end	ΔV (V) at E2, end	ΔV (V) at M2, end	Avg. start ΔV (V)
-	-	-	-	-	-	-	-	-

Fraction sample	Sample time (s)	C_p (g/L)	pH			C (g/L)	pH	Λ_0 (µS/cm)
1	0	0.073862	-		Pre-sample	0.001993	-	-
4	100	0.060929	-		Stock solution	0.110651	-	-
8	200	0.058852	-		Retentate(start)	0.105190	-	-
12	300	0.052486	-		Feed, (start)	0.105232	-	-
16	400	0.050643	-		Retentate(end)	-	-	-
20	500	0.054496	-		Feed (end)	-	-	-
24	600	0.056104	-					
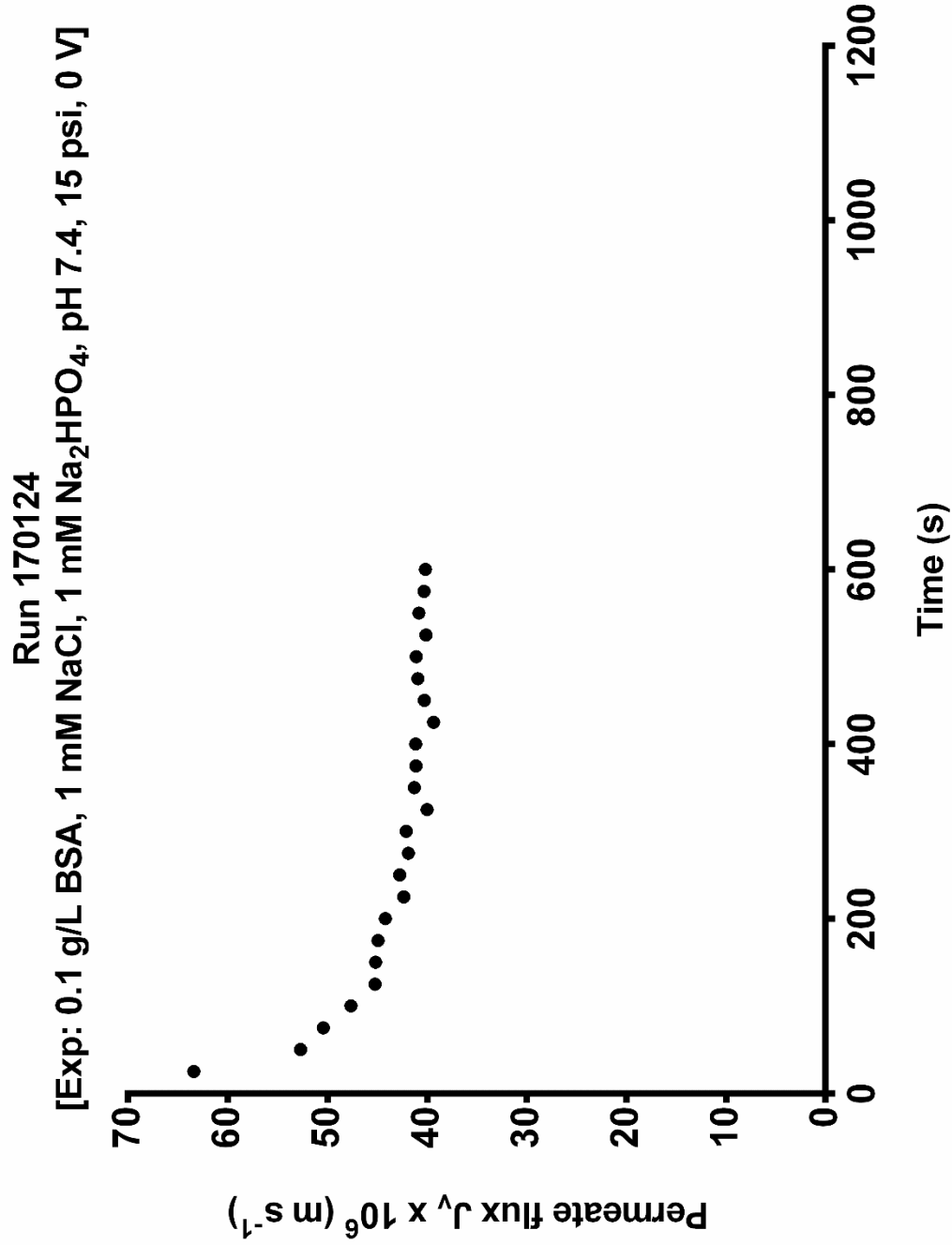
Figure 6.2 Permeate flux for single protein (BSA) EUF at 0 V [Run 170124].

Table 6.5 Data for single protein (BSA) EUF at -9 V [Run 170203].

Run 170203
Exp: 0.1 g/L BSA, 1 mM NaCl, 1 mM Na$_2$HPO$_4$, pH 7.4, -9 V

Power supply current (A), start	0.06
Power supply current (A), end	0.06
Membrane	20 [01-20-17_1]
Operating pressure	15 psi
Crossflow shear rate	440 s^{-1}

ΔP (psi)	$J_v \times 10^6$ (m/s)	Pre-HP $\times 10^{10}$ m/(s·Pa)		ΔP (psi)	$J_v \times 10^6$ (m/s)	Post-HP $\times 10^{10}$ m/(s·Pa)
0.6	4.1			1	3.6	
1.2	10.0			2	7.3	
1.8	14.9	12.8 ± 0.3		3	10.6	5.0 ± 0.1
2.5	20.9			4	14.0	

ΔV (V) at M1, start	ΔV (V) at E1, start	ΔV (V) at E2, start	ΔV (V) at M2, start	ΔV (V) at M1, end	ΔV (V) at E1, end	ΔV (V) at E2, end	ΔV (V) at M2, end	Avg. start ΔV (V)
-8.59	-3.77	-3.07	-8.62	-8.62	-3.81	-3.24	-8.66	-3.42

Fraction sample	Sample time (s)	C_p (g/L)	pH			C (g/L)	pH	Λ_0 (μS/cm)
1	0	0.059257	-		Pre-sample	0.009917	-	-
4	100	0.047642	-		Stock solution	0.118587	-	-
8	200	0.045813	-		Retentate(start)	0.115404	-	-
12	300	0.044120	-		Feed, (start)	0.116514	-	-
16	400	0.042867	-		Retentate(end)	-	-	-
20	500	0.042901	-		Feed (end)	-	-	-
24	600	0.039244	-					
28	700	0.031353	-					
32	800	0.036670	-					
36	900	0.036467	-					
40	1000	0.037517	-					
44	1100	0.046321	-					
48	1200	0.045542	-					

Figure 6.3 Permeate flux for single protein (BSA) EUF at -9 V [Run 170203].

Table 6.6 Data for single protein (BSA) EUF at -6 V [Run 170206].

Run 170206
Exp: 0.1 g/L BSA, 1 mM NaCl, 1 mM Na$_2$HPO$_4$, pH 7.4, -6 V

Power supply current (A), start	0.04
Power supply current (A), end	0.04
Membrane	20 [01-20-17_1]
Operating pressure	15 psi
Crossflow shear rate	440 s^{-1}

ΔP (psi)	$J_v \times 10^6$ (m/s)	Pre-HP $\times 10^{10}$ m/(s·Pa)		ΔP (psi)	$J_v \times 10^6$ (m/s)	Post-HP $\times 10^{10}$ m/(s·Pa)
0.6	3.5			1	4.7	
1.2	7.7			2	8.6	
1.8	11.6	9.0 ± 0.5		3	12.8	5.7 ± 0.2
2.5	15.2			3.7	15.1	

ΔV (V) at M1, start	ΔV (V) at E1, start	ΔV (V) at E2, start	ΔV (V) at M2, start	ΔV (V) at M1, end	ΔV (V) at E1, end	ΔV (V) at E2, end	ΔV (V) at M2, end	Avg. start ΔV (V)
-5.68	-3.13	-1.95	-5.75	-5.70	-3.14	-2.01	-5.77	-2.54

Fraction sample	Sample time (s)	C_p (g/L)	pH			C (g/L)	pH	Λ_0 (μS/cm)
1	0	0.068696	-		Pre-sample	0.000068	-	-
4	100	0.065190	-		Stock solution	0.109988	-	-
8	200	0.057020	-		Retentate(start)	0.112405	-	-
12	300	0.049497	-		Feed, (start)	0.111043	-	-
16	400	0.048850	-		Retentate(end)	-	-	-
20	500	0.046161	-		Feed (end)	-	-	-
24	600	0.042518	-					
28	700	0.036288	-					
32	800	0.040748	-					
36	900	0.058177	-					
40	1000	0.043573	-					
44	1100	0.031795	-					
48	1200	0.041224	-					

Run 170206

[Exp: 0.1 g/L BSA, 1 mM NaCl, 1 mM Na_2HPO_4, pH 7.4, 15 psi, -6 V]

Figure 6.4 Permeate flux for single protein (BSA) EUF at -6 V [Run 170206].

Table 6.7 Data for single protein (BSA) EUF at 0 V [Run 170208].

Run 170208
Exp: 0.1 g/L BSA, 1 mM NaCl, 1 mM Na$_2$HPO$_4$, pH 7.4, 0 V

Power supply current (A), start	-
Power supply current (A), end	-
Membrane	20 [01-20-17_1]
Operating pressure	15 psi
Crossflow shear rate	440 s^{-1}

ΔP (psi)	$J_v \times 10^6$ (m/s)	Pre-HP $\times 10^{10}$ m/(s·Pa)		ΔP (psi)	$J_v \times 10^6$ (m/s)	Post-HP $\times 10^{10}$ m/(s·Pa)
0.6	3.1			0.5	1.9	
1.2	7.0			1.3	5.4	
1.8	10.0	8.1 ± 0.3		2.7	10.8	5.6 ± 0.1
2.4	13.3			3.5	13.7	

ΔV (V) at M1, start	ΔV (V) at E1, start	ΔV (V) at E2, start	ΔV (V) at M2, start	ΔV (V) at M1, end	ΔV (V) at E1, end	ΔV (V) at E2, end	ΔV (V) at M2, end	Avg. start ΔV (V)
-	-	-	-	-	-	-	-	-

Fraction sample	Sample time (s)	C_p (g/L)	pH			C (g/L)	pH	Λ_0 (μS/cm)
1	0	0.069161	-		Pre-sample	0	-	-
4	100	0.064677	-		Stock solution	0.119951	-	-
8	200	0.055123	-		Retentate(start)	0.117578	-	-
12	300	0.048397	-		Feed, (start)	0.117923	-	-
16	400	0.045602	-		Retentate(end)	-	-	-
20	500	0.048884	-		Feed (end)	-	-	-
24	600	0.043133	-					
28	700	0.039461	-					
32	800	0.038908	-					
36	900	0.039136	-					
40	1000	0.038583	-					
44	1100	0.040696	-					
48	1200	0.037349	-					

Figure 6.5 Permeate flux for single protein (BSA) EUF at 0 V [Run 170208].

83

Table 6.8 Data for single protein (BSA) EUF at -9 V [Run 170210].

Run 170210								
Exp: 0.1 g/L BSA, 1 mM NaCl, 1 mM Na$_2$HPO$_4$, pH 7.4, -9 V								

Power supply current (A), start	0.05
Power supply current (A), end	0.05
Membrane	20 [01-20-17_1]
Operating pressure	15 psi
Crossflow shear rate	440 s^{-1}

ΔP (psi)	$J_v \times 10^6$ (m/s)	Pre-HP $\times 10^{10}$ m/(s·Pa)		ΔP (psi)	$J_v \times 10^6$ (m/s)	Post-HP $\times 10^{10}$ m/(s·Pa)
0.5	1.8			1	2.8	
1.5	6.8			2	5.8	
2.5	11.6	6.7 ± 0.2		3	8.7	4.3 ± 0.1
3.5	15.5			4	11.8	

ΔV (V) at M1, start	ΔV (V) at E1, start	ΔV (V) at E2, start	ΔV (V) at M2, start	ΔV (V) at M1, end	ΔV (V) at E1, end	ΔV (V) at E2, end	ΔV (V) at M2, end	Avg. start ΔV (V)
-8.67	-5.38	-2.91	-8.74	-8.67	-5.14	-3.17	-8.72	-4.15

Fraction sample	Sample time (s)	C_p (g/L)	pH			C (g/L)	pH	Λ_0 (µS/cm)
1	0	0.070393	-		Pre-sample	0.000129	-	-
4	100	0.065941	-		Stock solution	0.101340	-	-
8	200	0.064687	-		Retentate(start)	0.113004	-	-
12	300	0.057570	-		Feed, (start)	0.113232	-	-
16	400	0.053368	-		Retentate(end)	-	-	-
20	500	0.048853	-		Feed (end)	-	-	-
24	600	0.043147	-					
28	700	0.046502	-					
32	800	0.047881	-					
36	900	0.041987	-					
40	1000	0.042394	-					
44	1100	0.042018	-					
48	1200	0.044464	-					

Figure 6.6 Permeate flux for single protein (BSA) EUF at -9 V [Run 170210].

Table 6.9 Data for single protein (HEL) EUF at 0 V [Run 170327].

Run 170327								
Exp: 0.1 g/L HEL, 1 mM NaCl, 1 mM Na₂HPO₄, pH 7.4, 0 V								

Power supply current (A), start	-
Power supply current (A), end	-
Membrane	25 [02-25-17_2]
Operating pressure	15 psi
Crossflow shear rate	440 s^{-1}

ΔP (psi)	$J_v \times 10^6$ (m/s)	Pre-HP $\times 10^{10}$ m/(s·Pa)		ΔP (psi)	$J_v \times 10^6$ (m/s)	Post-HP $\times 10^{10}$ m/(s·Pa)
1.0	10.2			1	8.5	
2.0	19.5			2	15.7	
3.0	30.0	14.6 ± 0.3		3	23.0	10.5 ± 0.1
4.0	40.2			4	30.3	

ΔV (V) at M1, start	ΔV (V) at E1, start	ΔV (V) at E2, start	ΔV (V) at M2, start	ΔV (V) at M1, end	ΔV (V) at E1, end	ΔV (V) at E2, end	ΔV (V) at M2, end	Avg. start ΔV (V)
-	-	-	-	-	-	-	-	-

Fraction sample	Sample time (min)	C_p (g/L)	pH			C (g/L)	pH	Λ_0 (μS/cm)
1	0.25	0.105894	-		Pre-sample	0	-	-
4	1	0.109934	-		Stock solution	0.113974	-	-
8	2	0.108435	-		Retentate(start)	0.110924	-	-
12	3	0.101396	-		Feed, (start)	0.110899	-	-
16	4	0.099998	-		Retentate(end)	-	-	-
20	5	0.097152	-		Feed (end)	-	-	-
24	6	0.100608	-					
28	7	0.111331	-					
32	8	0.110391	-					
36	9	0.10818	-					
40	10	0.112297	-					
44	11	0.110035	-					
48	12	0.108994	-					

Figure 6.7 Permeate flux for single protein (HEL) EUF at 0 V [Run 170327].

Table 6.10 Data for single protein (HEL) EUF at 0 V [Run 170328].

Run 170328
Exp: 0.1 g/L HEL, 1 mM NaCl, 1 mM Na$_2$HPO$_4$, pH 7.4, 0 V

Power supply current (A), start	-
Power supply current (A), end	-
Membrane	25 [02-25-17_2]
Operating pressure	15 psi
Crossflow shear rate	440 s^{-1}

ΔP (psi)	$J_v \times 10^6$ (m/s)	Pre-HP $\times 10^{10}$ m/(s·Pa)		ΔP (psi)	$J_v \times 10^6$ (m/s)	Post-HP $\times 10^{10}$ m/(s·Pa)
0.7	10.1			1.1	11.1	
1.3	19.0			1.7	16.6	
1.9	28.3	21.1 ± 0.5		2.7	25.4	13.0 ± 0.1
2.5	36.1			3.5	32.6	

ΔV (V) at M1, start	ΔV (V) at E1, start	ΔV (V) at E2, start	ΔV (V) at M2, start	ΔV (V) at M1, end	ΔV (V) at E1, end	ΔV (V) at E2, end	ΔV (V) at M2, end	Avg. start ΔV (V)
-	-	-	-	-	-	-	-	-

Fraction sample	Sample time (min)	C_p (g/L)	pH			C (g/L)	pH	Λ_0 (μS/cm)
1	0.25	0.098347	-		Pre-sample	0	-	-
4	1	0.101421	-		Stock solution	0.111814	-	-
8	2	0.105233	-		Retentate(start)	0.110521	-	-
12	3	0.105233	-		Feed, (start)	0.110340	-	-
16	4	0.107012	-		Retentate(end)	-	-	-
20	5	0.110264	-		Feed (end)	-	-	-
24	6	0.108892	-					
28	7	0.107901	-					
32	8	0.108079	-					
36	9	0.110569	-					
40	10	0.1094	-					
44	11	0.110544	-					
48	12	0.11029	-					

Figure 6.8 Permeate flux for single protein (HEL) EUF at 0 V [Run 170328].

Table 6.11 Data for single protein (HEL) EUF at -9 V [Run 170329].

Run 170329			
Exp: 0.1 g/L HEL, 1 mM NaCl, 1 mM Na$_2$HPO$_4$, pH 7.4, -9 V			

Power supply current (A), start	0.06	
Power supply current (A), end	0.06	
Membrane	25 [02-25-17_2]	
Operating pressure	15 psi	
Crossflow shear rate	440 s^{-1}	

ΔP (psi)	$J_v \times 10^6$ (m/s)	Pre-HP $\times 10^{10}$ m/(s·Pa)		ΔP (psi)	$J_v \times 10^6$ (m/s)	Post-HP $\times 10^{10}$ m/(s·Pa)
0.9	11.3			1.0	3.8	
1.5	19.4			2.0	4.1	
2.3	29.8	18.8 ± 0.2		3.0	10.9	5.2 ± 0.1
3.0	38.5			4.0	14.4	

ΔV (V) at M1, start	ΔV (V) at E1, start	ΔV (V) at E2, start	ΔV (V) at M2, start	ΔV (V) at M1, end	ΔV (V) at E1, end	ΔV (V) at E2, end	ΔV (V) at M2, end	Avg. start ΔV (V)
-8.68	-4.32	-3.60	-8.67	-8.68	-4.40	-3.91	-8.67	-3.96

Fraction sample	Sample time (min)	C_p (g/L)	pH			C (g/L)	pH	Λ_0 (µS/cm)
1	0.25	0.078645	-		Pre-sample	0.001547	-	-
4	1	0.088000	-		Stock solution	0.102750	-	-
8	2	0.090804	-		Retentate(start)	0.102814	-	-
12	3	0.090191	-		Feed, (start)	0.102774	-	-
16	4	0.090804	-		Retentate(end)	-	-	-
20	5	0.093136	-		Feed (end)	-	-	-
24	6	0.093042	-					
28	7	0.091204	-					
32	8	0.090804	-					
36	9	0.088542	-					
40	10	0.088966	-					
44	11	0.088777	-					
48	12	0.088565	-					

Run 170329

[Exp: 0.1 g/L HEL, 1 mM NaCl, 1 mM Na$_2$HPO$_4$, pH 7.4, 15 psi, -9 V]

Permeate flux J_v x 10^6 (m s^{-1})
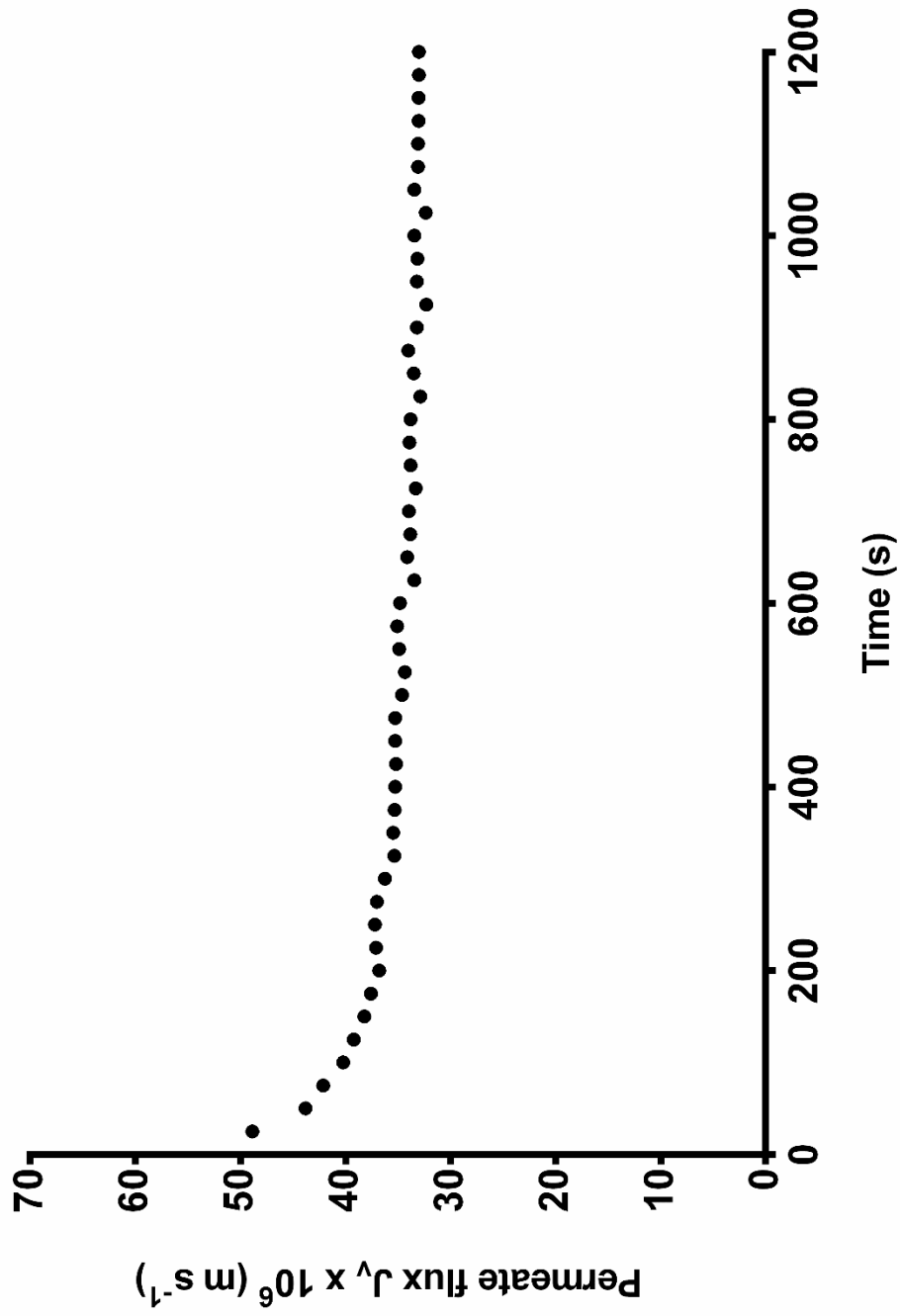
Time (s)
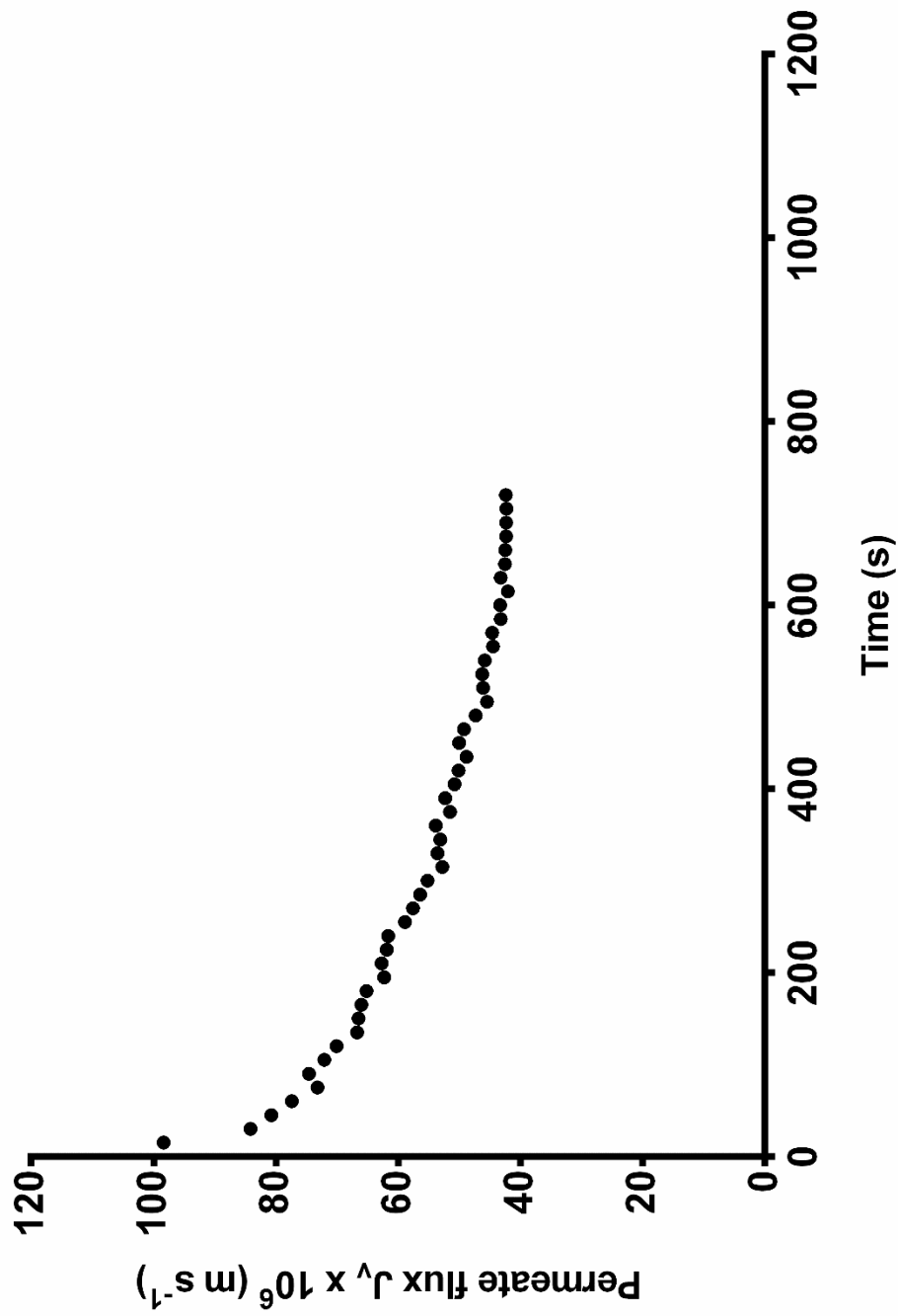
Figure 6.9 Permeate flux for single protein (HEL) EUF at -9 V [Run 170329].

Table 6.12 Data for single protein (αLA) EUF at 0 V [Run 170614].

Run 170614
Exp: 0.1 g/L αLA, 1 mM NaCl, 1 mM Na$_2$HPO$_4$, pH 7.4, 0 V

Power supply current (A), start	-
Power supply current (A), end	-
Membrane	33 [05-20-17_1]
Operating pressure	1 psi
Crossflow shear rate	555 s^{-1}

ΔP (psi)	$J_v \times 10^6$ (m/s)	Pre-HP $\times 10^{10}$ m/(s·Pa)		ΔP (psi)	$J_v \times 10^6$ (m/s)	Post-HP $\times 10^{10}$ m/(s·Pa)
1	6.8			1	5.3	
2	14.2			2	10.6	
3	21.7	10.5 ± 0.2		3	15.5	7.7 ± 0.2
4	28.5			4	21.4	

ΔV (V) at M1, start	ΔV (V) at E1, start	ΔV (V) at E2, start	ΔV (V) at M2, start	ΔV (V) at M1, end	ΔV (V) at E1, end	ΔV (V) at E2, end	ΔV (V) at M2, end	Avg. start ΔV (V)
-	-	-	-	-	-	-	-	-

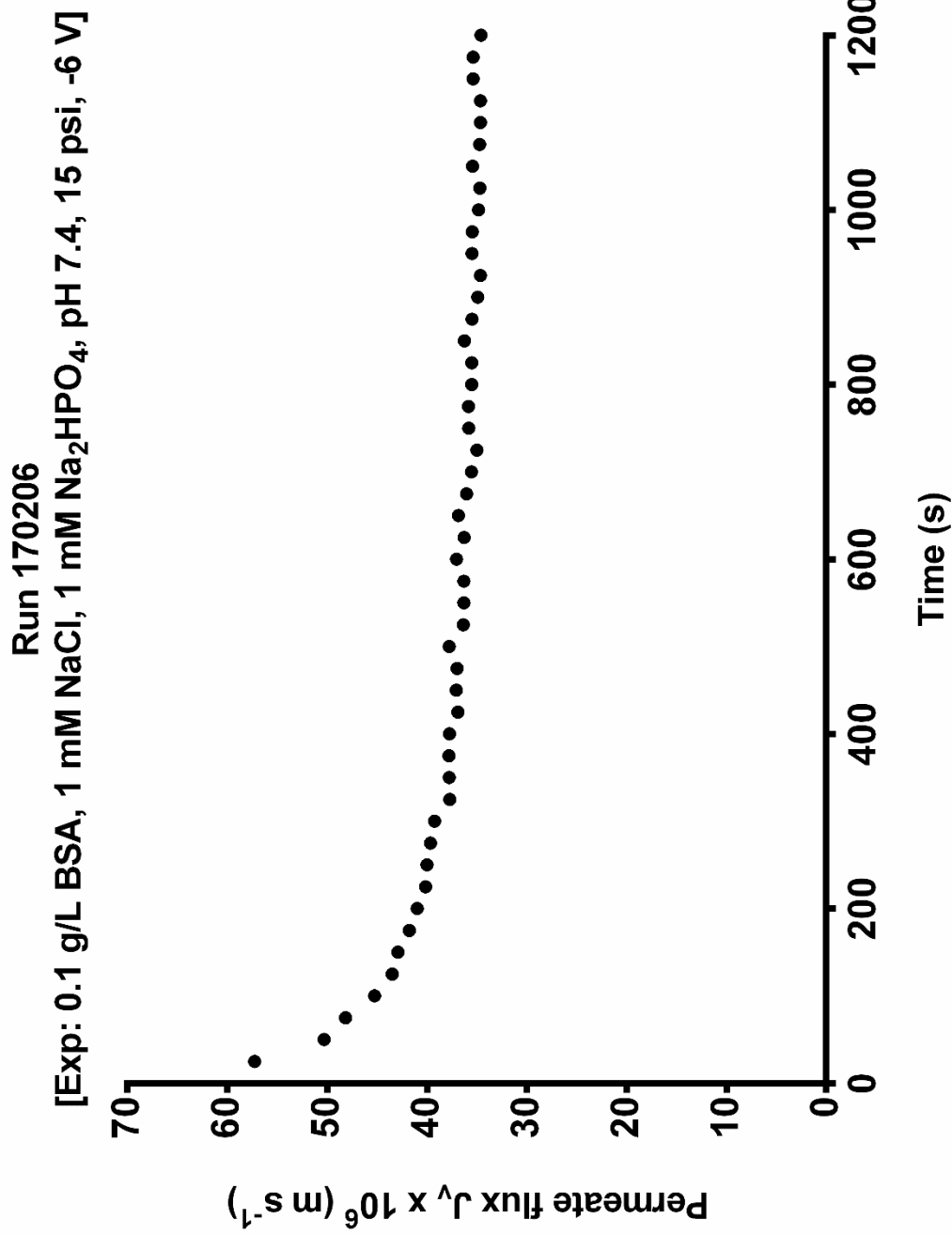| Fraction sample	Sample time (min)	C_p (g/L)	pH			C (g/L)	pH	Λ_0 (μS/cm)
1	5	0	7.061		Pre-sample	0	-	-
4	20	0	7.137		Stock solution	0.117231	-	-
8	40	0	7.147		Retentate(start)	0.114644	7.456	-
12	60	0	7.141		Feed, (start)	0.114100	7.345	-
16	80	0	7.145		Retentate(end)	0.119070	7.301	-
32	160	0	7.174		Feed (end)	0.118797	7.303	-
48	240	0	7.193					
64	320	0	7.181					
80	400	0.000849	7.141					
96	480	0.003879	7.111					
112	560	0.009325	7.059					

Figure 6.10 Permeate flux for single protein (αLA) EUF at 0 V [Run 170614].

Table 6.13 Data for single protein (αLA) EUF at -9 V [Run 170615].

Run 170615
Exp: 0.1 g/L αLA, 1 mM NaCl, 1 mM Na₂HPO₄, pH 7.4, -9 V

Power supply current (A), start	0.10
Power supply current (A), end	0.10
Membrane	33 [05-20-17_1]
Operating pressure	1 psi
Crossflow shear rate	555 s^{-1}

ΔP (psi)	$J_v \times 10^6$ (m/s)	Pre-HP $\times 10^{10}$ m/(s·Pa)		ΔP (psi)	$J_v \times 10^6$ (m/s)	Post-HP $\times 10^{10}$ m/(s·Pa)
1	7.2			1	6.0	
2	14.8			2	11.4	
3	22.3	11.0 ± 0.1		3	17.2	7.8 ± 0.2
4	29.9			4	22.0	

ΔV (V) at M1, start	ΔV (V) at E1, start	ΔV (V) at E2, start	ΔV (V) at M2, start	ΔV (V) at M1, end	ΔV (V) at E1, end	ΔV (V) at E2, end	ΔV (V) at M2, end	Avg. start ΔV (V)
-8.35	-6.06	-5.53	-8.33	-8.48	-6.42	-5.65	-8.48	-5.80

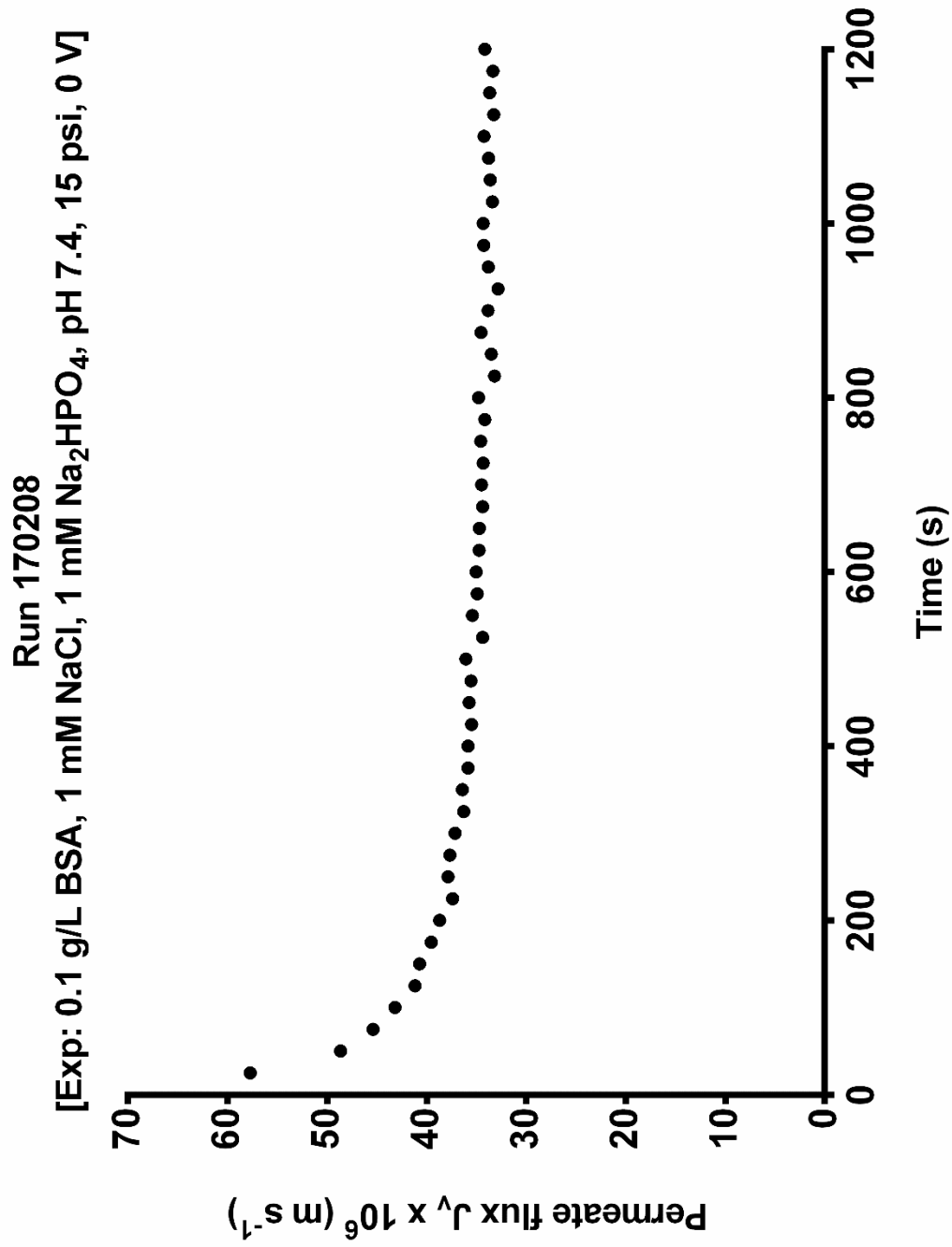| Fraction sample	Sample time (min)	C_p (g/L)	pH			C (g/L)	pH	Λ_0 (µS/cm)
1	5	0	8.8106		Pre-sample	0	-	-
4	20	0.008615	8.110		Stock solution	0.101636	-	-
8	40	0.013573	7.942		Retentate(start)	0.101739	7.435	-
12	60	0.011955	7.858		Feed, (start)	0.084044	7.311	-
16	80	0.009786	7.750		Retentate(end)	0.199132	6.751	-
32	160	0.010027	7.504		Feed (end)	0.103151	7.292	-
48	240	0.006963	7.317					
64	320	0.006997	7.122					
80	400	0.009476	6.985					
96	480	0.012368	6.914					
112	560	0.015501	6.880					

Figure 6.11 Permeate flux for single protein (αLA) EUF at -9 V [Run 170615].

Table 6.14 Data for single protein (αLA) EUF at 0 V [Run 170801].

Run 170801								
Exp: 0.1 g/L αLA, 1 mM NaCl, 1 mM Na$_2$HPO$_4$, pH 7.4, 0 V								

Power supply current (A), start	-
Power supply current (A), end	-
Membrane	33 [05-20-17_1]
Operating pressure	1 psi
Crossflow shear rate	555 s^{-1}

ΔP (psi)	$J_v \times 10^6$ (m/s)	Pre-HP $\times 10^{10}$ m/(s·Pa)		ΔP (psi)	$J_v \times 10^6$ (m/s)	Post-HP $\times 10^{10}$ m/(s·Pa)
0.9	10.5			1.1	9.4	
1.5	16.4			1.7	13.5	
2.1	22.6	14.2 ± 0.3		2.5	19.2	10.8 ± 0.3
2.7	28.0			3.3	25.7	

ΔV (V) at M1, start	ΔV (V) at E1, start	ΔV (V) at E2, start	ΔV (V) at M2, start	ΔV (V) at M1, end	ΔV (V) at E1, end	ΔV (V) at E2, end	ΔV (V) at M2, end	Avg. start ΔV (V)
-	-	-	-	-	-	-	-	-

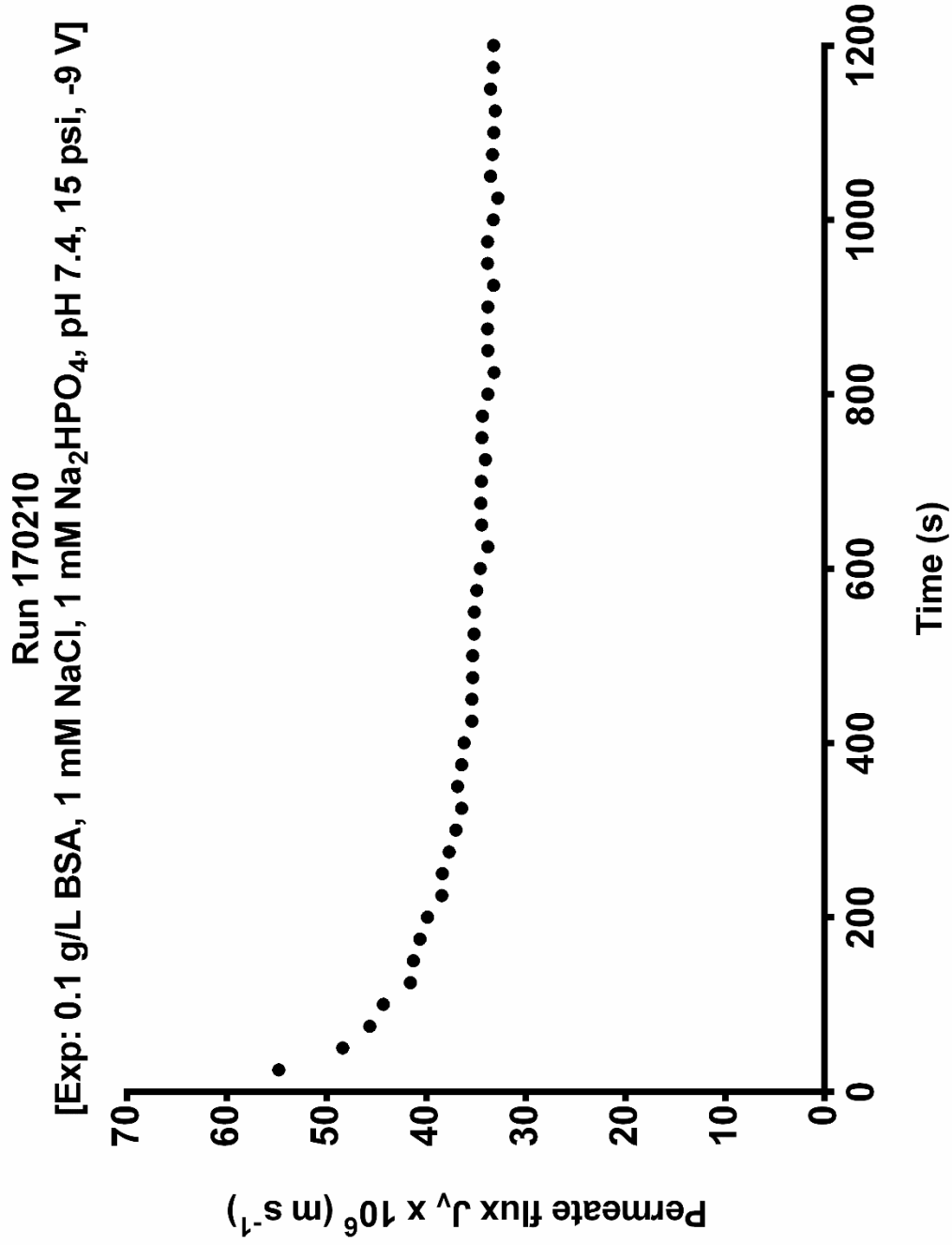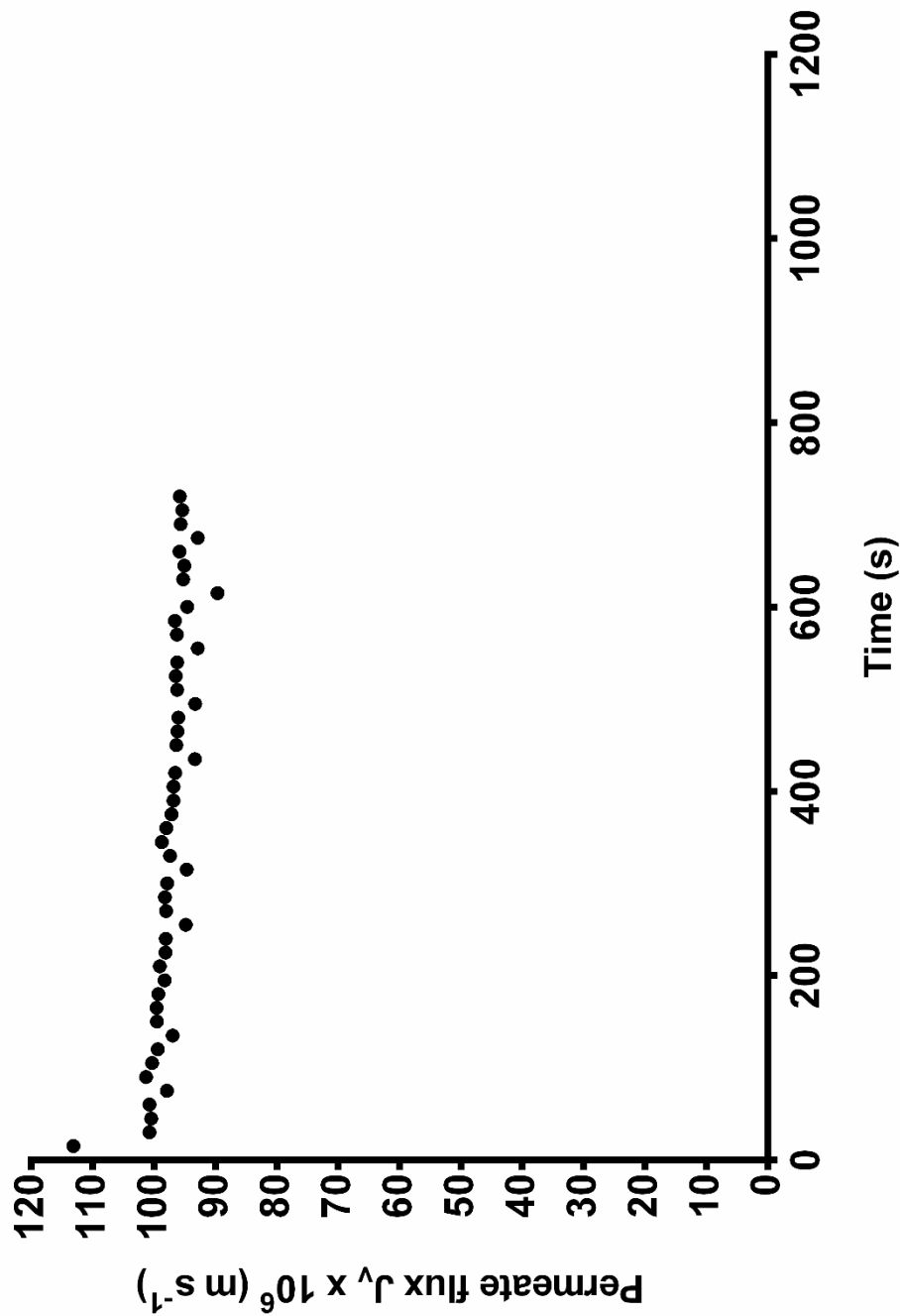| Fraction sample	Sample time (min)	C_p (g/L)	pH			C (g/L)	pH	Λ_0 (μS/cm)
1	5	0	7.044		Pre-sample	0	-	-
4	20	0	7.143		Stock solution	0.100305	-	-
8	40	0.002535	7.145		Retentate(start)	0.099811	7.519	77.7
12	60	0.003203	7.137		Feed, (start)	0.098794	7.334	118.7
16	80	0.002913	7.122		Retentate(end)	0.101758	7.328	-
32	160	0.006197	7.158		Feed (end)	0.108065	7.309	-
48	240	0.006633	7.187					
64	320	0.012591	7.189					
80	400	0.023519	7.212					
96	480	0.032325	7.246					
112	560	0.032354	7.248					

Figure 6.12 Permeate flux for single protein (αLA) EUF at 0 V [Run 170801].

Table 6.15 Data for single protein (αLA) EUF at -9 V [Run 170803].

Run 170803		
Exp: 0.1 g/L αLA, 1 mM NaCl, 1 mM Na$_2$HPO$_4$, pH 7.4, -9 V		

Power supply current (A), start	0.06	
Power supply current (A), end	0.06	
Membrane	33 [05-20-17_1]	
Operating pressure	1 psi	
Crossflow shear rate	555 s^{-1}	

ΔP (psi)	$J_v \times 10^6$ (m/s)	Pre-HP $\times 10^{10}$ m/(s·Pa)		ΔP (psi)	$J_v \times 10^6$ (m/s)	Post-HP $\times 10^{10}$ m/(s·Pa)
0.9	10.4			1	5.3	
1.5	16.2			2	10.9	
2.3	23.3	12.2 ± 0.7		3	15.2	7.5 ± 0.3
2.9	27.1			4	21.0	

ΔV (V) at M1, start	ΔV (V) at E1, start	ΔV (V) at E2, start	ΔV (V) at M2, start	ΔV (V) at M1, end	ΔV (V) at E1, end	ΔV (V) at E2, end	ΔV (V) at M2, end	Avg. start ΔV (V)
-8.62	-5.61	-6.54	-8.62	-8.48	-8.66	-6.05	-6.83	-6.08

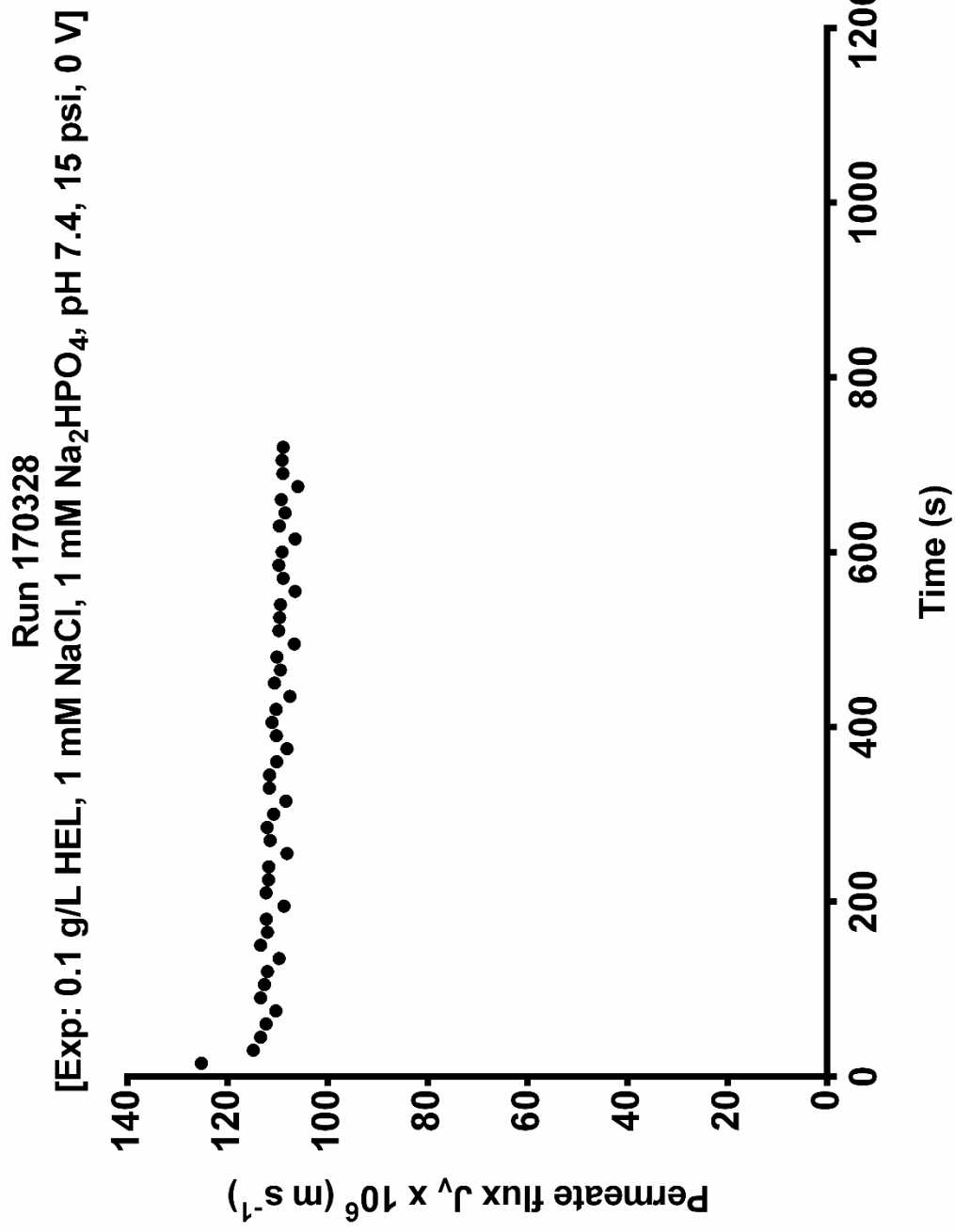| Fraction sample	Sample time (min)	C_p (g/L)	pH			C (g/L)	pH	Λ_0 (μS/cm)
1	5	0.022430	10.525		Pre-sample	0.000208	-	-
4	20	0.022847	10.338		Stock solution	0.091344	-	-
8	40	0.022783	10.067		Retentate(start)	0.091858	7.460	91.4
12	60	0.019154	10.096		Feed, (start)	0.096642	7.368	77.3
16	80	0.016714	9.972		Retentate(end)	0.151716	6.161	-
32	160	0.015397	7.910		Feed (end)	0.094908	7.259	-
48	240	0.016457	7.471					
64	320	0.021145	7.122					
80	400	0.026733	6.974					
96	480	0.030233	6.866					
112	560	0.033894	6.763					

Figure 6.13 Permeate flux for single protein (αLA) EUF at -9 V [Run 170803].

Table 6.16 Data for single protein (HEL) EUF at 0 V [Run 170710].

	Run 170710							
	Exp: 0.1 g/L HEL, 1 mM NaCl, 1 mM Na$_2$HPO$_4$, pH 7.4, 0 V							

Power supply current (A), start	-
Power supply current (A), end	-
Membrane	34 [05-20-17_2]
Operating pressure	1 psi
Crossflow shear rate	555 s^{-1}

ΔP (psi)	$J_v \times 10^6$ (m/s)	Pre-HP $\times 10^{10}$ m/(s·Pa)		ΔP (psi)	$J_v \times 10^6$ (m/s)	Post-HP $\times 10^{10}$ m/(s·Pa)
1	8.0			1.5	2.5	
2	16.4			2.5	4.2	
3	24.2	11.7 ± 0.1		3.5	5.4	2.1 ± 0.1
3.5	28.2			5	7.7	

ΔV (V) at M1, start	ΔV (V) at E1, start	ΔV (V) at E2, start	ΔV (V) at M2, start	ΔV (V) at M1, end	ΔV (V) at E1, end	ΔV (V) at E2, end	ΔV (V) at M2, end	Avg. start ΔV (V)
-	-	-	-	-	-	-	-	-

| Fraction sample	Sample time (min)	C_p (g/L)	pH			C (g/L)	pH	Λ_0 (µS/cm)
1	5	0	7.048		Pre-sample	0	-	-
4	20	0	7.252		Stock solution	0.126947	-	-
8	40	0.001965	7.242		Retentate(start)	0.122113	7.414	-
12	60	0.024935	7.227		Feed, (start)	0.127039	7.362	-
16	80	0.042148	7.240		Retentate(end)	0.123283	7.263	-
32	160	0.059268	7.231		Feed (end)	0.126978	7.359	-
48	240	0.062008	7.210					
64	320	0.062593	7.219					
80	400	0.064533	7.231					
96	480	0.070876	7.229					
112	560	0.066134	7.225					

Figure 6.14 Permeate flux for single protein (HEL) EUF at 0 V [Run 170710].

Table 6.17 Data for single protein (HEL) EUF at -9 V [Run 170711].

Run 170711								
Exp: 0.1 g/L HEL, 1 mM NaCl, 1 mM Na$_2$HPO$_4$, pH 7.4, -9 V								

Power supply current (A), start	0.10	
Power supply current (A), end	0.09	
Membrane	34 [05-20-17_2]	
Operating pressure	1 psi	
Crossflow shear rate	555 s^{-1}	

ΔP (psi)	$J_v \times 10^6$ (m/s)	Pre-HP $\times 10^{10}$ m/(s·Pa)		ΔP (psi)	$J_v \times 10^6$ (m/s)	Post-HP $\times 10^{10}$ m/(s·Pa)
1	7.9			1.5	3.5	
2	15.0			2.5	5.7	
3	22.6	10.5 ± 0.2		3.5	7.6	2.7 ± 0.1
3.5	25.8			5	10.1	

ΔV (V) at M1, start	ΔV (V) at E1, start	ΔV (V) at E2, start	ΔV (V) at M2, start	ΔV(V) at M1, end	ΔV (V) at E1, end	ΔV (V) at E2, end	ΔV (V) at M2, end	Avg. start ΔV (V)
-8.48	-6.11	-6.57	-8.46	-8.42	-6.19	-7.08	-8.41	-6.34

Fraction sample	Sample time (min)	C_p (g/L)	pH			C (g/L)	pH	Λ_0 (μS/cm)
1	5	0.000531	8.883		Pre-sample	0	-	-
4	20	0.007004	8.568		Stock solution	0.131414	-	-
8	40	0.035338	8.446		Retentate(start)	0.130477	7.454	-
12	60	0.115202	8.450		Feed, (start)	0.130477	7.374	-
16	80	0.143707	8.377		Retentate(end)	0.122641	6.569	-
32	160	0.125508	8.076		Feed (end)	0.132294	7.632	-
48	240	0.109695	7.765					
64	320	0.095953	7.576					
80	400	0.089906	7.479					
96	480	0.082638	6.796					
112	560	0.074688	6.447					

Run 170711

[Exp: 0.1 g/L HEL, 1 mM NaCl, 1 mM Na_2HPO_4, pH 7.4, 1 psi, -9 V]
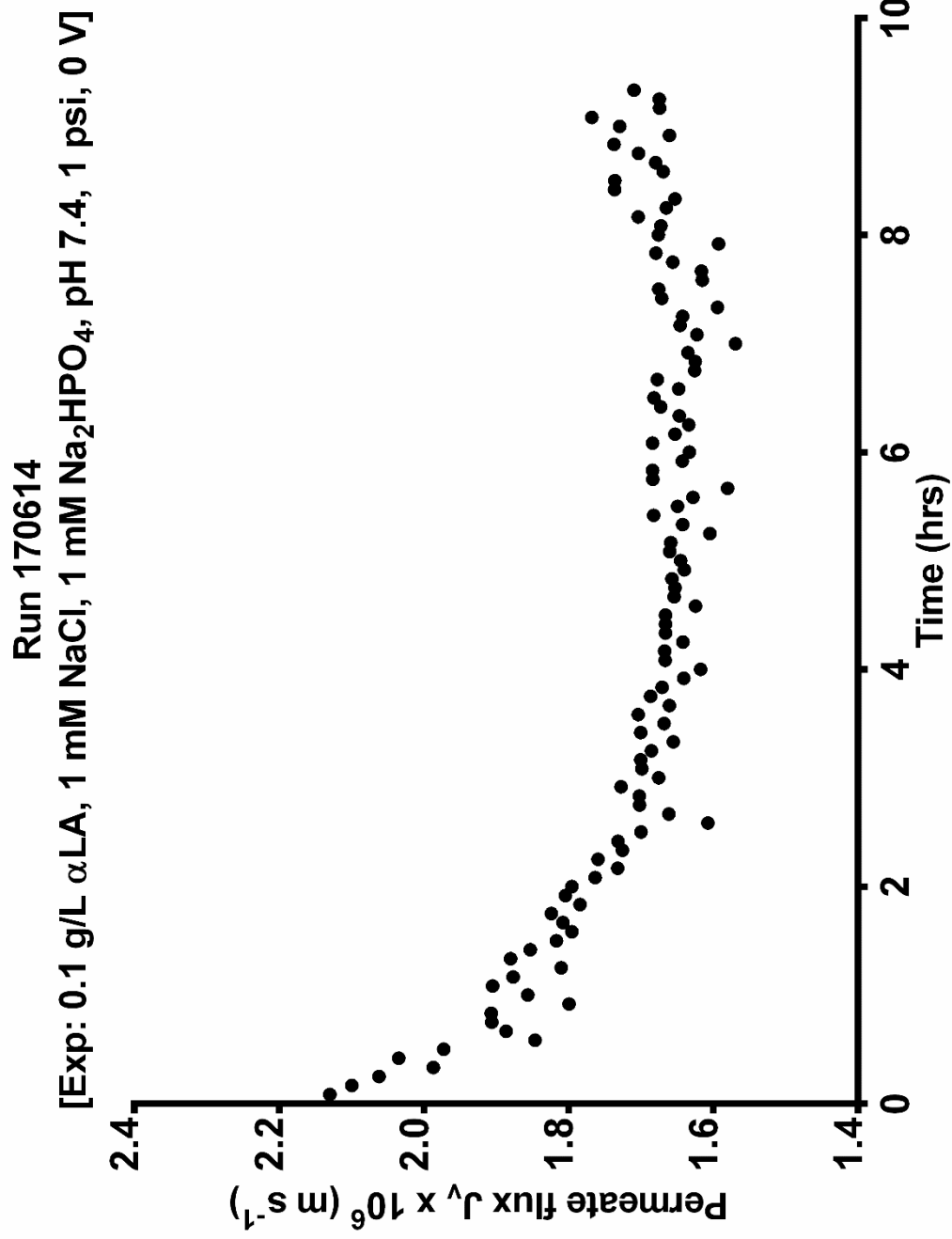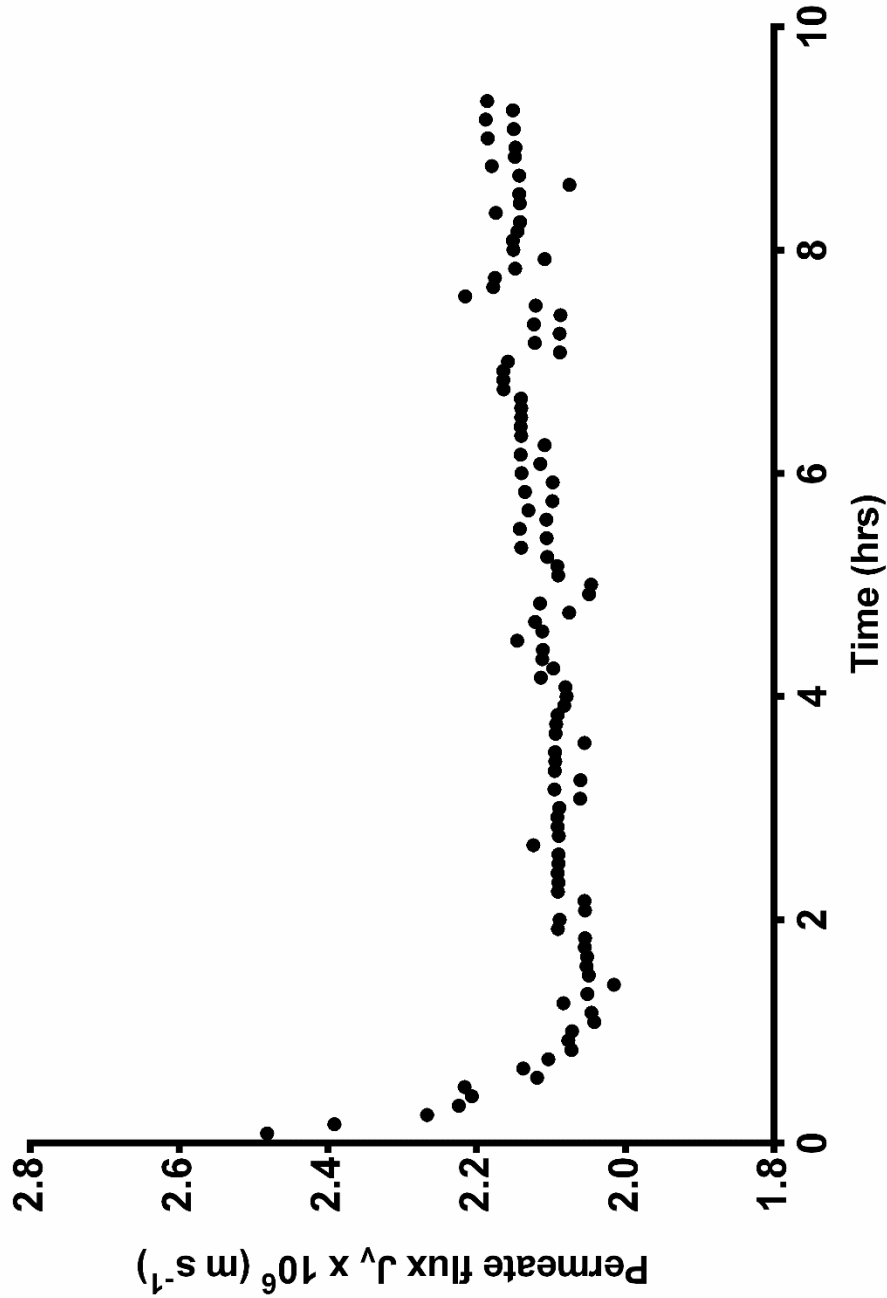
Permeate flux J_v x 10^6 (m s^{-1})

Time (hrs)
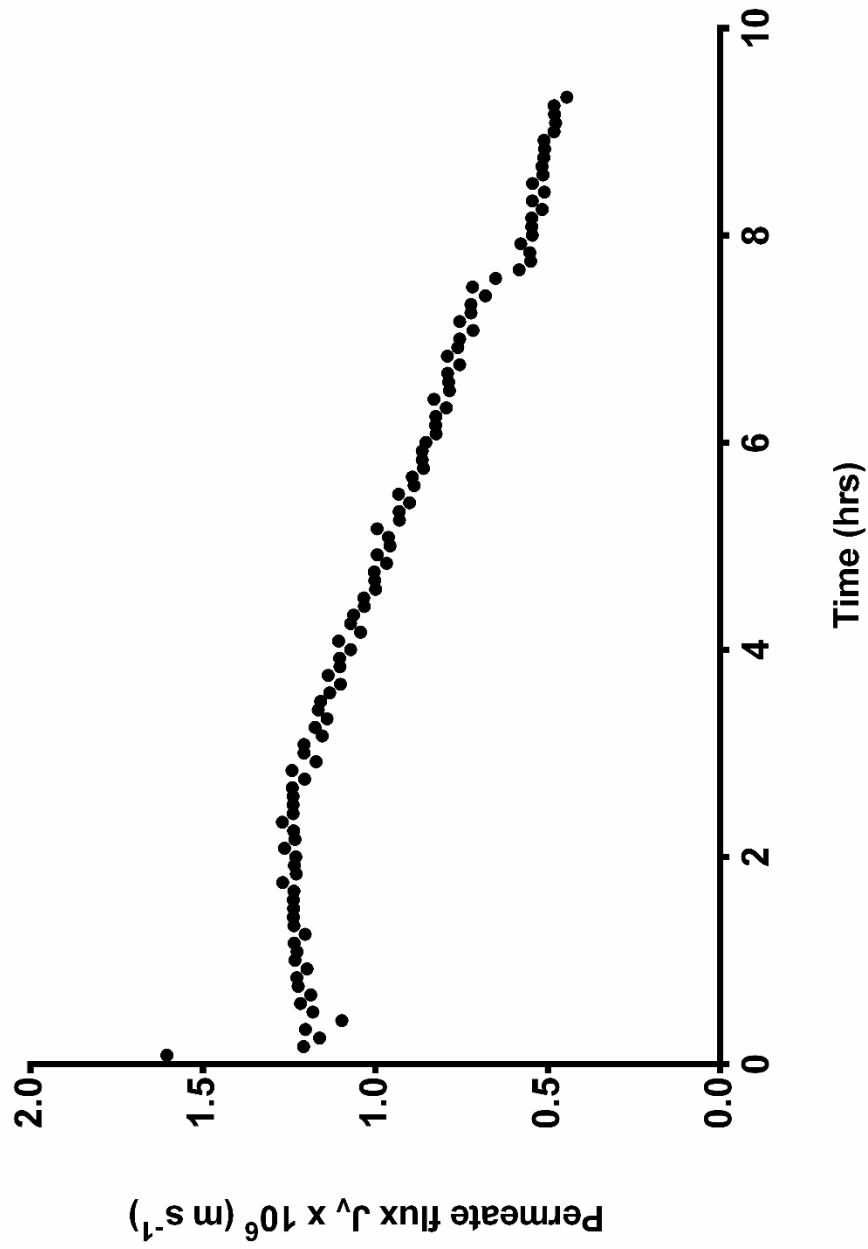
Figure 6.15 Permeate flux for single protein (HEL) EUF at -9 V [Run 170711].

Table 6.18 Data for single protein (HEL) EUF at 0 V [Run 170717].

Run 170717
Exp: 0.1 g/L HEL, 1 mM NaCl, 1 mM Na₂HPO₄, pH 7.4, 0 V

Power supply current (A), start	-
Power supply current (A), end	-
Membrane	34 [05-20-17_2]
Operating pressure	1 psi
Crossflow shear rate	555 s^{-1}

ΔP (psi)	$J_v \times 10^6$ (m/s)	Pre-HP $\times 10^{10}$ m/(s·Pa)		ΔP (psi)	$J_v \times 10^6$ (m/s)	Post-HP $\times 10^{10}$ m/(s·Pa)
1	7.3			1.5	3.7	
2	13.7			2.5	6.0	
3	20.4	9.6 ± 0.1		3.5	8.4	3.2 ± 0.1
3.5	23.9			5	11.5	

ΔV (V) at M1, start	ΔV (V) at E1, start	ΔV (V) at E2, start	ΔV (V) at M2, start	ΔV (V) at M1, end	ΔV (V) at E1, end	ΔV (V) at E2, end	ΔV (V) at M2, end	Avg. start ΔV (V)
-	-	-	-	-	-	-	-	-

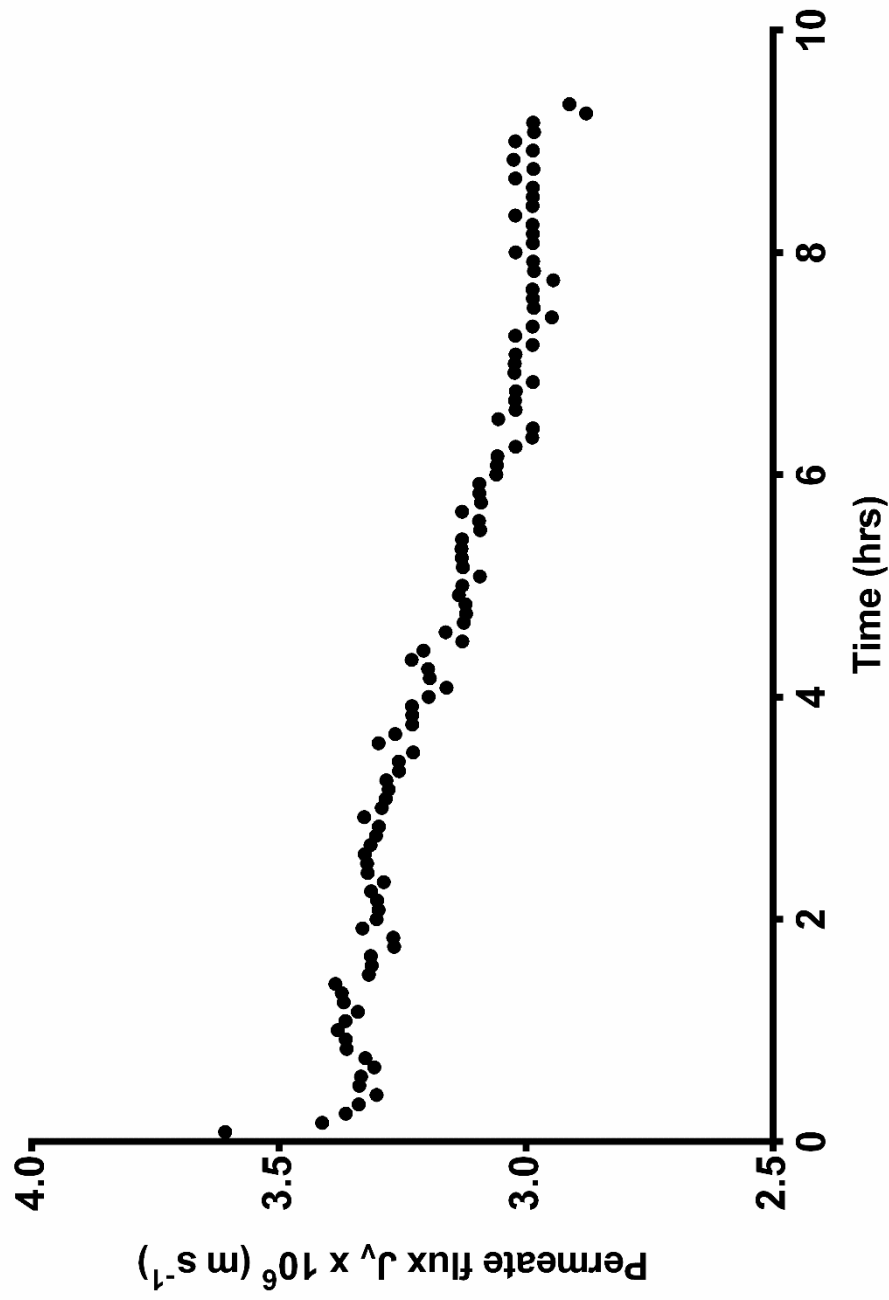| Fraction sample	Sample time (min)	C_p (g/L)	pH			C (g/L)	pH	Λ_0 (µS/cm)
1	5	0.003359	6.990		Pre-sample	0.000008	-	-
4	20	0	7.233		Stock solution	0.133537	-	-
8	40	0.015114	7.254		Retentate(start)	0.130270	7.372	-
12	60	0.047114	7.269		Feed, (start)	0.131275	7.319	-
16	80	0.060517	7.265		Retentate(end)	0.144678	7.248	-
32	160	0.073781	7.261		Feed (end)	0.127561	7.301	-
48	240	0.076238	7.250					
64	320	0.078584	7.231					
80	400	0.081711	7.254					
96	480	0.084085	7.250					
112	560	0.086318	7.271					

Figure 6.16 Permeate flux for single protein (HEL) EUF at 0 V [Run 170717].

Table 6.19 Data for single protein (HEL) EUF at -9 V [Run 170719].

Run 170719								
Exp: 0.1 g/L HEL, 1 mM NaCl, 1 mM Na$_2$HPO$_4$, pH 7.4, -9 V								

Power supply current (A), start	0.07	
Power supply current (A), end	0.06	
Membrane	34 [05-20-17_2]	
Operating pressure	1 psi	
Crossflow shear rate	555 s^{-1}	

ΔP (psi)	$J_v \times 10^6$ (m/s)	Pre-HP $\times 10^{10}$ m/(s·Pa)		ΔP (psi)	$J_v \times 10^6$ (m/s)	Post-HP $\times 10^{10}$ m/(s·Pa)
1	7.8			1.5	2.9	
2	14.2			2.5	4.4	
3	21.0	9.9 ± 0.3		3.5	6.0	2.1 ± 0.1
3.5	25.0			5	7.8	

ΔV (V) at M1, start	ΔV (V) at E1, start	ΔV (V) at E2, start	ΔV (V) at M2, start	ΔV (V) at M1, end	ΔV (V) at E1, end	ΔV (V) at E2, end	ΔV (V) at M2, end	Avg. start ΔV (V)
-8.62	-5.44	-5.67	-8.62	-8.65	-5.81	-6.40	-8.66	-5.56

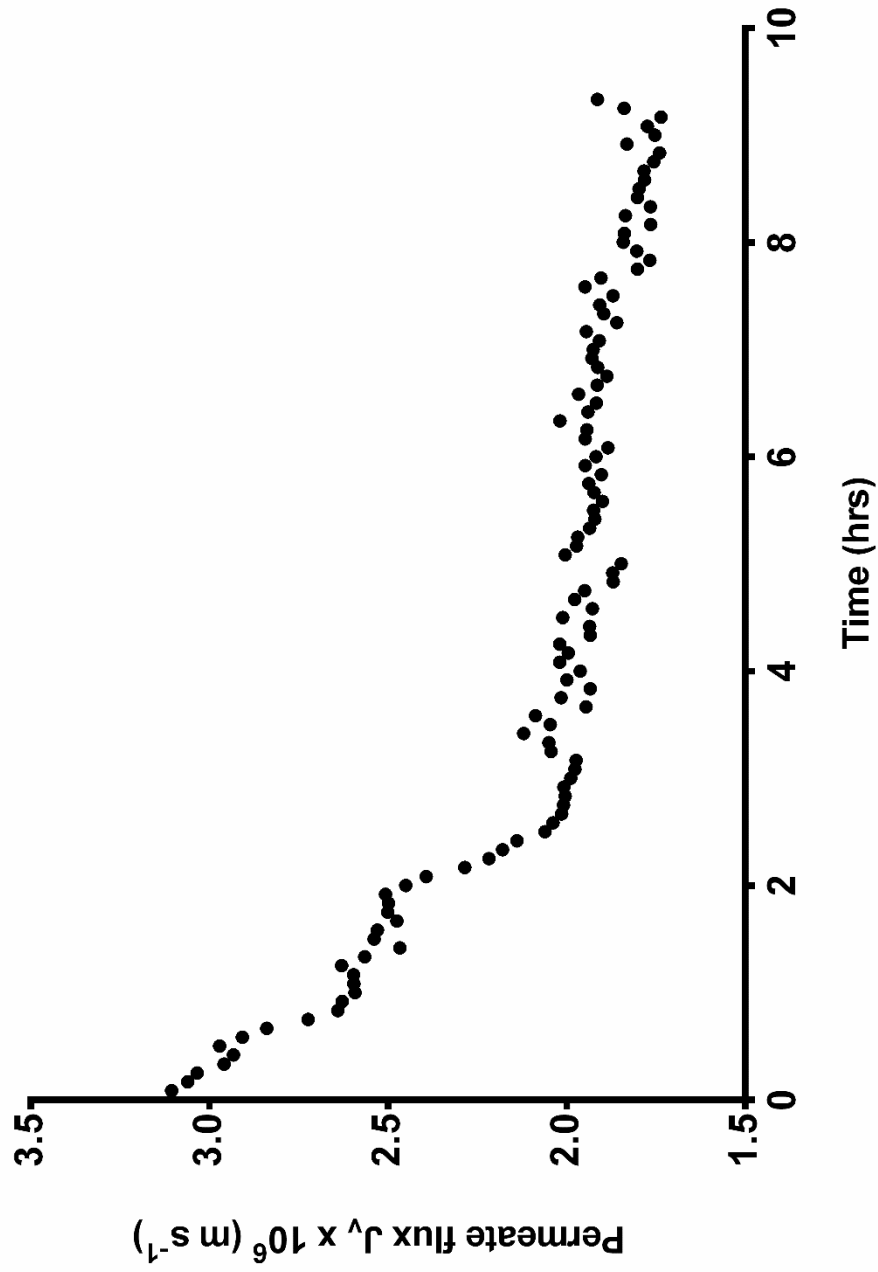| Fraction sample	Sample time (min)	C_p (g/L)	pH			C (g/L)	pH	Λ_0 (µS/cm)
1	5	0.004001	9.968		Pre-sample	0	-	-
4	20	0.011857	9.541		Stock solution	0.132575	-	-
8	40	0.027292	9.073		Retentate(start)	0.129176	7.376	-
12	60	0.074403	9.005		Feed, (start)	0.132268	7.317	-
16	80	0.133606	8.970		Retentate(end)	0.118227	6.355	-
32	160	0.134302	8.213		Feed (end)	0.133411	7.326	-
48	240	0.111680	7.954					
64	320	0.099672	6.658					
80	400	0.092902	6.595					
96	480	0.095410	6.897					
112	560	0.082928	7.205					

Figure 6.17 Permeate flux for single protein (HEL) EUF at -9 V [Run 170719].

Table 6.20 Data for single protein (HEL) EUF at 0 V [Run 170730].

Run 170730
Exp: 0.1 g/L HEL, 1 mM NaCl, 1 mM Na$_2$HPO$_4$, pH 7.4, 0 V

Power supply current (A), start	-	
Power supply current (A), end	-	
Membrane	34 [05-20-17_2]	
Operating pressure	1 psi	
Crossflow shear rate	555 s^{-1}	

ΔP (psi)	$J_v \times 10^6$ (m/s)	Pre-HP $\times 10^{10}$ m/(s·Pa)		ΔP (psi)	$J_v \times 10^6$ (m/s)	Post-HP $\times 10^{10}$ m/(s·Pa)
1.5	6.8			1.5	1.8	
2.5	11.6			2.5	2.7	
3.5	16.2	7.0 ± 0.1		3.5	3.8	1.5 ± 0.1
4.5	21.3			5	5.4	

ΔV (V) at M1, start	ΔV (V) at E1, start	ΔV (V) at E2, start	ΔV (V) at M2, start	ΔV (V) at M1, end	ΔV (V) at E1, end	ΔV (V) at E2, end	ΔV (V) at M2, end	Avg. start ΔV (V)
-	-	-	-	-	-	-	-	-

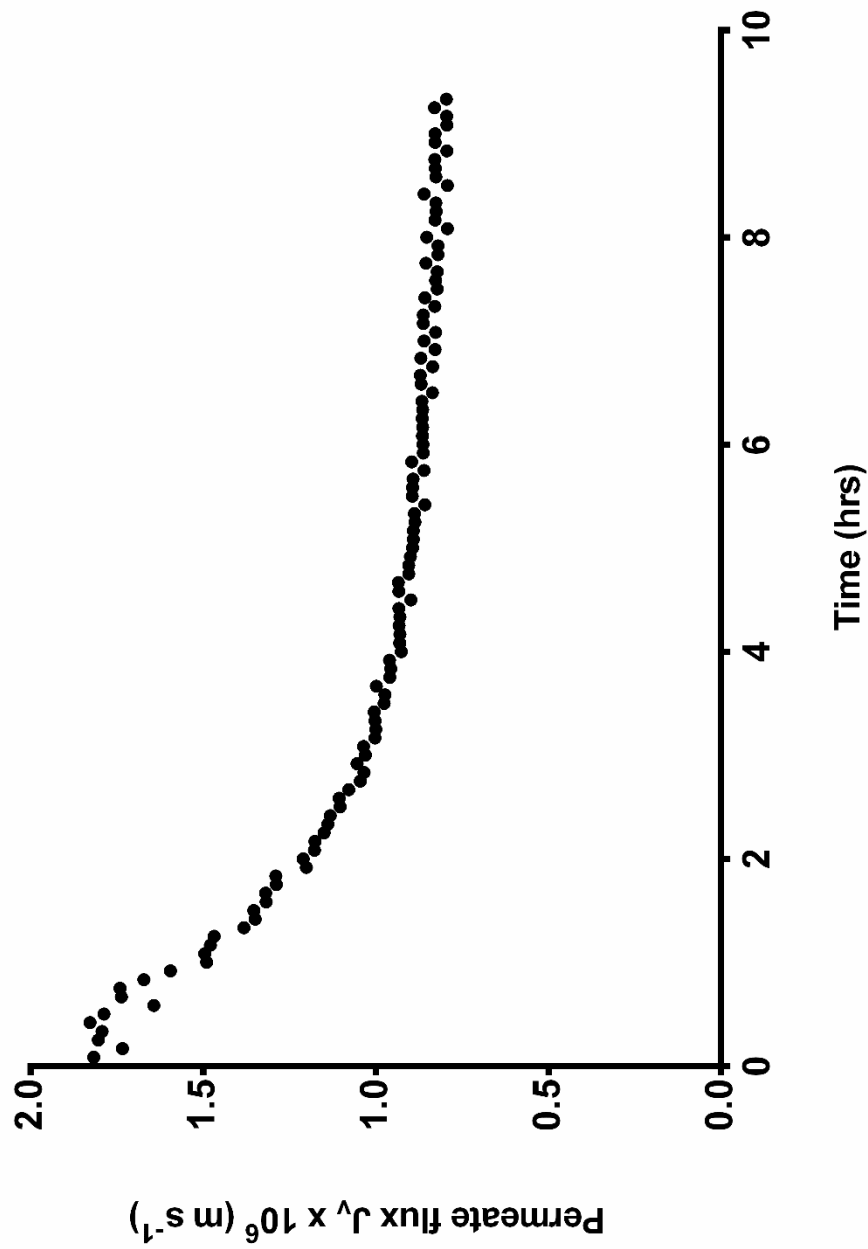| Fraction sample	Sample time (min)	C_p (g/L)	pH			C (g/L)	pH	Λ_0 (µS/cm)
1	5	0.000583	6.827		Pre-sample	0.002253	-	-
4	20	0	7.219		Stock solution	0.135439	-	-
8	40	0.001149	7.204		Retentate(start)	0.132382	7.439	-
12	60	0.005055	7.189		Feed, (start)	0.135298	7.408	-
16	80	0.013066	7.204		Retentate(end)	0.105773	7.256	-
32	160	0.033391	7.198		Feed (end)	0.137987	7.412	-
48	240	0.039052	7.235					
64	320	0.042563	7.256					
80	400	0.042166	-					
96	480	0.044572	-					
112	560	0.040892	-					

Figure 6.18 Permeate flux for single protein (HEL) EUF at 0 V [Run 170730].

Table 6.21 Data for single protein (HEL) EUF at -9 V [Run 170731].

Run 170731
Exp: 0.1 g/L HEL, 1 mM NaCl, 1 mM Na$_2$HPO$_4$, pH 7.4, -9 V

Power supply current (A), start	0.07
Power supply current (A), end	0.07
Membrane	34 [05-20-17_2]
Operating pressure	1 psi
Crossflow shear rate	555 s^{-1}

ΔP (psi)	$J_v \times 10^6$ (m/s)	Pre-HP $\times 10^{10}$ m/(s·Pa)		ΔP (psi)	$J_v \times 10^6$ (m/s)	Post-HP $\times 10^{10}$ m/(s·Pa)
1	5.3			1	1.0	
2	10.3			2	1.9	
3	15.5	7.1 ± 0.1		3	2.7	1.1 ± 0.1
4	20.0			4	3.3	

ΔV (V) at M1, start	ΔV (V) at E1, start	ΔV (V) at E2, start	ΔV (V) at M2, start	ΔV (V) at M1, end	ΔV (V) at E1, end	ΔV (V) at E2, end	ΔV (V) at M2, end	Avg. start ΔV (V)
-8.52	-5.62	-5.47	-8.53	-8.49	-5.80	-5.98	-8.50	-5.55

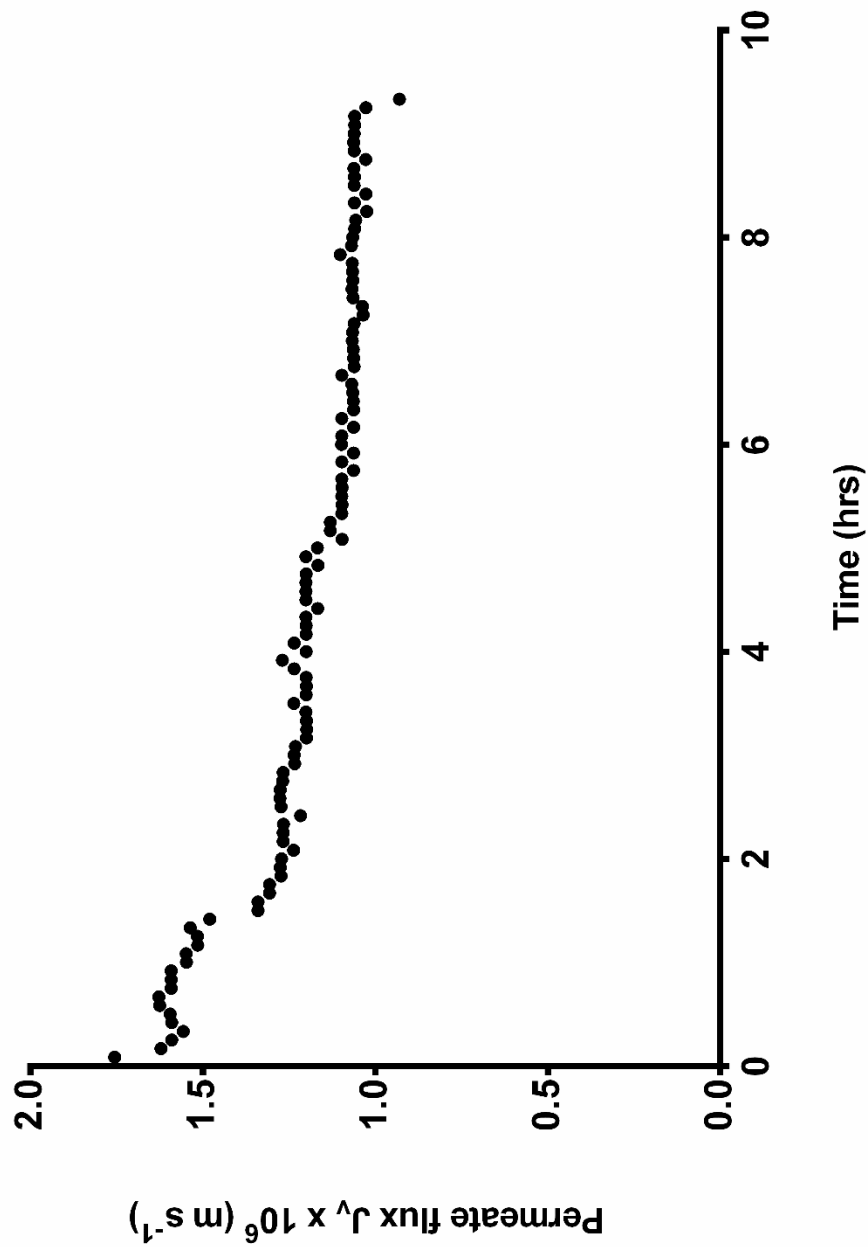| Fraction sample	Sample time (min)	C_p (g/L)	pH			C (g/L)	pH	Λ_0 (μS/cm)
1	5	0.009651	8.095	Pre-sample		0.003107	-	-
4	20	0.016132	7.921	Stock solution		0.151320	-	-
8	40	0.019327	7.862	Retentate(start)		0.150390	7.446	-
12	60	0.046153	8.160	Feed, (start)		0.145769	7.334	-
16	80	0.086285	8.104	Retentate(end)		0.102505	6.569	-
32	160	0.118570	8.450	Feed (end)		0.149459	7.349	-
48	240	0.130200	7.643					
64	320	0.119469	7.166					
80	400	0.092767	-					
96	480	0.072546	-					
112	560	0.075957	-					

Figure 6.19 Permeate flux for single protein (HEL) EUF at -9 V [Run 170731].

Table 6.22 Data for binary protein (BSA-HEL) EUF at 0 V [Run 170310].

| **Run 170310** |
| **Exp: 0.1 g/L BSA, 0.1 g/L HEL, 1 mM NaCl, 1 mM Na$_2$HPO$_4$, pH 7.4, 0 V** |

Power supply current (A), start	-
Power supply current (A), end	-
Membrane	26 [02-25-17_3]
Operating pressure	15 psi
Crossflow shear rate	440 s^{-1}

ΔP (psi)	$J_v \times 10^6$ (m/s)	Pre-HP $\times 10^{10}$ m/(s·Pa)		ΔP (psi)	$J_v \times 10^6$ (m/s)	Post-HP $\times 10^{10}$ m/(s·Pa)
0.7	8.6			2.5	3.8	
1.3	16.1			5.0	6.2	
1.9	24.8	18 ± 1		7.5	8.6	1.1 ± 0.2
2.5	30.4			10.0	9.1	

ΔV (V) at M1, start	ΔV (V) at E1, start	ΔV (V) at E2, start	ΔV (V) at M2, start	ΔV (V) at M1, end	ΔV (V) at E1, end	ΔV (V) at E2, end	ΔV (V) at M2, end	Avg. start ΔV (V)
-	-	-	-	-	-	-	-	-

Fraction sample	Sample time (s)	$C_{p,HEL}$ (g/L)	$C_{p,\,BSA}$ (g/L)	pH		C_{Total} (g/L)	pH	Λ_0 (μS/cm)
1	25	-	-	-	Pre-sample	0.000629	-	-
4	100	-	-	-	Stock	0.223277	-	-
8	200	-	-	-	Retent. (start)	0.220850	-	-
12	300	-	-	-	Feed (start)	0.220850	-	-
16	400	-	-	-	Retent. (end)	-	-	-
20	500	-	-	-	Feed (end)	-	-	-
24	600	-	-	-				
28	700	-	-	-				
32	800	-	-	-				
36	900	-	-	-				
40	1000	-	-	-				
44	1100	-	-	-				
48	1200	0.021018	0.005505	-				

Figure 6.20 Permeate flux for binary protein (BSA-HEL) EUF at 0 V [Run 170310].

Table 6.23 Data for binary protein (BSA-HEL) EUF at -9 V [Run 170321].

Run 170321				
Exp: 0.1 g/L BSA, 0.1 g/L HEL, 1 mM NaCl, 1 mM Na$_2$HPO$_4$, pH 7.4, -9 V				

Power supply current (A), start	0.05	
Power supply current (A), end	0.05	
Membrane	26 [02-25-17_3]	
Operating pressure	15 psi	
Crossflow shear rate	440 s^{-1}	

ΔP (psi)	$J_v \times 10^6$ (m/s)	Pre-HP $\times 10^{10}$ m/(s·Pa)		ΔP (psi)	$J_v \times 10^6$ (m/s)	Post-HP $\times 10^{10}$ m/(s·Pa)
1.1	9.6			1.5	1.2	
1.7	14.5			2.5	1.9	
2.3	20.7	12.9 ± 0.5		3.5	3.6	0.9 ± 0.4
2.9	25.3			5.0	3.3	

ΔV (V) at M1, start	ΔV (V) at E1, start	ΔV (V) at E2, start	ΔV (V) at M2, start	ΔV (V) at M1, end	ΔV (V) at E1, end	ΔV (V) at E2, end	ΔV (V) at M2, end	Avg. start ΔV (V)
-8.70	-3.77	-4.15	-8.71	-8.71	-3.89	-4.07	-8.70	-3.96

Fraction sample	Sample time (s)	$C_{p,HEL}$ (g/L)	$C_{p,BSA}$ (g/L)	pH		C_{Total} (g/L)	pH	Λ_0 (μS/cm)
1	25	-	-	-	Pre-sample	0.002488	-	-
4	100	-	-	-	Stock	0.219495	-	-
8	200	-	-	-	Retent. (start)	0.197530	-	-
12	300	-	-	-	Feed (start)	0.197421	-	-
16	400	-	-	-	Retent. (end)	-	-	-
20	500	-	-	-	Feed (end)	-	-	-
24	600	-	-	-				
28	700	-	-	-				
32	800	-	-	-				
36	900	-	-	-				
40	1000	-	-	-				
44	1100	-	-	-				
48	1200	0	0	-				

Figure 6.21 Permeate flux for binary protein (BSA-HEL) EUF at -9 V [Run 170321].

115

Table 6.24 Data for binary protein (BSA-HEL) EUF at -9 V [Run 170322].

Run 170322
Exp: 0.1 g/L BSA, 0.1 g/L HEL, 1 mM NaCl, 1 mM Na$_2$HPO$_4$, pH 7.4, -9 V

Power supply current (A), start	0.04
Power supply current (A), end	0.04
Membrane	26 [02-25-17_3]
Operating pressure	15 psi
Crossflow shear rate	440 s^{-1}

ΔP (psi)	$J_v \times 10^6$ (m/s)	Pre-HP $\times 10^{10}$ m/(s·Pa)		ΔP (psi)	$J_v \times 10^6$ (m/s)	Post-HP $\times 10^{10}$ m/(s·Pa)
1.5	2.9			1.5	0.6	
2.5	5.1			2.5	1.1	
3.5	7.8	2.8 ± 0.4		3.5	1.6	0.4 ± 0.2
5.0	9.5			5.0	1.5	

ΔV (V) at M1, start	ΔV (V) at E1, start	ΔV (V) at E2, start	ΔV (V) at M2, start	ΔV (V) at M1, end	ΔV (V) at E1, end	ΔV (V) at E2, end	ΔV (V) at M2, end	Avg. start ΔV (V)
-8.75	-8.00	-4.36	-8.73	-8.72	-7.99	-4.43	-8.71	-6.18

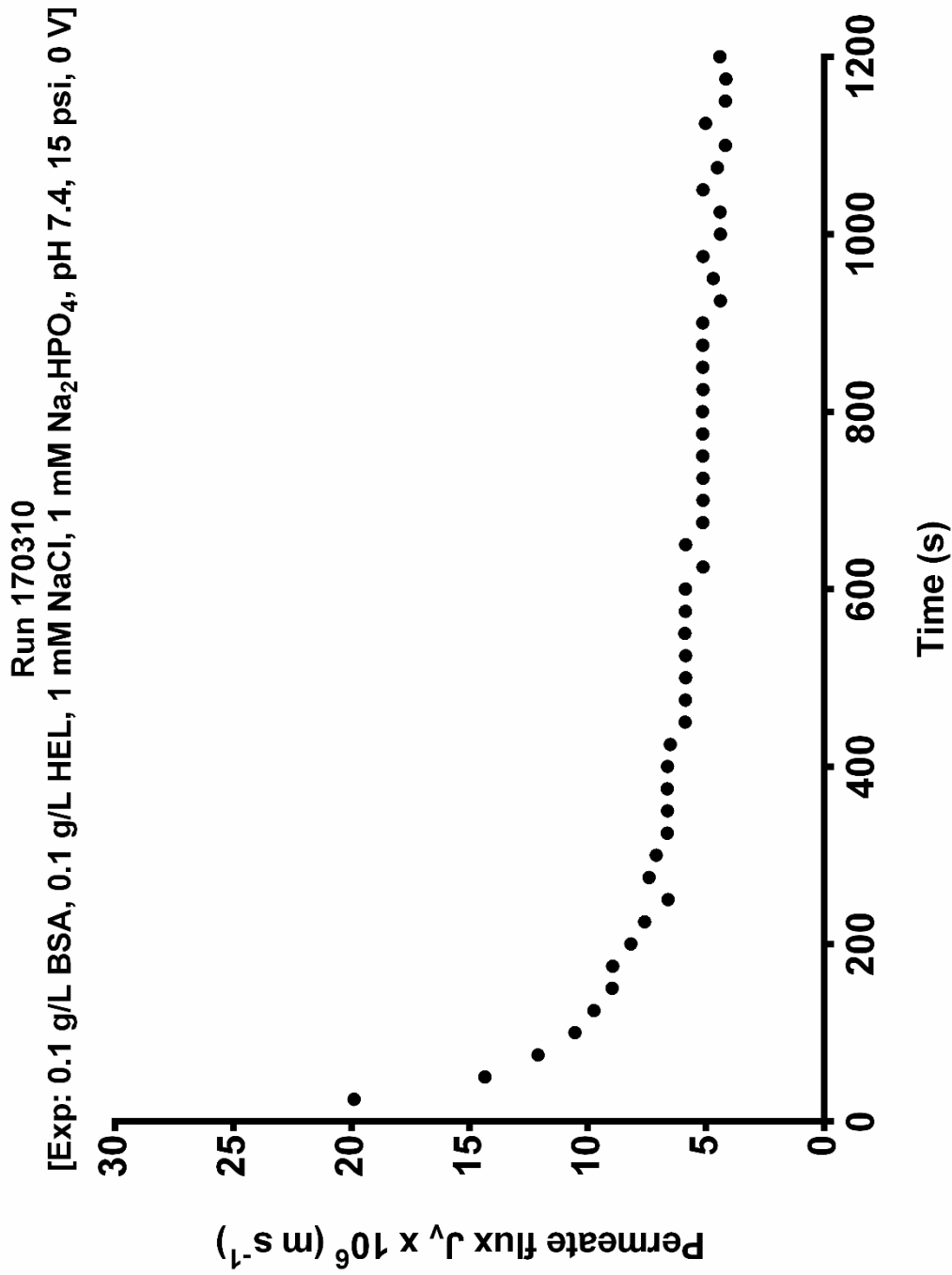| Fraction sample	Sample time (s)	$C_{p,HEL}$ (g/L)	$C_{p,BSA}$ (g/L)	pH		C_{Total} (g/L)	pH	Λ_0 (µS/cm)
1	25	-	-	-	Pre-sample	0.001046	-	-
4	100	-	-	-	Stock	0.212715	-	-
8	200	-	-	-	Retent. (start)	0.223223	-	-
12	300	-	-	-	Feed (start)	0.223053	-	-
16	400	-	-	-	Retent. (end)	-	-	-
20	500	-	-	-	Feed (end)	-	-	-
24	600	-	-	-				
28	700	-	-	-				
32	800	-	-	-				
36	900	-	-	-				
40	1000	-	-	-				
44	1100	-	-	-				
48	1200	0	0	-				

Figure 6.22 Permeate flux for binary protein (BSA-HEL) EUF at -9 V [Run 170322].

117

Table 6.25 Data for binary protein (αLA-HEL) EUF at 0 V [Run 170404].

Run 170404
Exp: 0.1 g/L αLA, 0.1 g/L HEL, 1 mM NaCl, 1 mM Na$_2$HPO$_4$, pH 7.4, 0 V

Power supply current (A), start	-	
Power supply current (A), end	-	
Membrane	24 [02-25-17_1]	
Operating pressure	15 psi	
Crossflow shear rate	555 s^{-1}	

ΔP (psi)	$J_v \times 10^6$ (m/s)	Pre-HP $\times 10^{10}$ m/(s·Pa)		ΔP (psi)	$J_v \times 10^6$ (m/s)	Post-HP $\times 10^{10}$ m/(s·Pa)
0.7	7.0			1.0	7.6	
1.3	13.9			2.0	15.4	
1.7	17.1	14.9 ± 0.6		3.0	22.4	10.9 ± 0.2
2.3	23.7			3.5	26.6	

ΔV (V) at M1, start	ΔV (V) at E1, start	ΔV (V) at E2, start	ΔV (V) at M2, start	ΔV (V) at M1, end	ΔV (V) at E1, end	ΔV (V) at E2, end	ΔV (V) at M2, end	Avg. start ΔV (V)
-	-	-	-	-	-	-	-	-

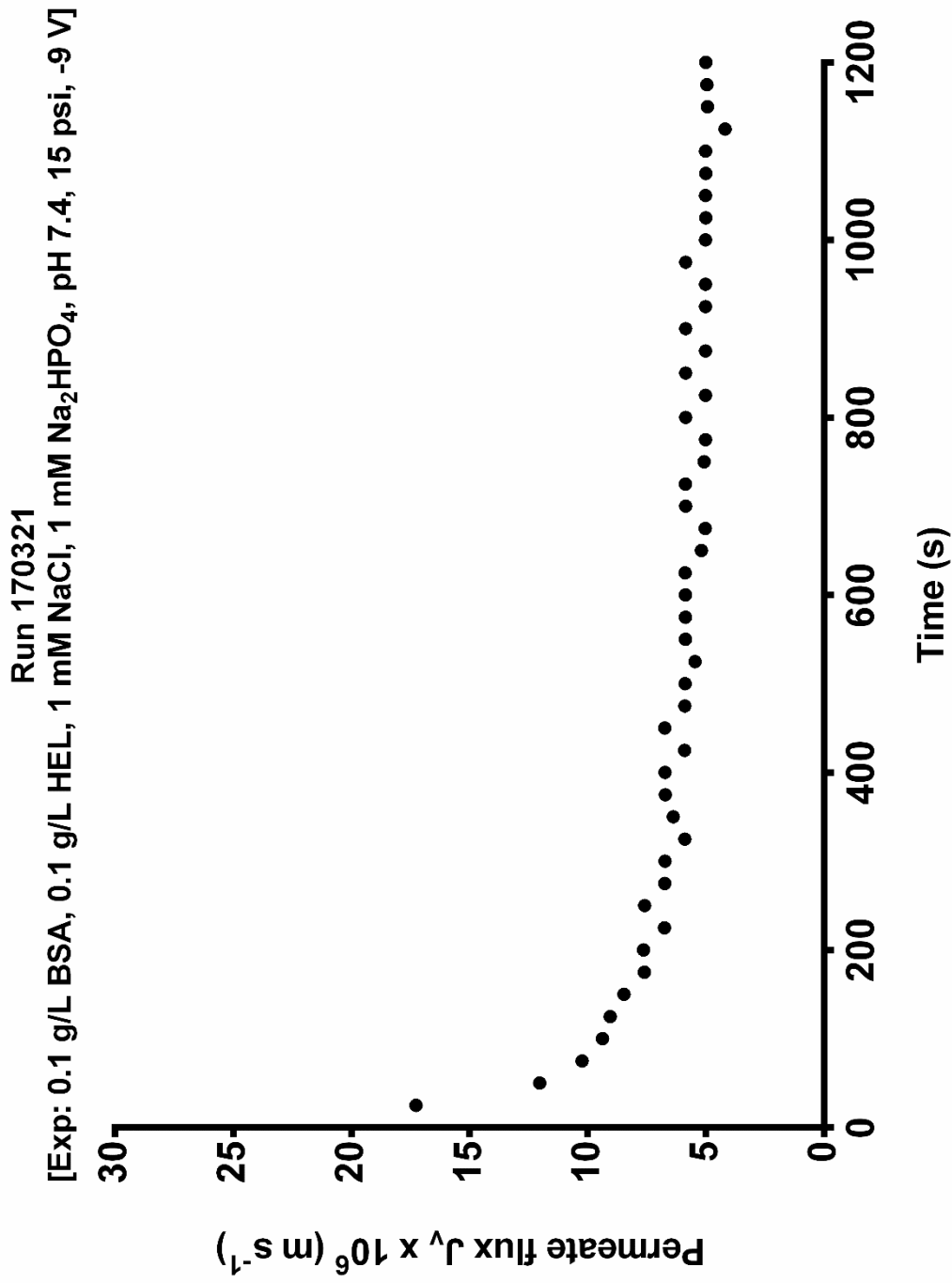| Fraction sample	Sample time (s)	$C_{p,HEL}$ (g/L)	$C_{p,\alpha LA}$ (g/L)	pH		C (g/L)	pH	Λ_0 (μS/cm)
1	15	-	-	-				
4	60	-	-	-		C_{HEL}		
8	120	-	-	-	Retent. (start)	0.096817	-	-
12	180	-	-	-	Feed (start)	0.096914	-	-
16	240	-	-	-	Retent. (end)	-	-	-
20	300	-	-	-	Feed (end)	-	-	-
24	360	-	-	-				
28	420	-	-	-				
32	480	-	-	-				
36	540	-	-	-				
40	600	-	-	-				
44	660	-	-	-		$C_{\alpha LA}$		
48	720	0.111167	0.087475	-	Retent. (start)	0.119223	-	-
52	780	-	-	-	Feed (start)	0.119312	-	-
56	840	-	-	-	Retent. (end)	-	-	-
60	900	-	-	-	Feed (end)	-	-	-
64	960	0.116119	0.098447	-				

Figure 6.23 Permeate flux for binary protein (αLA-HEL) EUF at 0 V [Run 170404].

Table 6.26 Data for binary protein (αLA-HEL) EUF at -9 V [Run 170405].

	Run 170405							
	Exp: 0.1 g/L αLA, 0.1 g/L HEL, 1 mM NaCl, 1 mM Na$_2$HPO$_4$, pH 7.4, -9 V							

Power supply current (A), start	0.07			
Power supply current (A), end	0.06			
Membrane	24 [02-25-17_1]			
Operating pressure	15 psi			
Crossflow shear rate	555 s^{-1}			

ΔP (psi)	$J_v \times 10^6$ (m/s)	Pre-HP $\times 10^{10}$ m/(s·Pa)		ΔP (psi)	$J_v \times 10^6$ (m/s)	Post-HP $\times 10^{10}$ m/(s·Pa)
0.7	9.8			1.5	1.1	
1.3	18.8			3.0	2.4	
1.9	27.4	21.7 ± 0.2		4.5	3.6	1.3 ± 0.1
2.5	36.8			6.0	5.0	

ΔV (V) at M1, start	ΔV (V) at E1, start	ΔV (V) at E2, start	ΔV (V) at M2, start	ΔV (V) at M1, end	ΔV (V) at E1, end	ΔV (V) at E2, end	ΔV (V) at M2, end	Avg. start ΔV (V)
-8.61	-4.01	-5.25	-8.65	-8.68	-3.98	-4.54	-8.68	-4.63

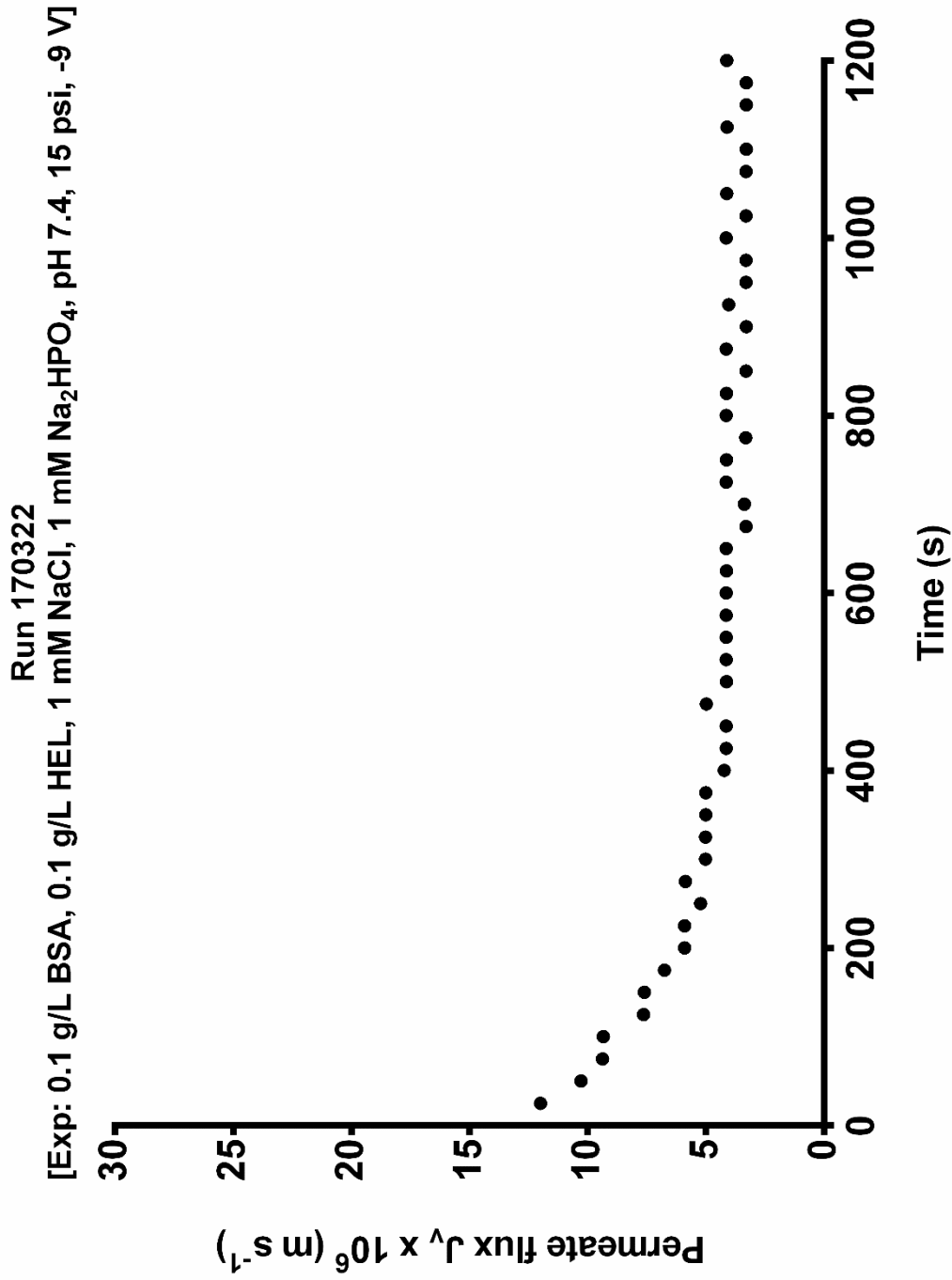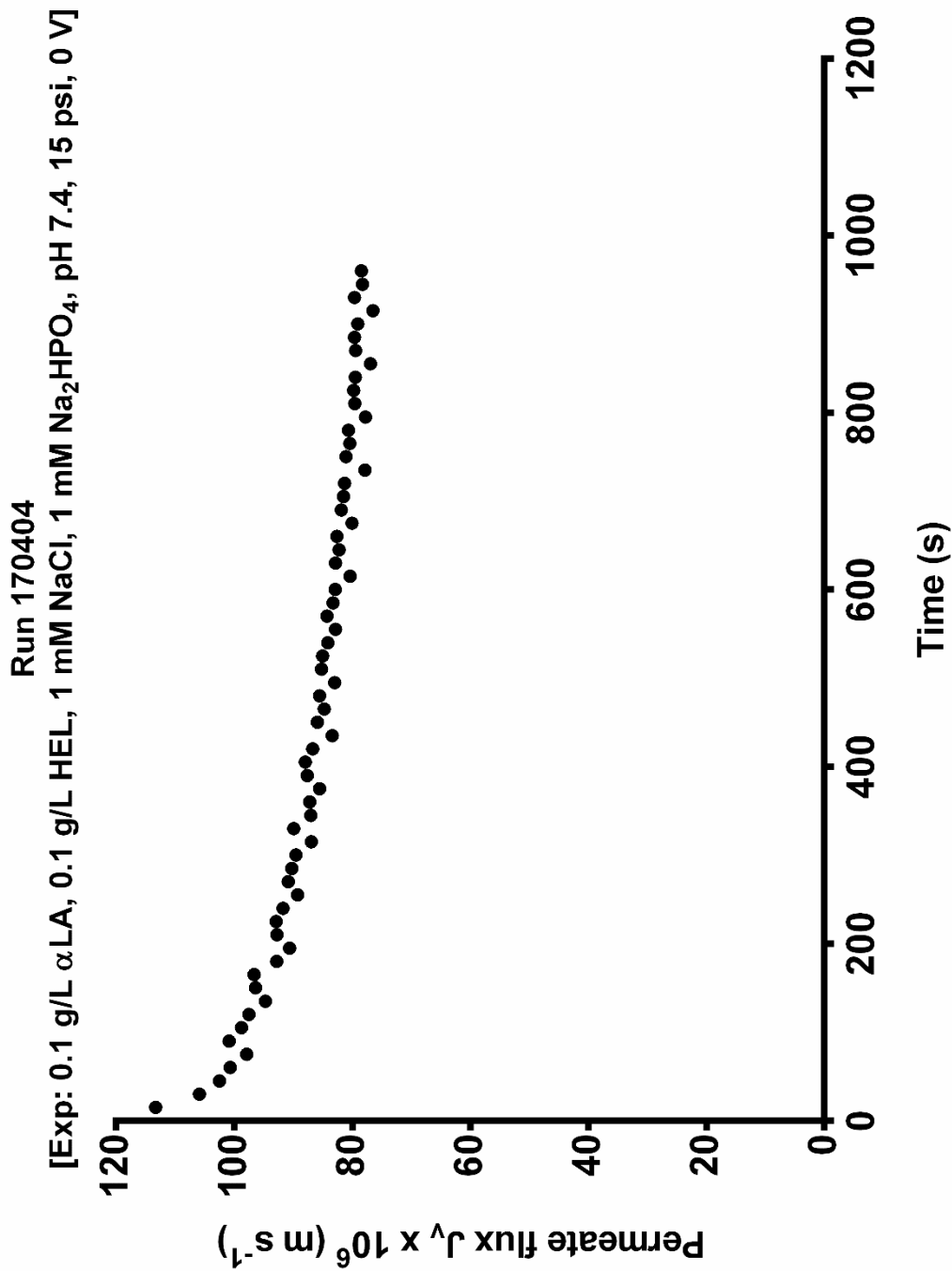| Fraction sample	Sample time (s)	$C_{p,HEL}$ (g/L)	$C_{p,\alpha LA}$ (g/L)	pH		C (g/L)	pH	Λ_0 (µS/cm)
1	15	-	-	-				
4	60	-	-	-	C_{HEL}			
8	120	-	-	-	Retent. (start)	0.100289	-	-
12	180	-	-	-	Feed (start)	0.100301	-	-
16	240	-	-	-	Retent. (end)	-	-	-
20	300	-	-	-	Feed (end)	-	-	-
24	360	-	-	-				
28	420	-	-	-				
32	480	-	-	-				
36	540	-	-	-				
40	600	-	-	-				
44	660	-	-	-	$C_{\alpha LA}$			
48	720	0.020121	0.113479	-	Retent. (start)	0.114646	-	-
52	780	-	-	-	Feed (start)	0.114941	-	-
56	840	-	-	-	Retent. (end)	-	-	-
60	900	-	-	-	Feed (end)	-	-	-
64	960	0.029169	0.105497	-				

Figure 6.24 Permeate flux for binary protein (αLA-HEL) EUF at -9 V [Run 170405].

Table 6.27 Data for binary protein (αLA-HEL) EUF at 0 V [Run 170509].

Run 170509	
Exp: 0.1 g/L αLA, 0.1 g/L HEL, 1 mM NaCl, 1 mM Na$_2$HPO$_4$, pH 7.4, 0 V	
Power supply current (A), start	-
Power supply current (A), end	-
Membrane	31 [04-02-17_3]
Operating pressure	15 psi
Crossflow shear rate	555 s^{-1}

ΔP (psi)	$J_v \times 10^6$ (m/s)	Pre-HP $\times 10^{10}$ m/(s·Pa)		ΔP (psi)	$J_v \times 10^6$ (m/s)	Post-HP $\times 10^{10}$ m/(s·Pa)
1.5	2.8			1.5	2.4	
2.5	4.9			2.5	4.0	
3.5	6.9	4.0 ± 0.5		3.5	5.5	2.4 ± 0.1
5	12.6			5.0	8.1	

ΔV (V) at M1, start	ΔV (V) at E1, start	ΔV (V) at E2, start	ΔV (V) at M2, start	ΔV (V) at M1, end	ΔV (V) at E1, end	ΔV (V) at E2, end	ΔV (V) at M2, end	Avg. start ΔV (V)
-	-	-	-	-	-	-	-	-

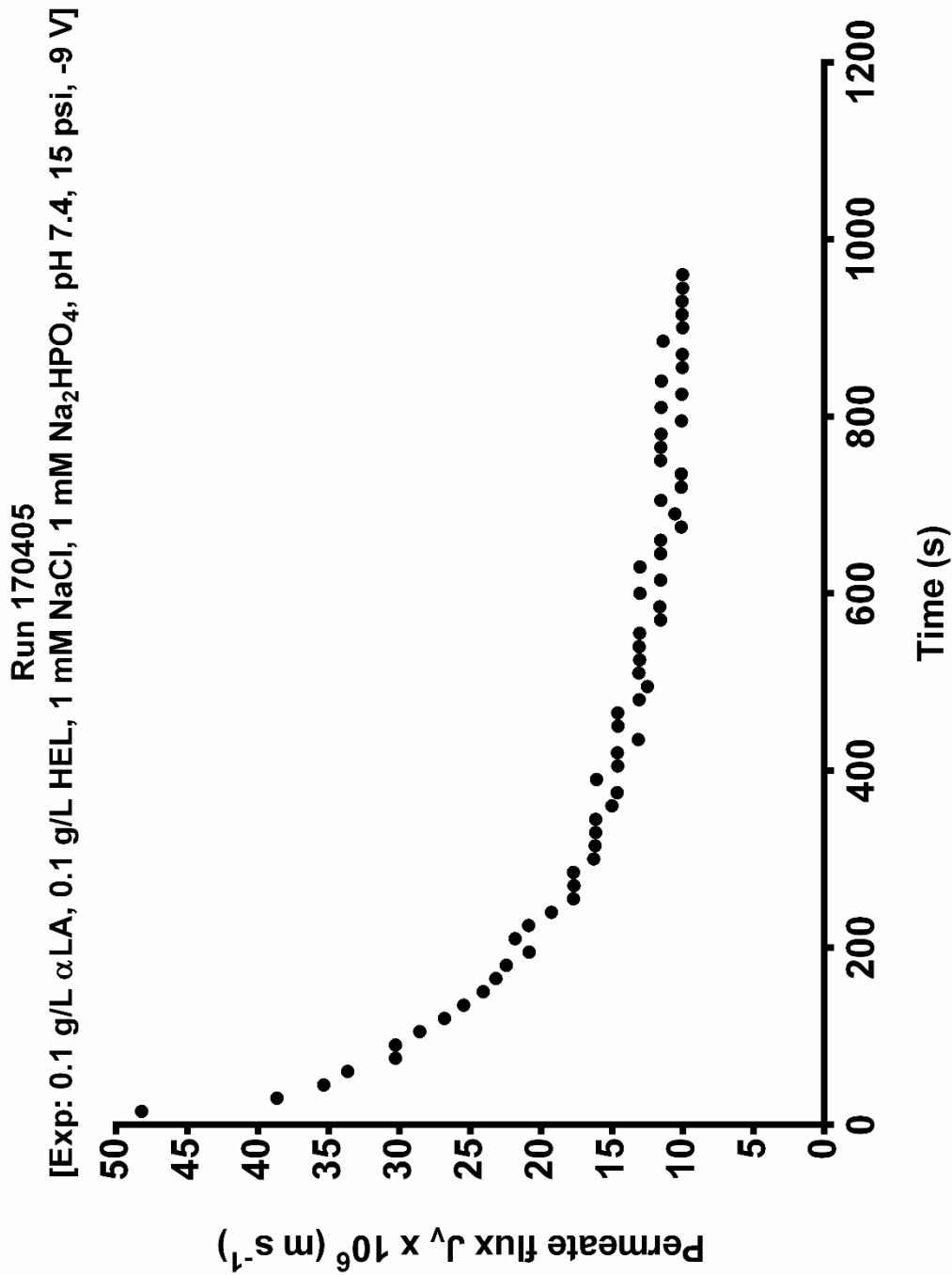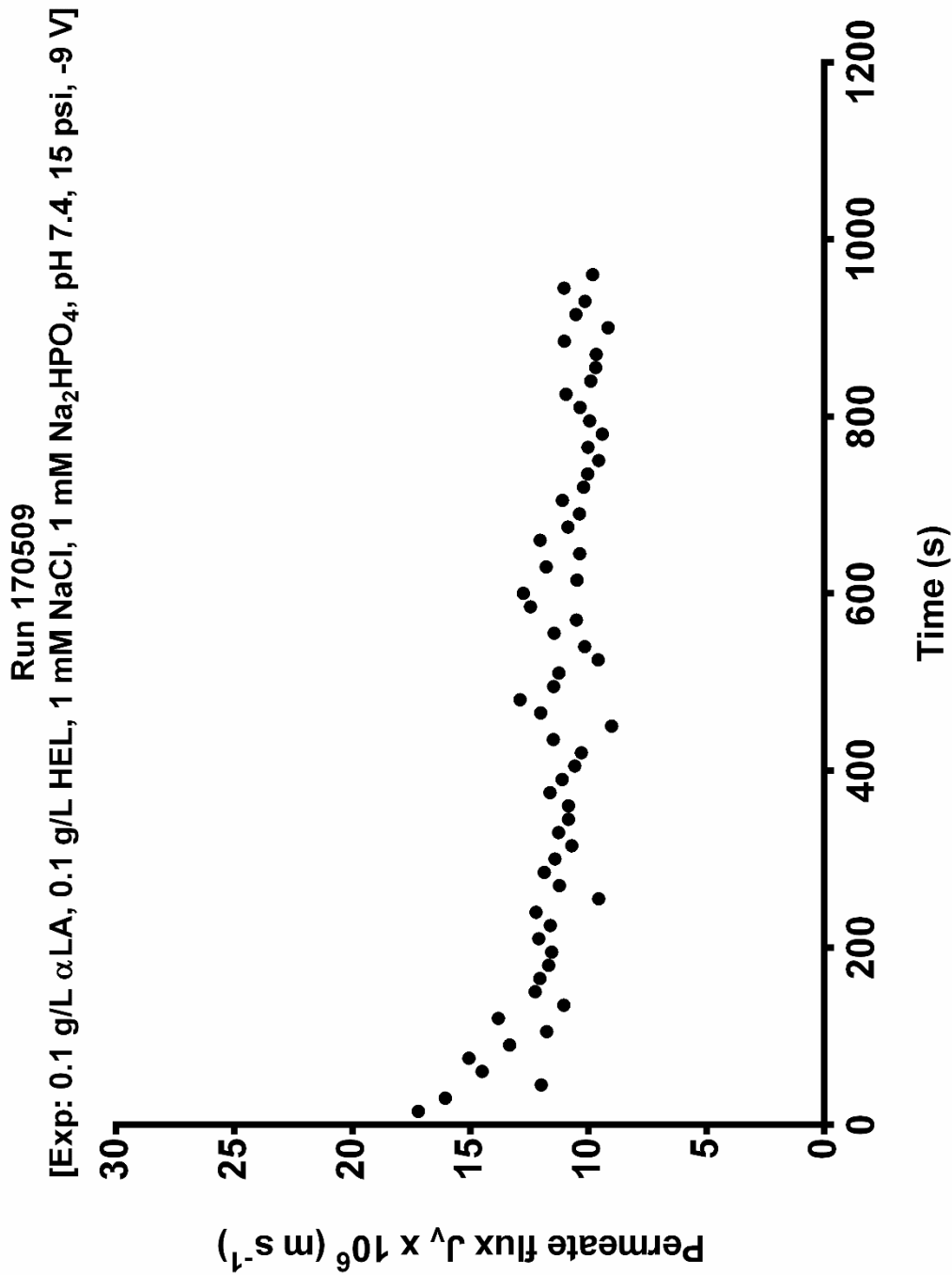| Fraction sample	Sample time (s)	$C_{p,HEL}$ (g/L)	$C_{p,\alpha LA}$ (g/L)	pH		C (g/L)	pH	Λ_0 (μS/cm)
1	15	-	-	-				
4	60	-	-	-	C_{HEL}			
8	120	-	-	-	Retent. (start)	0.140902	-	-
12	180	-	-	-	Feed (start)	0.140956	-	-
16	240	-	-	-	Retent. (end)	-	-	-
20	300	-	-	-	Feed (end)	-	-	-
24	360	-	-	-				
28	420	-	-	-				
32	480	-	-	-				
36	540	-	-	-				
40	600	-	-	-				
44	660	-	-	-	$C_{\alpha LA}$			
48	720	-	-	-	Retent. (start)	0.091404	-	-
52	780	-	-	-	Feed (start)	0.091463	-	-
56	840	-	-	-	Retent. (end)	-	-	-
60	900	-	-	-	Feed (end)	-	-	-
64	960	0.133378	0.065876	-				

Figure 6.25 Permeate flux for binary protein (αLA-HEL) EUF at 0 V [Run 170509].

Table 6.28 Data for binary protein (αLA-HEL) EUF at -9 V [Run 170510].

Run 170510
Exp: 0.1 g/L αLA, 0.1 g/L HEL, 1 mM NaCl, 1 mM Na$_2$HPO$_4$, pH 7.4, -9 V

Power supply current (A), start	0.06	
Power supply current (A), end	0.06	
Membrane	31 [04-02-17_3]	
Operating pressure	15 psi	
Crossflow shear rate	555 s^{-1}	

ΔP (psi)	$J_v \times 10^6$ (m/s)	Pre-HP $\times 10^{10}$ m/(s·Pa)	ΔP (psi)	$J_v \times 10^6$ (m/s)	Post-HP $\times 10^{10}$ m/(s·Pa)
1.0	7.1		1.0	2.1	
2.0	13.3		2.0	3.6	
3.0	19.3	9.3 ± 0.3	3.0	4.9	2.0 ± 0.1
4.0	26.5		4.0	6.2	

ΔV (V) at M1, start	ΔV (V) at E1, start	ΔV (V) at E2, start	ΔV (V) at M2, start	ΔV (V) at M1, end	ΔV (V) at E1, end	ΔV (V) at E2, end	ΔV (V) at M2, end	Avg. start ΔV (V)
-8.64	-4.16	-3.12	-8.52	-8.56	-4.57	-3.52	-8.56	-3.64

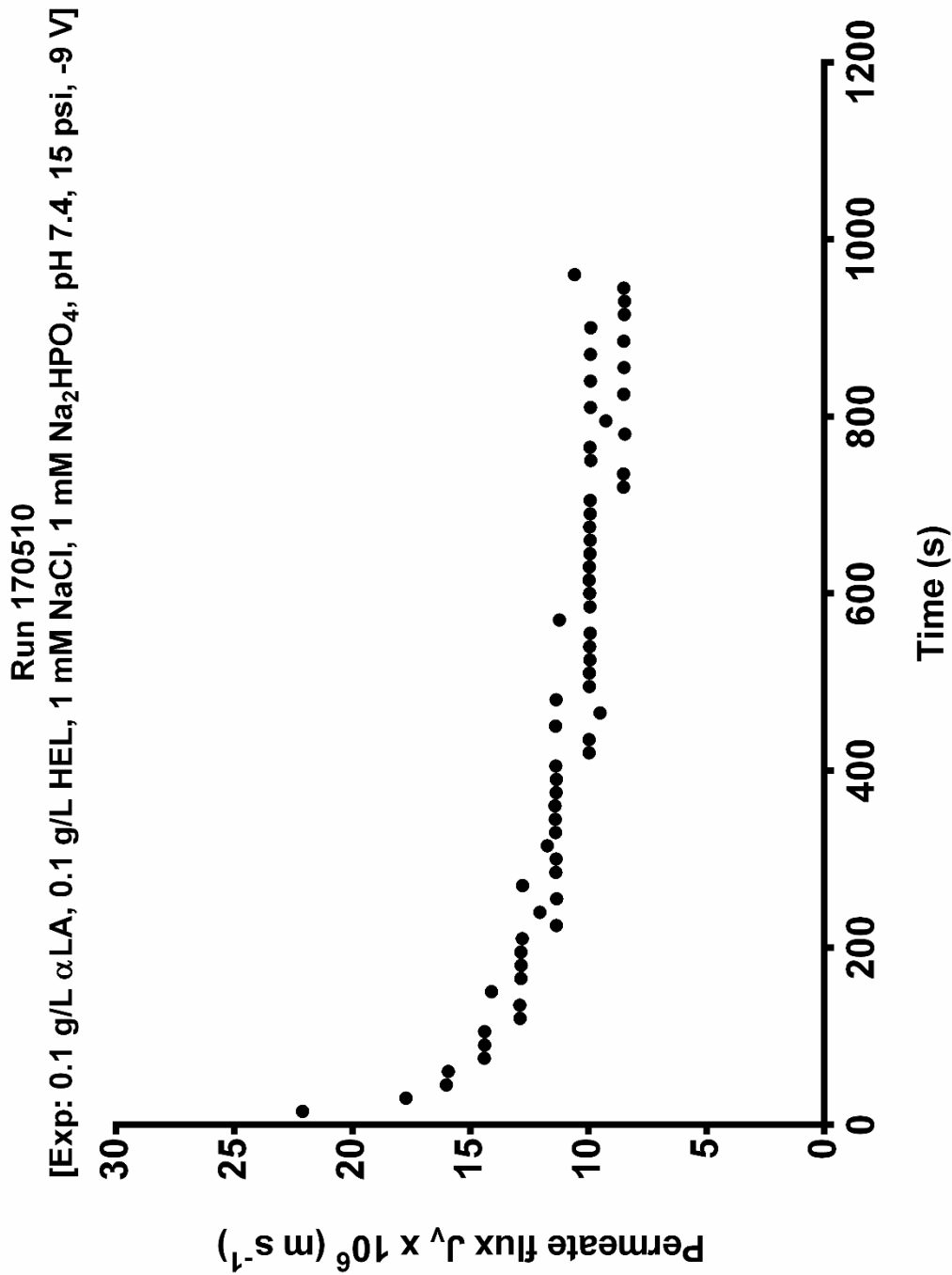| Fraction sample	Sample time (s)	$C_{p,HEL}$ (g/L)	$C_{p,\alpha LA}$ (g/L)	pH			C (g/L)	pH	Λ_0 (μS/cm)
1	15	-	-	-					
4	60	-	-	-		C_{HEL}			
8	120	-	-	-	Retent. (start)		0.146747	-	-
12	180	-	-	-	Feed (start)		0.146782	-	-
16	240	-	-	-	Retent. (end)		-	-	-
20	300	-	-	-	Feed (end)		-	-	-
24	360	-	-	-					
28	420	-	-	-					
32	480	-	-	-					
36	540	-	-	-					
40	600	-	-	-					
44	660	-	-	-		$C_{\alpha LA}$			
48	720	-	-	-	Retent. (start)		0.075359	-	-
52	780	-	-	-	Feed (start)		0.075401	-	-
56	840	-	-	-	Retent. (end)		-	-	-
60	900	-	-	-	Feed (end)		-	-	-
64	960	0.046447	0.062851	-					

Figure 6.26 Permeate flux for binary protein (αLA-HEL) EUF at -9 V [Run 170510].

Table 6.29 Data for binary protein (αLA-HEL) EUF at 0 V [Run 170605].

Run 170605								
Exp: 0.1 g/L αLA, 0.1 g/L HEL, 1 mM NaCl, 1 mM Na$_2$HPO$_4$, pH 7.4, 0 V								

Power supply current (A), start	-			
Power supply current (A), end	-			
Membrane	32 [04-02-17_4]			
Operating pressure	1 psi			
Crossflow shear rate	555 s^{-1}			

ΔP (psi)	$J_v \times 10^6$ (m/s)	Pre-HP $\times 10^{10}$ m/(s·Pa)		ΔP (psi)	$J_v \times 10^6$ (m/s)	Post-HP $\times 10^{10}$ m/(s·Pa)
0.5	5.0			2.0	0.5	
1.3	13.0			4.0	0.9	
2.1	21.0	14.5 ± 0.1		6.0	1.4	0.3 ± 0.1
2.7	27.0			8.0	1.7	

ΔV (V) at M1, start	ΔV (V) at E1, start	ΔV (V) at E2, start	ΔV (V) at M2, start	ΔV (V) at M1, end	ΔV (V) at E1, end	ΔV (V) at E2, end	ΔV (V) at M2, end	Avg. start ΔV (V)
-	-	-	-	-	-	-	-	-

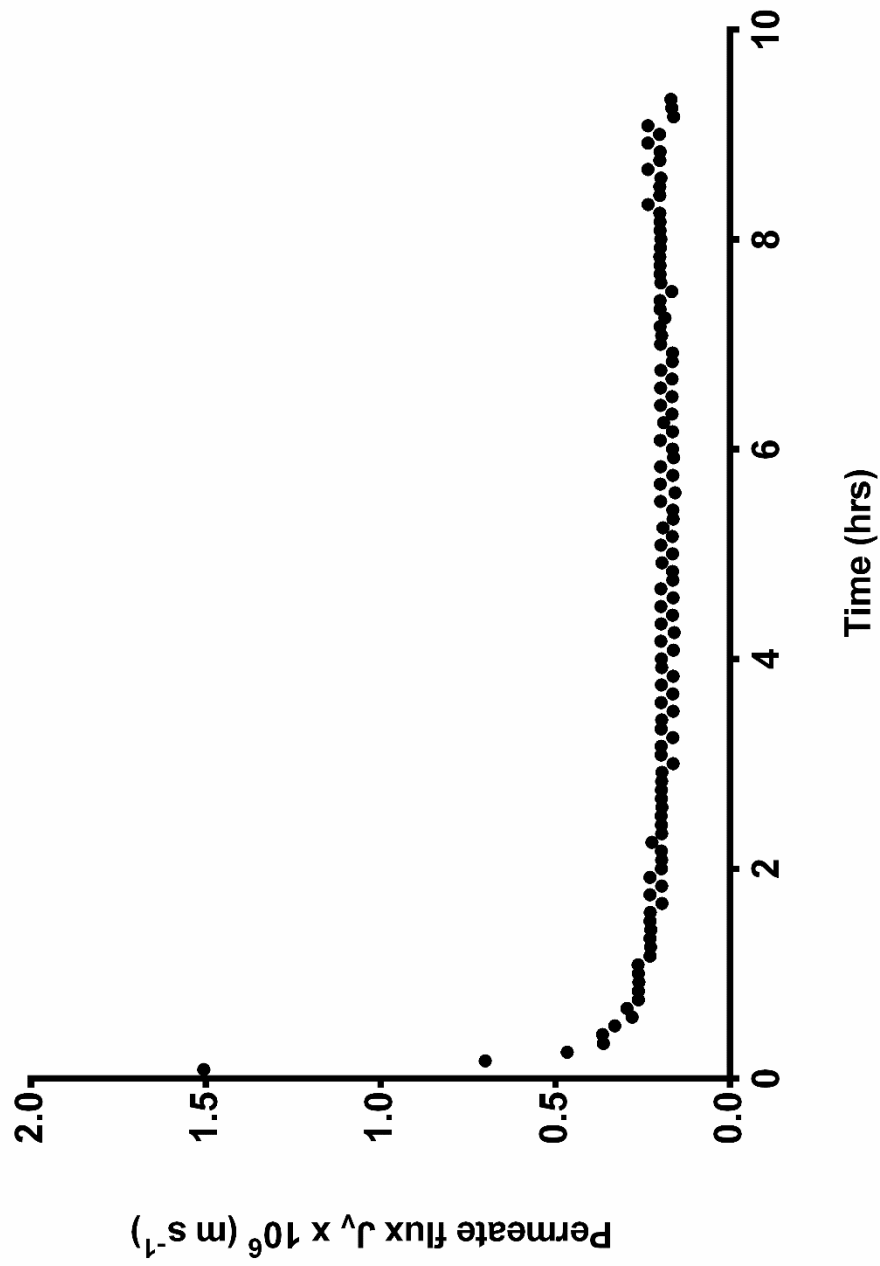| Fraction sample	Sample time (min)	$C_{p,HEL}$ (g/L)	$C_{p,\alpha LA}$ (g/L)	pH			C (g/L)	pH	Λ_0 (µS/cm)
1	10	0.000100	0.000283	-					
4	40	0.008462	0.000277	-		C_{HEL}			
8	80	0.001400	0.004959	-	Retent. (start)		-	-	-
16	160	0.002113	0.000100	-	Feed (start)		0.100021	7.444	-
48	480	0.003216	0.000100	-	Retent. (end)		-	-	-
80	800	0.002548	0.003595	-	Feed (end)		-	7.246	-
112	1120	0.001459	0.008902	-					
						$C_{\alpha LA}$			
					Retent. (start)		-	-	-
					Feed (start)		0.082210	7.444	-
					Retent. (end)		-	-	-
					Feed (end)		-	7.246	-

Figure 6.27 Permeate flux for binary protein (αLA-HEL) EUF at 0 V [Run 170605].

Table 6.30 Data for binary protein (αLA-HEL) EUF at -9 V [Run 170607].

		Run 170605						
		Exp: 0.1 g/L αLA, 0.1 g/L HEL, 1 mM NaCl, 1 mM Na$_2$HPO$_4$, pH 7.4, -9 V						

Power supply current (A), start	0.09			
Power supply current (A), end	0.09			
Membrane	32 [04-02-17_4]			
Operating pressure	1 psi			
Crossflow shear rate	555 s^{-1}			

ΔP (psi)	$J_v \times 10^6$ (m/s)	Pre-HP $\times 10^{10}$ m/(s·Pa)		ΔP (psi)	$J_v \times 10^6$ (m/s)	Post-HP $\times 10^{10}$ m/(s·Pa)
1.0	5.2			2.0	1.3	
2.0	10.7			4.0	2.5	
3.0	16.3	7.9 ± 0.1		6.0	3.3	0.6 ± 0.1
4.0	21.5			8.0	3.8	

ΔV (V) at M1, start	ΔV (V) at E1, start	ΔV (V) at E2, start	ΔV (V) at M2, start	ΔV (V) at M1, end	ΔV (V) at E1, end	ΔV (V) at E2, end	ΔV (V) at M2, end	Avg. start ΔV (V)
-8.71	-4.79	-4.87	-8.64	-8.69	-5.04	-5.36	-8.66	-4.83

Fraction sample	Sample time (min)	$C_{p,HEL}$ (g/L)	$C_{p,\alpha LA}$ (g/L)	pH			C (g/L)	pH	Λ_0 (μS/cm)
1	10	0.000260	0.027670	-					
4	40	0.000100	0.010729	-		C_{HEL}			
8	80	0.000100	0.009409	-	Retent. (start)		-	-	-
16	160	0.000100	0.022979	-	Feed (start)		0.100103	7.431	-
48	480	0.017178	0.012839	-	Retent. (end)		-	-	-
80	800	0.046271	0.000100	-	Feed (end)		-	6.868	-
112	1120	0.020978	0.029179	-					
						$C_{\alpha LA}$			
					Retent. (start)		-	-	-
					Feed (start)		0.104184	7.431	-
					Retent. (end)		-	-	-
					Feed (end)		-	6.868	-

Run 170607

[Exp: 0.1 g/L αLA, 0.1 g/L HEL, 1 mM NaCl, 1 mM Na$_2$HPO$_4$, pH 7.4, 1 psi, -9 V]

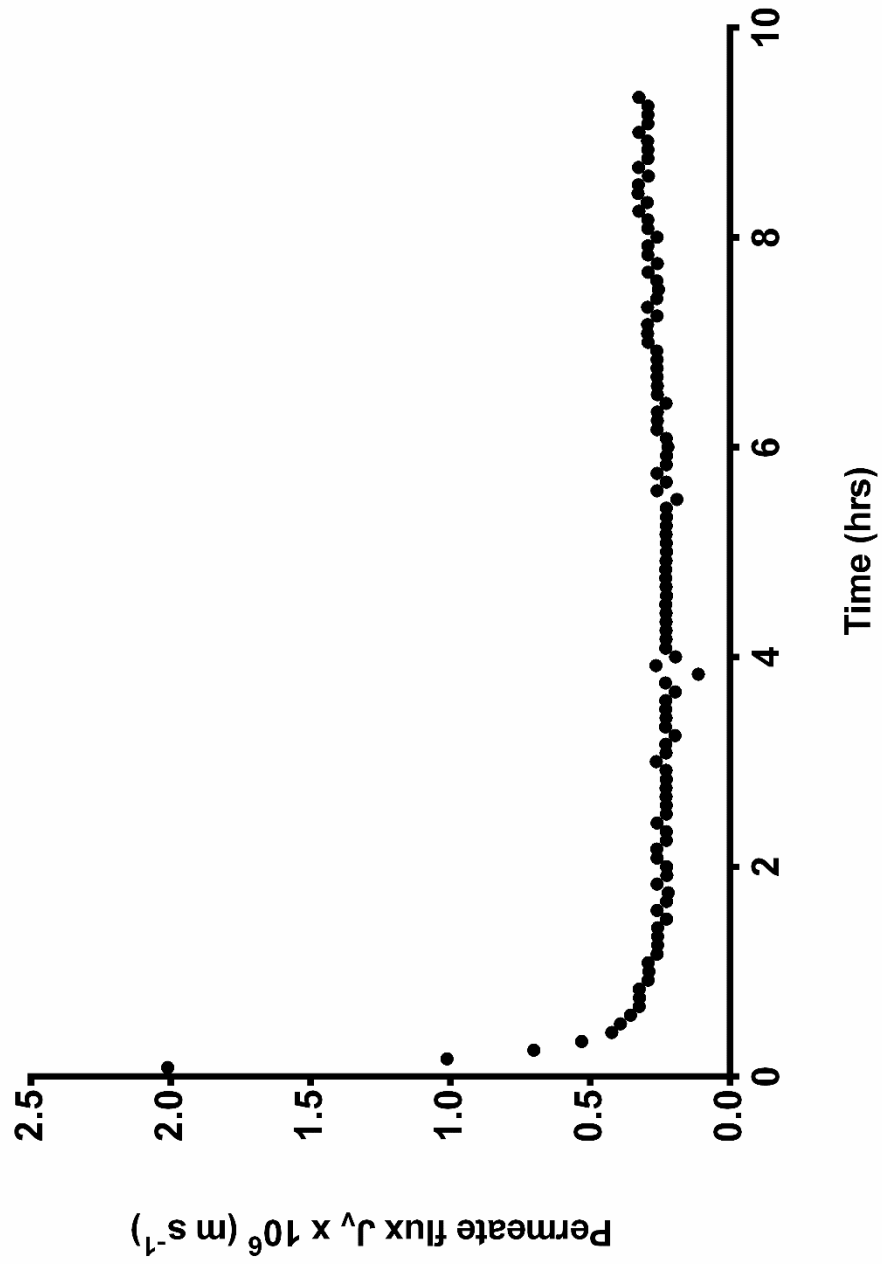Permeate flux J_v x 10^6 (m s^{-1})

Time (hrs)

Figure 6.28 Permeate flux for binary protein (αLA-HEL) EUF at -9 V [Run 170607].

6.1.2 Zeta potential data

Table 6.31 Parameters for the Helmholtz-Smoluchowski (H-S) equation for 10 mM NaCl electrolyte solution at 25 °C.

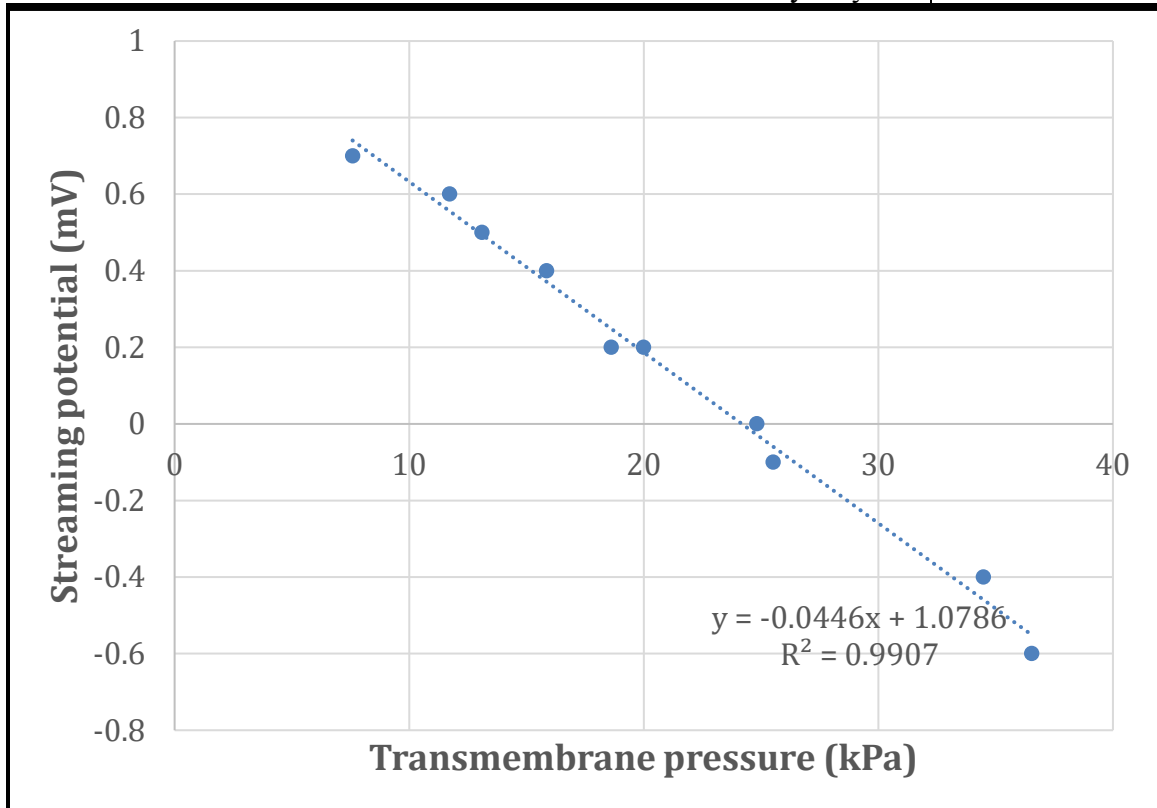| Parameters for calculation of zeta potential using the H-S equation; 10 mM NaCl electrolyte solution at 25 °CTable 6.31 Parameters for the Helmholtz-Smoluchowski (H-S) equation for 10 mM NaCl electrolyte solution at 25 °C.		
Parameter	Symbol	Value
Permittivity of free space	ε_0	8.86519×10^{-12} $C^2 \cdot N^{-1} \cdot m^{-2}$
Dielectric constant	ε_r	78.6 [69]
Solution viscosity	η	1 $N \cdot s \cdot m^{-2}$
Solution conductivity	Λ_0	118.45 $N \cdot V^{-2} \cdot s^{-1}$ [80]

Table 6.32 Zeta potential measurement data for the virgin polycarbonate (PC) membrane.

170810 - Zeta potential measurement for virgin polycarbonate (PC) membrane				
ΔP (psi)	ΔP (kPa)	Streaming potential (mV)	Membrane	PC
1.1	7.584236	0.7	Electrolyte	10 mM NaCl
1.9	13.10004	0.5	pH	7.4
2.7	18.61585	0.2		
3.7	25.51061	-0.1	N	10
5	34.4738	-0.4	Δ	8193.601
5.3	36.54223	-0.6	σ_y	0.043691
3.6	24.82114	0	σ_B	0.001526
2.9	19.9948	0.2		
2.3	15.85795	0.4	Zeta potential, ζ (mV)	-7.6
1.7	11.72109	0.6	Uncertainty in ζ	0.3

$y = -0.0446x + 1.0786$
$R^2 = 0.9907$

Table 6.33 Zeta potential measurement data for the virgin polysulfone support (PS-35) membrane.

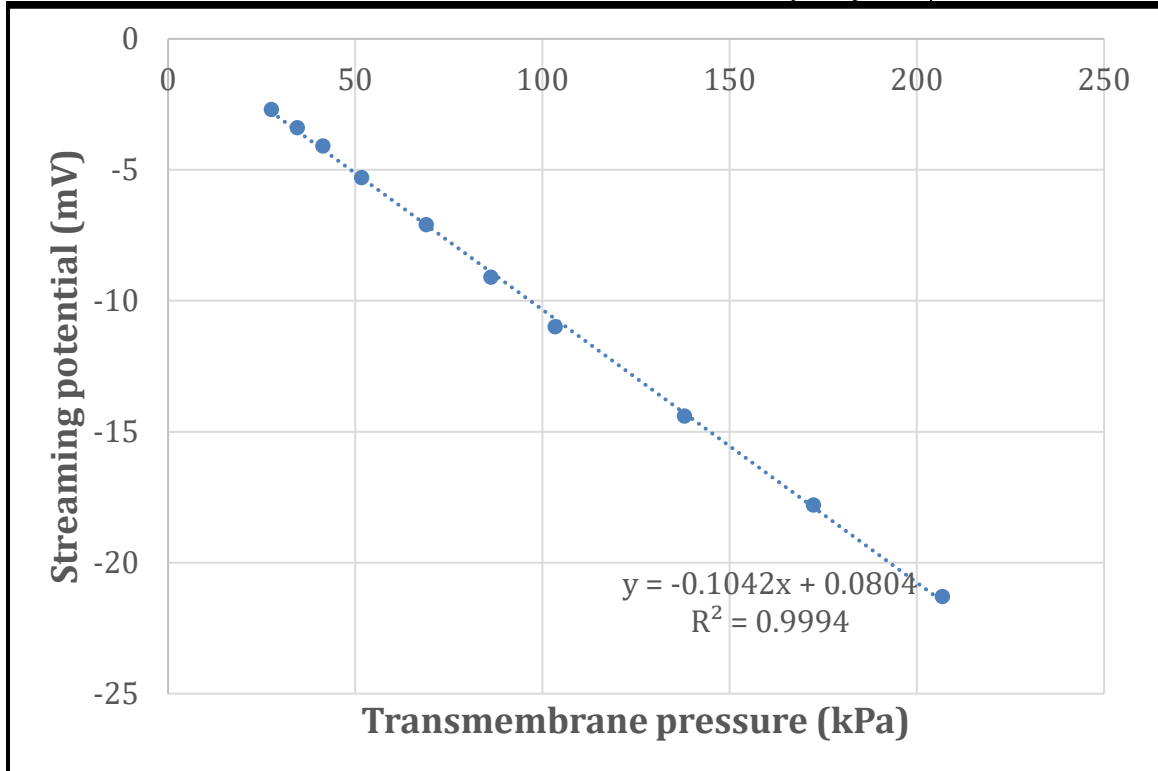|				
170811 - Zeta potential measurement for virgin polysulfone support only (PS-35) membrane				
ΔP (psi)	ΔP (kPa)	Streaming potential (mV)	Membrane	PS-35
30	206.8428	-21.3	Electrolyte	10 mM NaCl
25	172.369	-17.8	pH	7.4
20	137.8952	-14.4		
15	103.4214	-11	N	10
10	68.9476	-7.1	Δ	340845.4
7.5	51.7107	-5.3	σ_y	0.165564
6	41.36856	-4.1	σ_B	0.000897
5	34.4738	-3.4		
4	27.57904	-2.7	Zeta potential, ζ (mV)	-17.7
12.5	86.1845	-9.1	Uncertainty in ζ	0.2

Table 6.34 Zeta potential measurement data for the virgin PVA-CNT/PS-35 membrane.

170811 - Zeta potential measurement for virgin PVA-CNT/PS-35 membrane				
ΔP (psi)	ΔP (kPa)	Streaming potential (mV)	Membrane	PVA-CNT/PS-35 [Membrane 42]
30	206.8428	-20.5	Electrolyte	10 mM NaCl
25	172.369	-17.1	pH	7.4
20	137.8952	-13.5		
15	103.4214	-10.1	N	10
10	68.9476	-6.4	Δ	345468.5
7.5	51.7107	-4.6	σ_y	0.09771
5	34.4738	-2.9	σ_B	0.000526
3.5	24.13166	-1.9		
6	41.36856	-3.8	Zeta potential, ζ (mV)	-17.4
12.5	86.1845	-8.1	Uncertainty in ζ	0.1

$y = -0.1022x + 0.5858$
$R^2 = 0.9998$

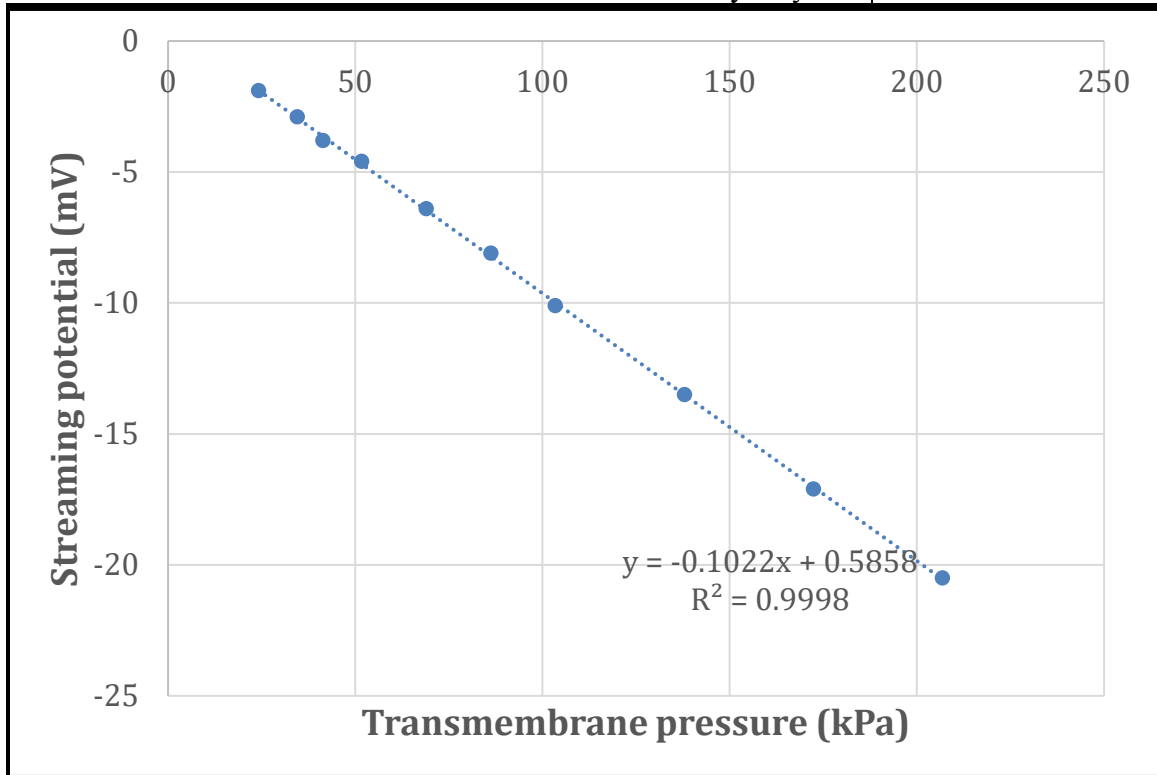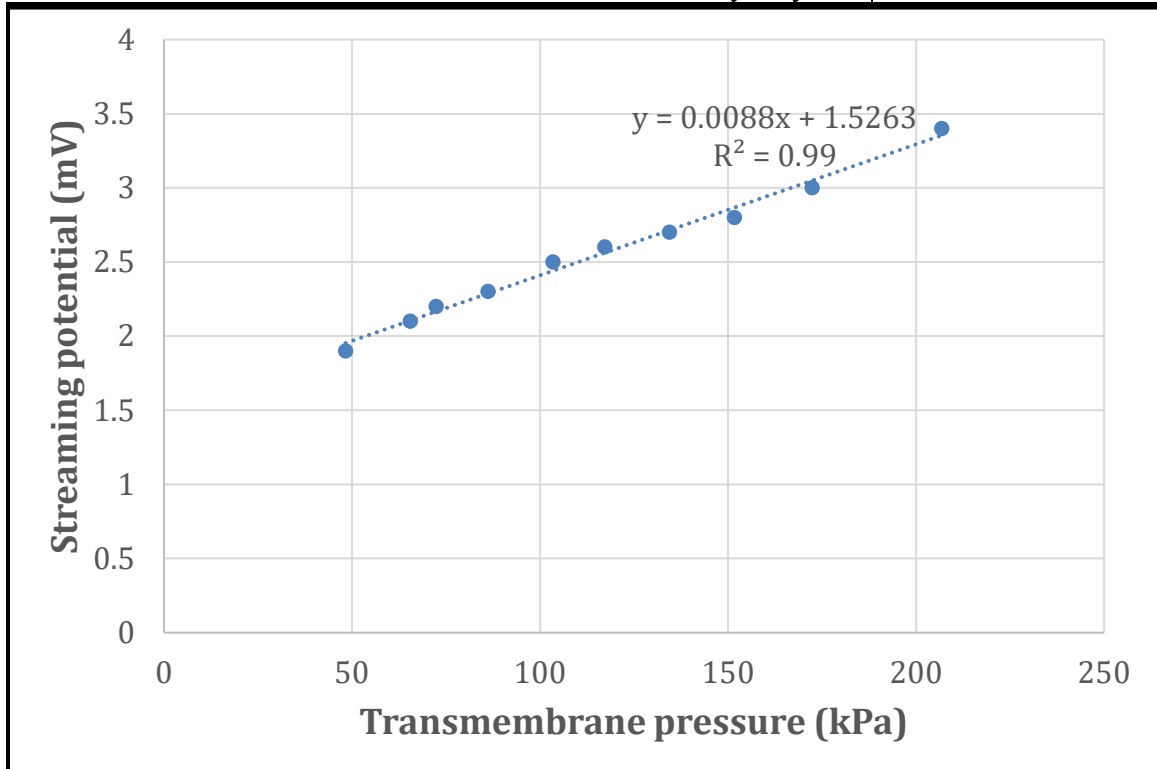Streaming potential (mV) vs. Transmembrane pressure (kPa)

Table 6.35 Zeta potential measurement data for the PVA-CNT/PS-35 membrane post-binary protein (αLA & HEL) EUF at -9 V.

170824 - Zeta potential measurement for PVA-CNT/PS-35 membrane post-binary protein EUF: [EUF exp: 0.1 g/L αLA & 0.1 g/L HEL; 4 mM ionic strength; pH 7.4; -9 V]				
ΔP (psi)	ΔP (kPa)	Streaming potential (mV)	Membrane	PVA-CNT/PS-35 [Membrane 36]
30	206.8428	3.4	Electrolyte	10 mM NaCl
25	172.369	3	pH	7.4
22	151.6847	2.8		
19.5	134.4478	2.7	N	10
17	117.2109	2.6	Δ	231318.5
15	103.4214	2.5	σ_y	0.047875
12.5	86.1845	2.3	σ_B	0.000315
10.5	72.39498	2.2		
9.5	65.50022	2.1	Zeta potential, ζ (mV)	1.5
7	48.26332	1.9	Uncertainty in ζ	0.1

Table 6.36 Zeta potential measurement data for the PVA-CNT/PS-35 membrane post-binary protein (αLA & HEL) UF at 0 V.

170824 - Zeta potential measurement for PVA-CNT/PS-35 membrane post-binary protein UF: [EUF exp: 0.1 g/L αLA & 0.1 g/L HEL; 4 mM ionic strength; pH 7.4; 0 V]				
ΔP (psi)	ΔP (kPa)	Streaming potential (mV)	Membrane	PVA-CNT/PS-35 [Membrane 37]
30	206.8428	-3.2	Electrolyte	10 mM NaCl
29	199.948	-3	pH	7.4
27.5	189.6059	-2.6		
24.5	168.9216	-1.9	N	10
23	158.5795	-1.5	Δ	74871.9
22.5	155.1321	-1.3	σ_y	0.072155
21.5	148.2373	-1.2	σ_B	0.000834
20	137.8952	-0.9		
19	131.0004	-0.7	Zeta potential, ζ (mV)	-5.7
18	124.1057	-0.5	Uncertainty in ζ	0.1

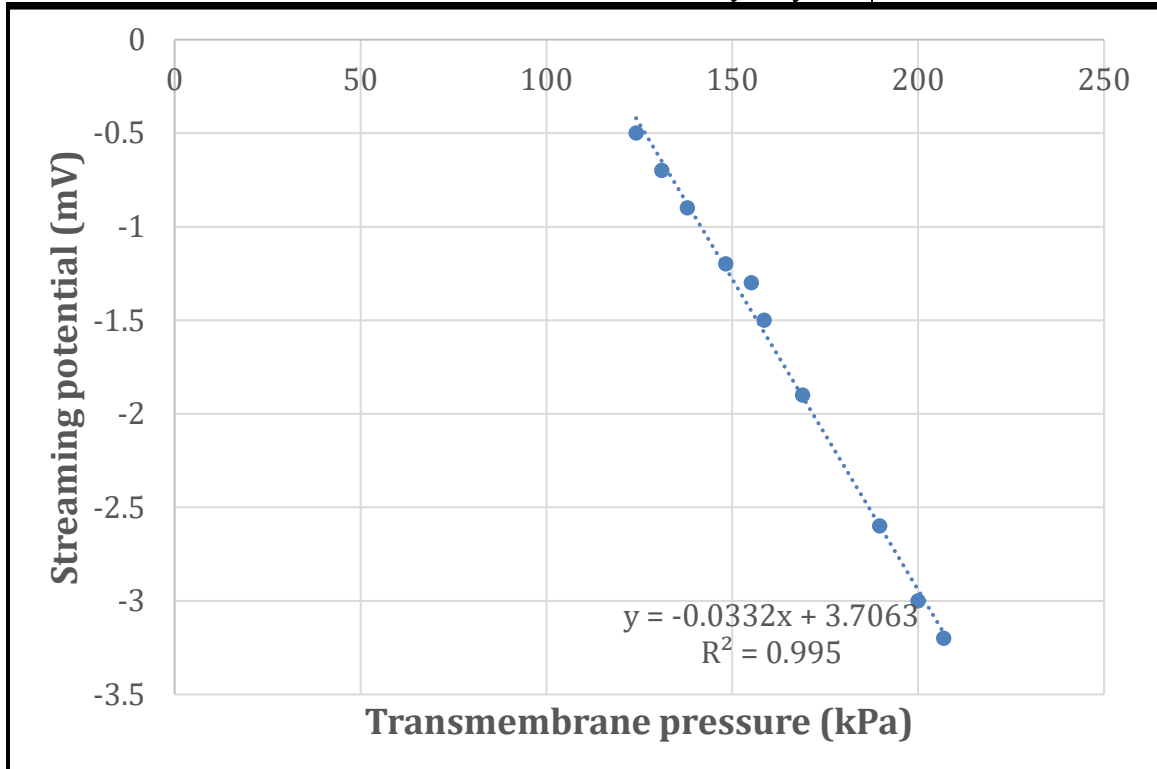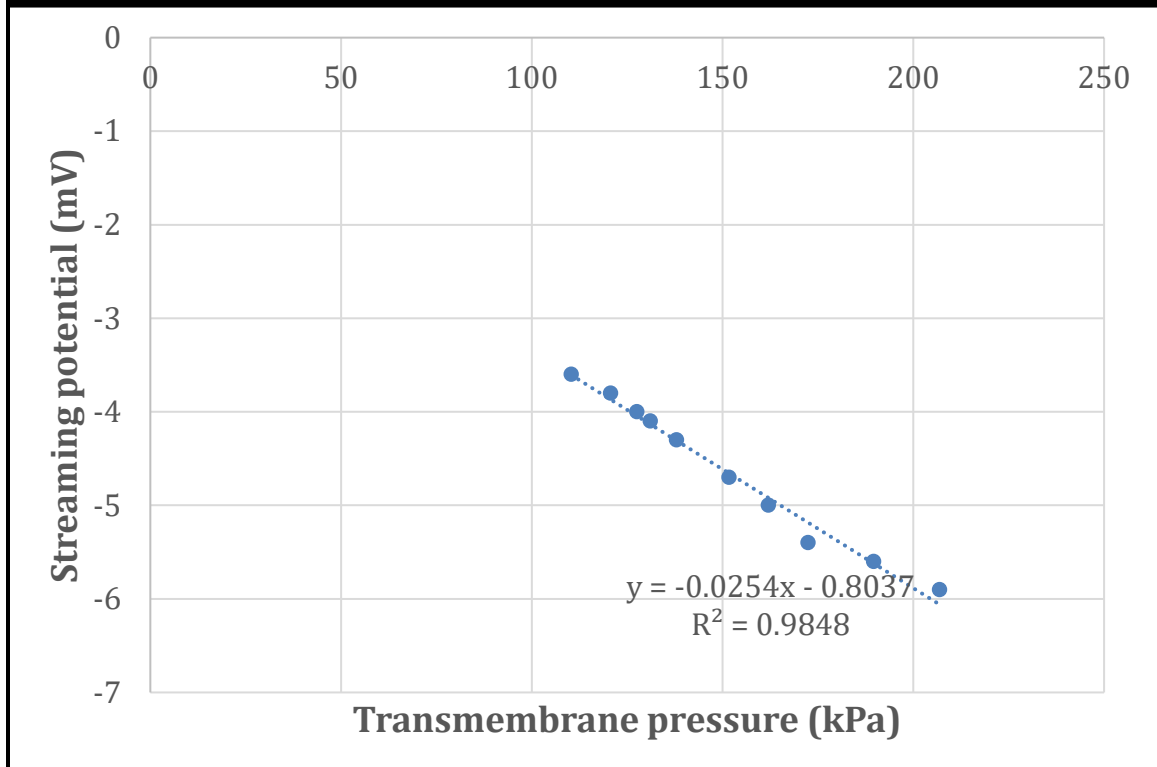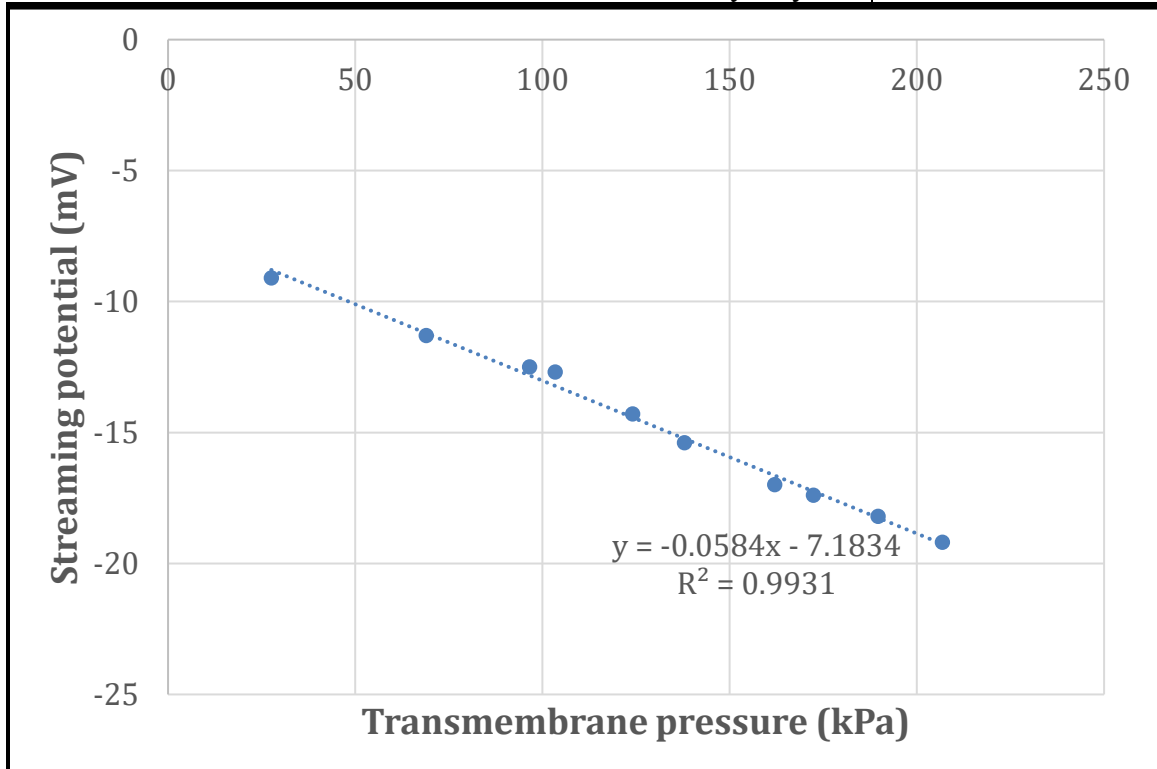$y = -0.0332x + 3.7063$
$R^2 = 0.995$

Table 6.37 Zeta potential measurement data for the PVA-CNT/PS-35 membrane post-single protein (αLA) UF at 0 V.

170828 - Zeta potential measurement for PVA-CNT/PS-35 membrane post-single protein UF: [EUF exp: 0.1 g/L αLA; 4 mM ionic strength; pH 7.4; 0 V]				
ΔP (psi)	ΔP (kPa)	Streaming potential (mV)	Membrane	PVA-CNT/PS-35 [Membrane 38]
30	206.8428	-5.9	Electrolyte	10 mM NaCl
27.5	189.6059	-5.6	pH	7.4
25	172.369	-5.4		
23.5	162.0269	-5	N	10
22	151.6847	-4.7	Δ	88847.99
20	137.8952	-4.3	σ_y	0.105361
18.5	127.5531	-4	σ_B	0.001118
17.5	120.6583	-3.8		
16	110.3162	-3.6	Zeta potential, ζ (mV)	-4.3
19	131.0004	-4.1	Uncertainty in ζ	0.2

$y = -0.0254x - 0.8037$
$R^2 = 0.9848$

X-axis: Transmembrane pressure (kPa)
Y-axis: Streaming potential (mV)

Table 6.38 Zeta potential measurement data for the PVA-CNT/PS-35 membrane post-single protein (αLA) EUF at -9 V.

170828 - Zeta potential measurement for PVA-CNT/PS-35 membrane post-single protein EUF: [EUF exp: 0.1 g/L αLA; 4 mM ionic strength; pH 7.4; -9 V]				
ΔP (psi)	ΔP (kPa)	Streaming potential (mV)	Membrane	PVA-CNT/PS-35 [Membrane 41]
30	206.8428	-19.2	Electrolyte	10 mM NaCl
27.5	189.6059	-18.2	pH	7.4
25	172.369	-17.4		
23.5	162.0269	-17	N	10
20	137.8952	-15.4	Δ	284085.4
18	124.1057	-14.3	σ_y	0.290965
15	103.4214	-12.7	σ_B	0.001726
14	96.52664	-12.5		
4	27.57904	-9.1	Zeta potential, ζ (mV)	-9.9
10	68.9476	-11.3	Uncertainty in ζ	0.3

$y = -0.0584x - 7.1834$
$R^2 = 0.9931$

X-axis: Transmembrane pressure (kPa)
Y-axis: Streaming potential (mV)

Table 6.39 Zeta potential measurement data for the PVA-CNT/PS-35 membrane post-single protein (HEL) UF at 0 V.

\$\Delta P\$ (psi)	\$\Delta P\$ (kPa)	Streaming potential (mV)	Membrane	PVA-CNT/PS-35 [Membrane 40]
170828 - Zeta potential measurement for PVA-CNT/PS-35 membrane post-single protein UF: [EUF exp: 0.1 g/L HEL; 4 mM ionic strength; pH 7.4; 0 V]				
30	206.8428	-20.3	Electrolyte	10 mM NaCl
28	193.0533	-18.8	pH	7.4
25	172.369	-16.8		
22.5	155.1321	-15.2	N	10
20	137.8952	-13.6	\$\Delta\$	148602.9
18	124.1057	-12.4	\$\sigma_y\$	0.108736
17	117.2109	-11.6	\$\sigma_B\$	0.000892
13	89.63188	-9.3		
15.5	106.869	-10.8	Zeta potential, \$\zeta\$ (mV)	-15.9
14	96.5266	-9.8	Uncertainty in \$\zeta\$	0.2

y = -0.0936x - 0.7605
\$R^2\$ = 0.9993

(x-axis) **Transmembrane pressure (kPa)**
(y-axis) **Streaming potential (mV)**

Table 6.40 Zeta potential measurement data for the PVA-CNT/PS-35 membrane post-single protein (HEL) EUF at -9 V.

170828 - Zeta potential measurement for PVA-CNT/PS-35 membrane post-single protein EUF: [EUF exp: 0.1 g/L HEL; 4 mM ionic strength; pH 7.4; -9 V]				
ΔP (psi)	ΔP (kPa)	Streaming potential (mV)	Membrane	PVA-CNT/PS-35 [Membrane 39]
30	206.8428	-1.9	Electrolyte	10 mM NaCl
27.5	189.6059	-1.5	pH	7.4
21.5	148.2373	-0.9		
20	137.8952	-0.7	N	10
18.5	127.5531	-0.4	Δ	174713
14	96.52664	0.1	σ_y	0.057405
12	82.73712	0.3	σ_B	0.000434
10	68.9476	0.6		
17	117.211	-0.2	Zeta potential, ζ (mV)	-3.0
16	110.316	-0.1	Uncertainty in ζ	0.1

$y = -0.0179x + 1.831$
$R^2 = 0.9953$

Streaming potential (mV) vs Transmembrane pressure (kPa)
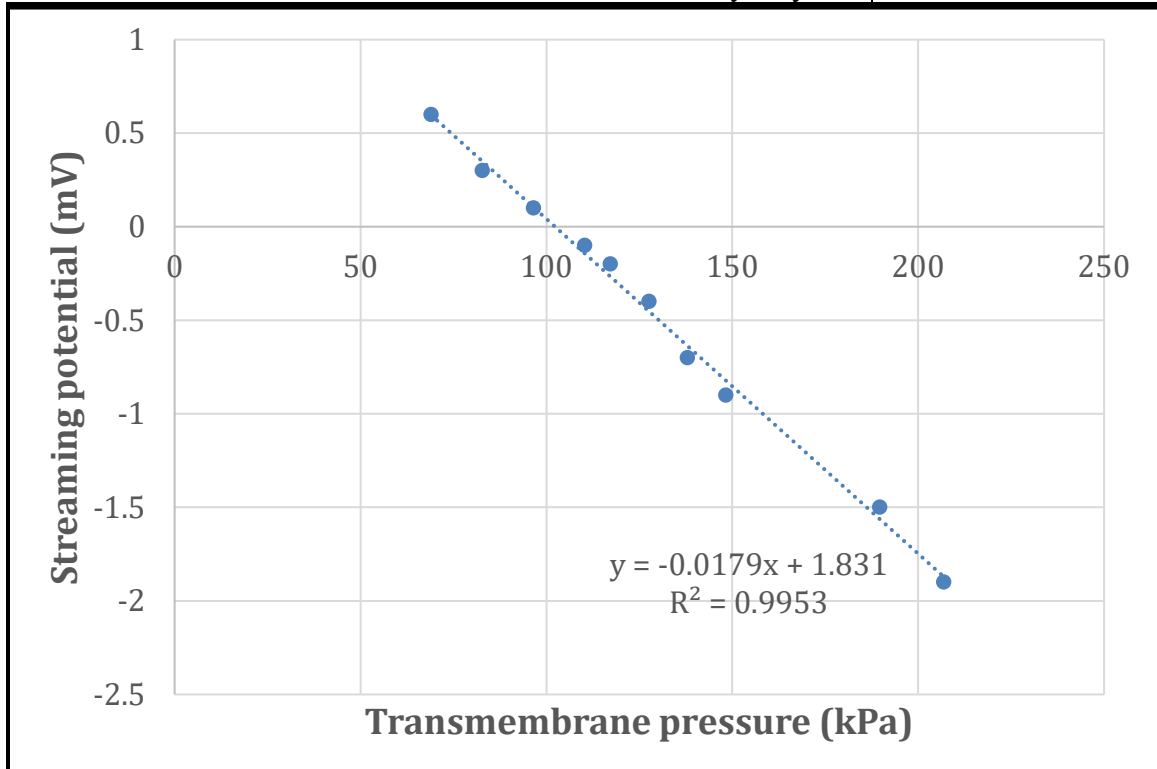
6.1.3 SEM analysis
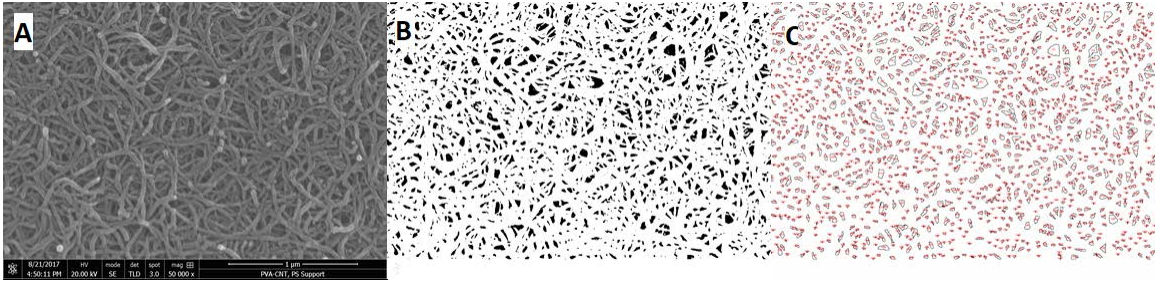
Figure 6.29 Porosity analysis using ImageJ: A) Original membrane surface SEM image of virgin PVA-CNT/PS-35 membrane; B) Binary Image; C) Analyzed outlines of pores.
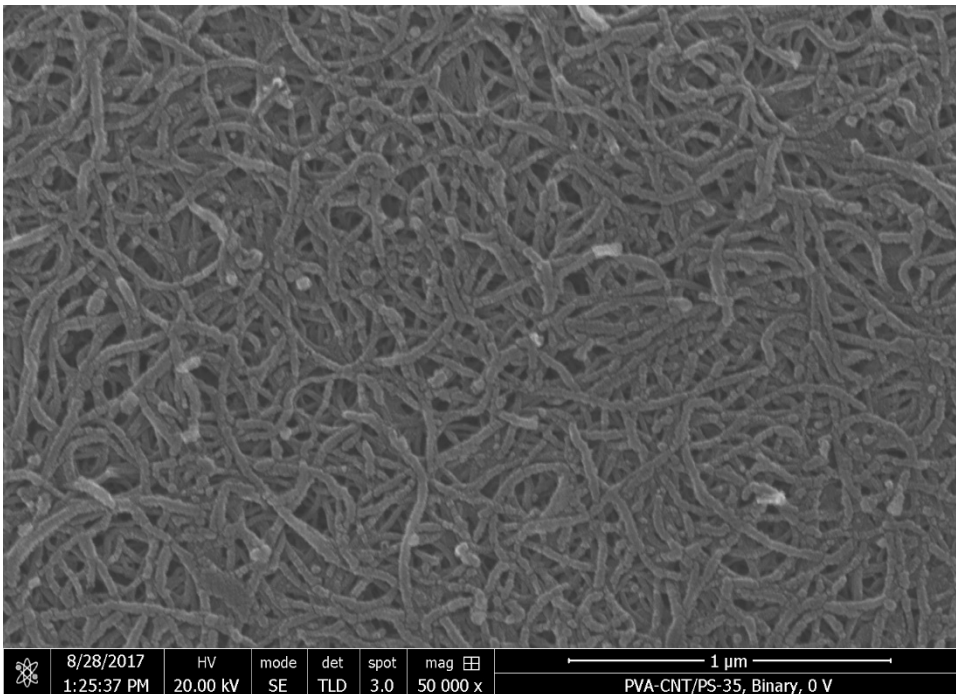
Figure 6.30 SEM image (1/1) of the PVA-CNT membrane surface following binary protein (0.1 g/L αLA and 0.1 g/L HEL) ultrafiltration at 0 V.
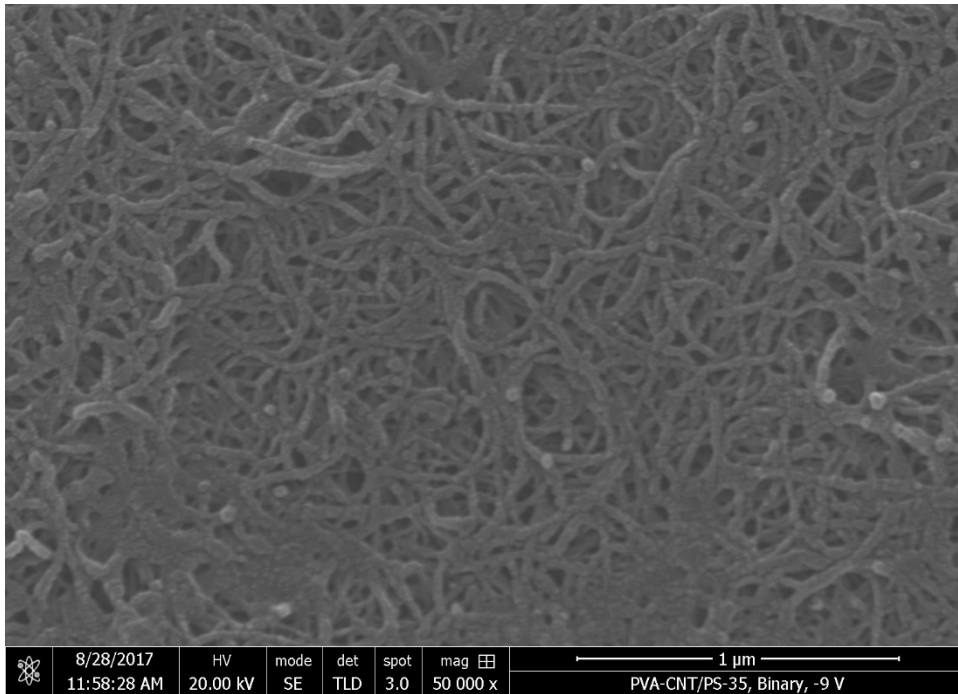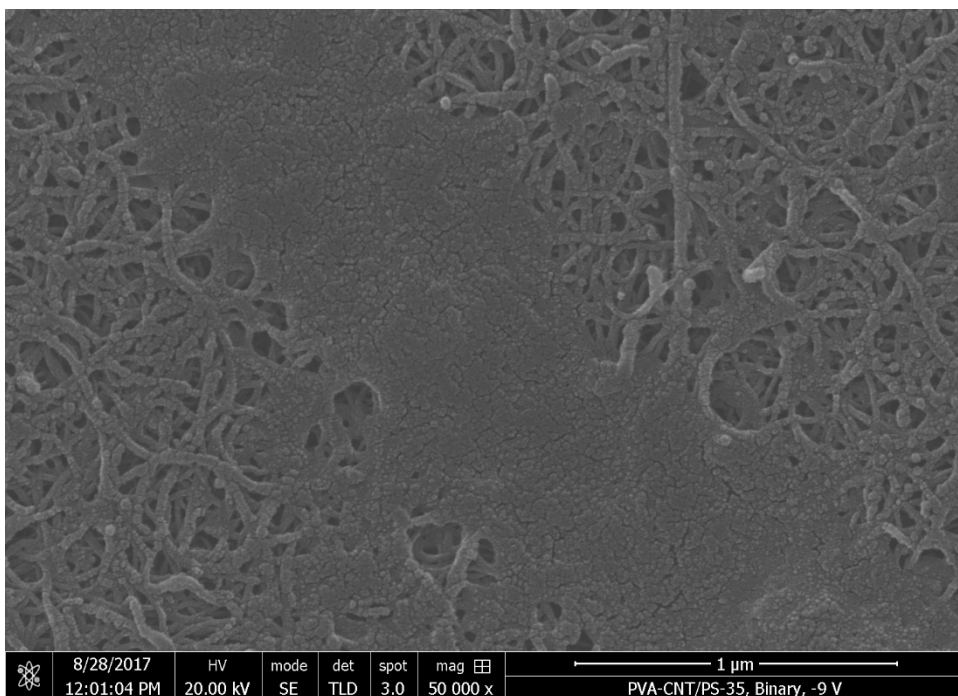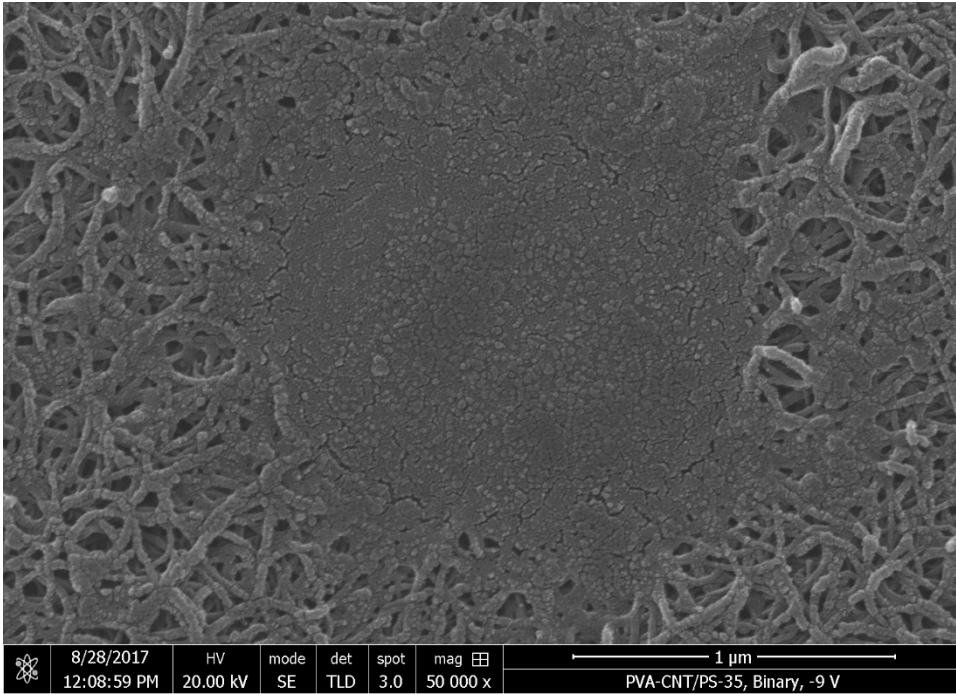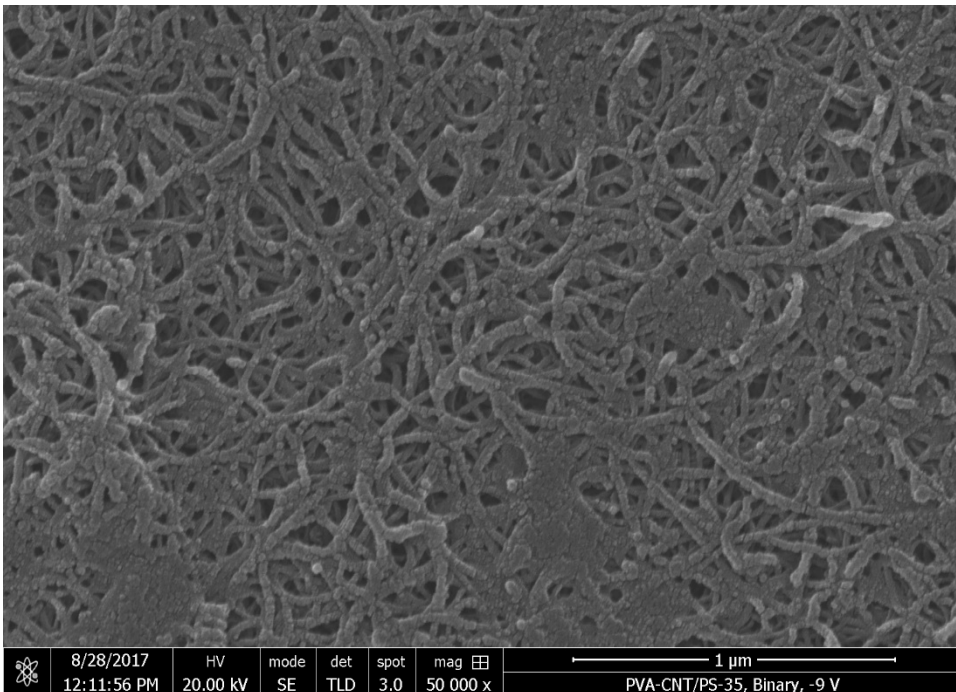
Figure 6.31 SEM image (1/4) of the PVA-CNT membrane surface following binary protein (0.1 g/L αLA and 0.1 g/L HEL) electroultrafiltration at -9 V.

Figure 6.32 SEM image (2/4) of the PVA-CNT membrane surface following binary protein (0.1 g/L αLA and 0.1 g/L HEL) electroultrafiltration at -9 V.

Figure 6.33 SEM image (3/4) of the PVA-CNT membrane surface following binary protein (0.1 g/L αLA and 0.1 g/L HEL) electroultrafiltration at -9 V.

Figure 6.34 SEM image (4/4) of the PVA-CNT membrane surface following binary protein (0.1 g/L αLA and 0.1 g/L HEL) electroultrafiltration at -9 V.
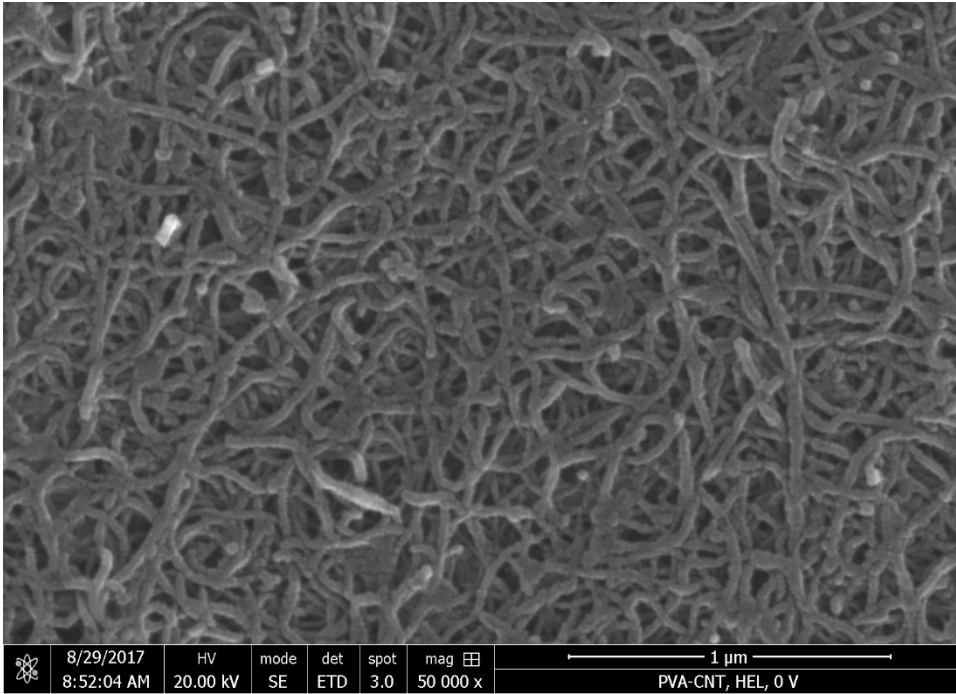
8/29/2017 | HV | mode | det | spot | mag ⊞ | 1 μm
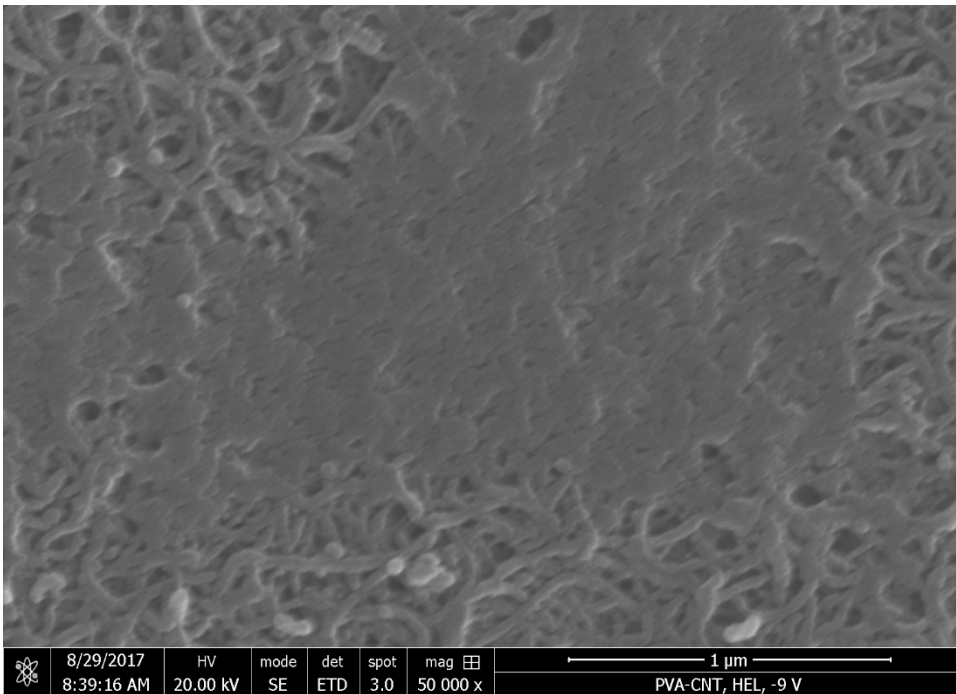8:52:04 AM | 20.00 kV | SE | ETD | 3.0 | 50 000 x | PVA-CNT, HEL, 0 V

Figure 6.35 SEM image (1/1) of the PVA-CNT membrane surface following single protein (0.1 g/L HEL) ultrafiltration at 0 V.

8/29/2017 | HV | mode | det | spot | mag ⊞ | 1 μm
8:39:16 AM | 20.00 kV | SE | ETD | 3.0 | 50 000 x | PVA-CNT, HEL, -9 V

Figure 6.36 SEM image (1/2) of the PVA-CNT membrane surface following single protein (0.1 g/L HEL) electroultrafiltration at -9 V.
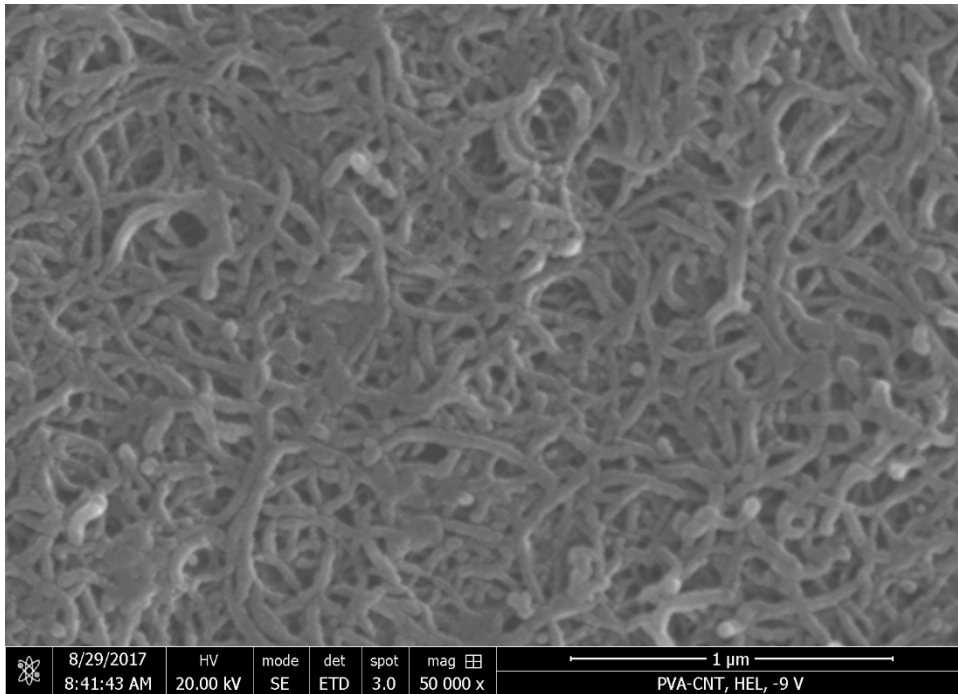
143

Figure 6.37 SEM image (2/2) of the PVA-CNT membrane surface following single protein (0.1 g/L HEL) electroultrafiltration at -9 V.
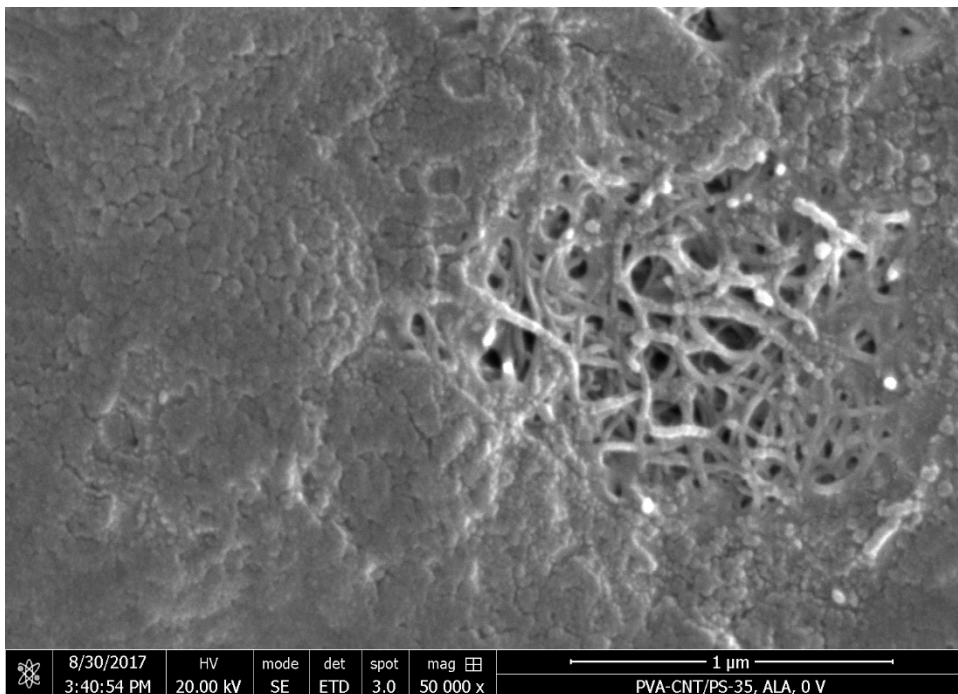

Figure 6.38 SEM image (1/2) of the PVA-CNT membrane surface following single protein (0.1 g/L αLA) ultrafiltration at 0 V.
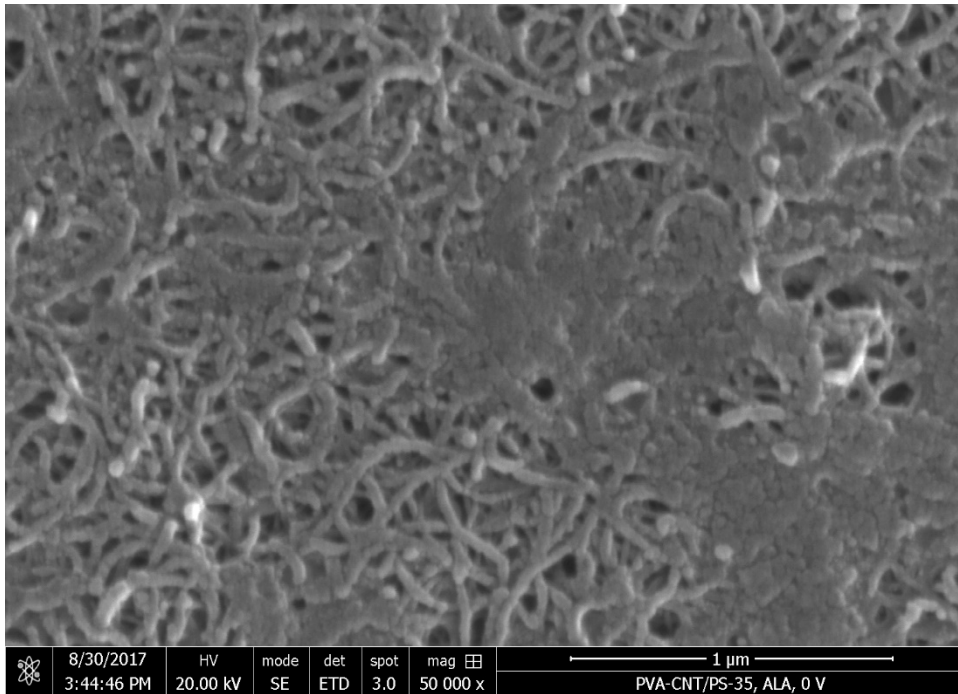
Figure 6.39 SEM image (2/2) of the PVA-CNT membrane surface following single protein (0.1 g/L αLA) ultrafiltration at 0 V.
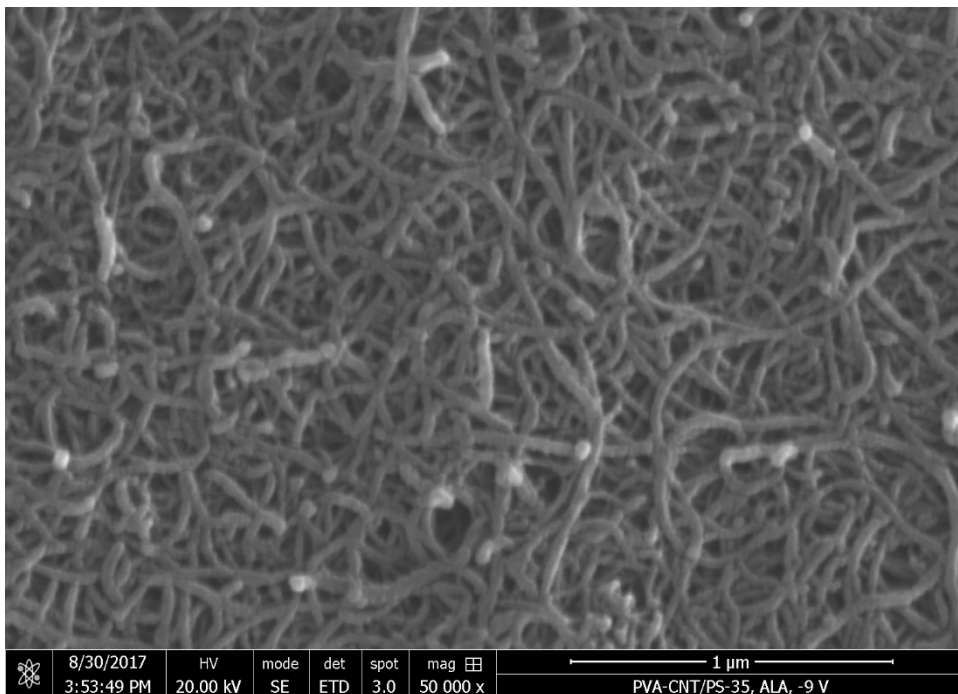

Figure 6.40 SEM image (1/3) of the PVA-CNT membrane surface following single protein (0.1 g/L αLA) electroultrafiltration at -9 V.
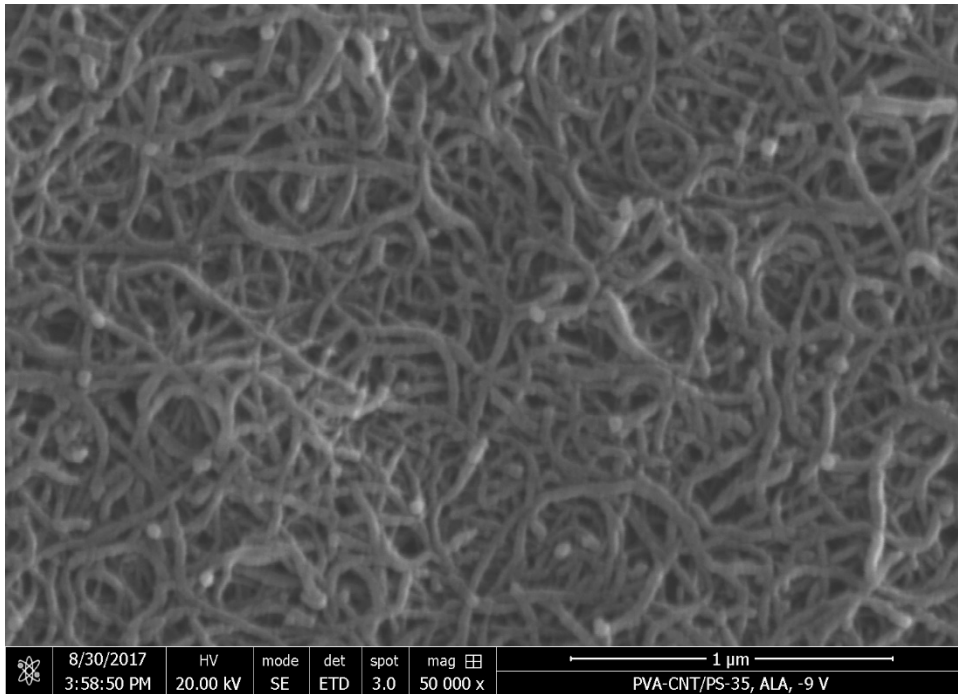
Figure 6.41 SEM image (2/3) of the PVA-CNT membrane surface following single protein (0.1 g/L αLA) electroultrafiltration at -9 V.
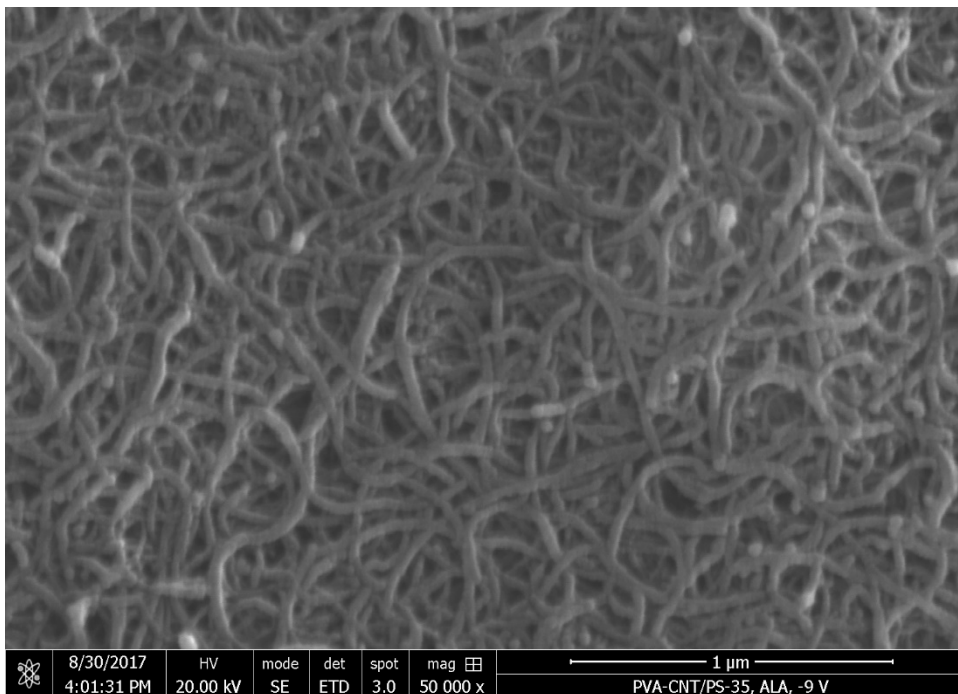

Figure 6.42 SEM image (3/3) of the PVA-CNT membrane surface following single protein (0.1 g/L αLA) electroultrafiltration at -9 V.
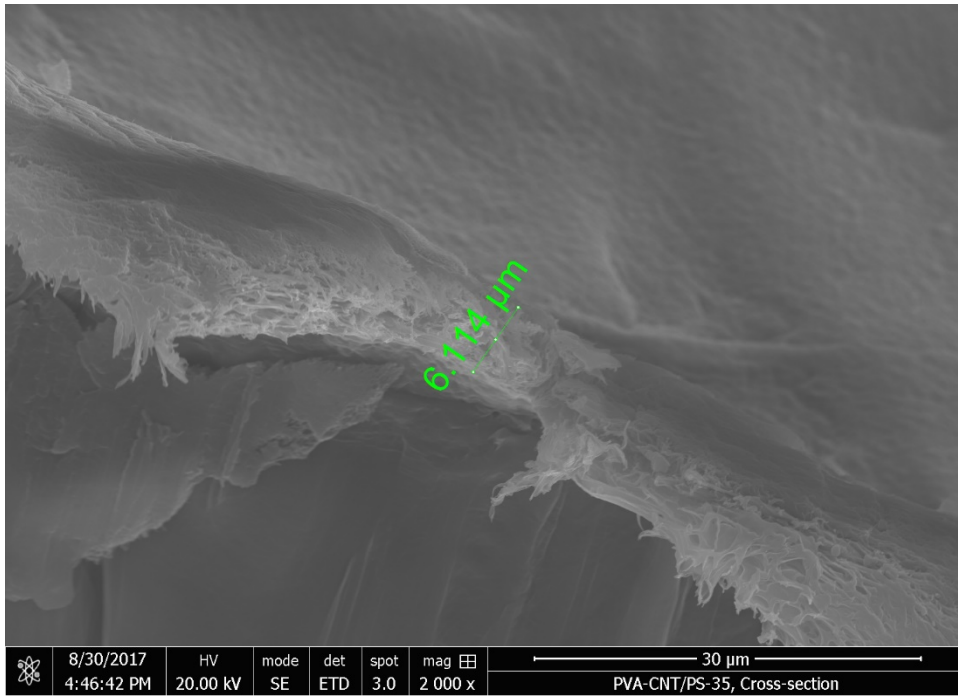
Figure 6.43 SEM image of the PVA-CNT/PS-35 membrane cross-section.

Table 6.41 Summary of the porosity analysis of the PVA-CNT membrane following protein electroultrafiltration. The measurements were acquired using the ImageJ imaging software.

Protein electroUF study	SEM image	ImageJ analyzed particle count	% Porosity	Average % porosity
-	170828_PVA-CNT (Virgin)_Image1	1657	11.8	11.8
Binary protein (0.1 g/L αLA & 0.1 g/L HEL) at 0 V	170828_Binary_0V_Image1	1728	9.1	9.1
Binary protein (0.1 g/L αLA & 0.1 g/L HEL) at -9 V	170828_Binary_-9V_Image1	1186	8.4	6.9
	170828_Binary_-9V_Image2	1049	3.7	
	170828_Binary_-9V_Image3	1995	7.9	
	170828_Binary_-9V_Image4	1338	7.6	
Single protein (0.1 g/L HEL) at 0 V	170829_HEL_0V_Image1	1202	10.6	10.6
Single protein (0.1 g/L HEL) at -9 V	170829_HEL_-9V_Image1	422	2.9	5.0
	170829_HEL_-9V_Image2	813	7.1	
Single protein (0.1 g/L αLA) at 0 V	170830_ALA_0V_Image1	288	2.0	3.7
	170830_ALA_0V_Image2	510	5.4	
Single protein (0.1 g/L αLA) at -9 V	170830_ALA_-9V_Image1	983	11.2	10.7
	170830_ALA_-9V_Image2	881	10.8	
	170830_ALA_-9V_Image3	806	10.1	

References

[1] M.C. Manning, K. Patel, R.T. Borchardt, Stability of protein pharmaceuticals, Pharmaceutical research, 6 (1989) 903-918.

[2] G. Walsh, D.R. Headon, Protein Biotechnology, John Wiley & Sons, West Sussex, England, 1994.

[3] D.S. Dimitrov, Therapeutic proteins, Therapeutic Proteins: Methods and Protocols, (2012) 1-26.

[4] B. Leader, Q.J. Baca, D.E. Golan, Protein therapeutics: a summary and pharmacological classification, Nature reviews. Drug discovery, 7 (2008) 21.

[5] A.L. Zydney, Membrane technology for purification of therapeutic proteins, Biotechnology and bioengineering, 103 (2009) 227-230.

[6] T. Lai, Y. Yang, S.K. Ng, Advances in mammalian cell line development technologies for recombinant protein production, Pharmaceuticals, 6 (2013) 579-603.

[7] F.M. Wurm, Production of recombinant protein therapeutics in cultivated mammalian cells, Nature biotechnology, 22 (2004) 1393-1398.

[8] M.C. Manning, D.K. Chou, B.M. Murphy, R.W. Payne, D.S. Katayama, Stability of protein pharmaceuticals: an update, Pharmaceutical research, 27 (2010) 544-575.

[9] G. Guiochon, L.A. Beaver, Separation science is the key to successful biopharmaceuticals, Journal of Chromatography A, 1218 (2011) 8836-8858.

[10] N.E. Levy, K.N. Valente, L.H. Choe, K.H. Lee, A.M. Lenhoff, Identification and characterization of host cell protein product-associated impurities in monoclonal antibody bioprocessing, Biotechnology and bioengineering, 111 (2014) 904-912.

[11] J. Thömmes, M. Etzel, Alternatives to chromatographic separations, Biotechnology progress, 23 (2007) 42-45.

[12] R. Ghosh, Protein bioseparation using ultrafiltration: theory, applications and new developments, World Scientific, 2003.

[13] M. Cheryan, Ultrafiltration and microfiltration handbook, CRC press, 1998.

[14] J. Howell, V. Sanchez, R.W. Field, Membranes in bioprocessing: theory and applications, Springer Science & Business Media, 2012.

[15] C. Charcosset, Membrane processes in biotechnology: an overview, Biotechnology advances, 24 (2006) 482-492.

[16] R. Van Reis, A. Zydney, Membrane separations in biotechnology, Current Opinion in Biotechnology, 12 (2001) 208-211.

[17] A. Saxena, B.P. Tripathi, M. Kumar, V.K. Shahi, Membrane-based techniques for the separation and purification of proteins: an overview, Advances in Colloid and Interface Science, 145 (2009) 1-22.

[18] A. Fane, C. Fell, A. Suki, The effect of pH and ionic environment on the ultrafiltration of protein solutions with retentive membranes, Journal of Membrane Science, 16 (1983) 195-210.

[19] A. Fane, C. Fell, A. Waters, Ultrafiltration of protein solutions through partially permeable membranes—the effect of adsorption and solution environment, Journal of membrane science, 16 (1983) 211-224.

[20] R. Ghosh, Z. Cui, Fractionation of BSA and lysozyme using ultrafiltration: effect of pH and membrane pretreatment, Journal of Membrane Science, 139 (1998) 17-28.

[21] R.H. van Eijndhoven, S. Saksena, A.L. Zydney, Protein fractionation using electrostatic interactions in membranel filtration, Biotechnology and bioengineering, 48 (1995) 406-414.

[22] S. Saksena, A.L. Zydney, Effect of solution pH and ionic strength on the separation of albumin from immunoglobulins (IgG) by selective filtration, Biotechnology and bioengineering, 43 (1994) 960-968.

[23] A. Arunkumar, M.R. Etzel, Fractionation of α-lactalbumin and β-lactoglobulin from bovine milk serum using staged, positively charged, tangential flow ultrafiltration membranes, Journal of Membrane Science, 454 (2014) 488-495.

[24] A. Arunkumar, M.R. Etzel, Negatively charged tangential flow ultrafiltration membranes for whey protein concentration, Journal of Membrane Science, 475 (2015) 340-348.

[25] S. Bhushan, M. Etzel, Charged ultrafiltration membranes increase the selectivity of whey protein separations, Journal of food science, 74 (2009).

[26] M. Nyström, P. Aimar, S. Luque, M. Kulovaara, S. Metsämuuronen, Fractionation of model proteins using their physiochemical properties, Colloids and Surfaces A: Physicochemical and Engineering Aspects, 138 (1998) 185-205.

[27] D.B. Burns, A.L. Zydney, Effect of solution pH on protein transport through ultrafiltration membranes, Biotechnology and bioengineering, 64 (1999) 27-37.

[28] N.S. Pujar, A.L. Zydney, Electrostatic effects on protein partitioning in size-exclusion chromatography and membrane ultrafiltration, Journal of Chromatography A, 796 (1998) 229-238.

[29] R. Van Reis, J. Brake, J. Charkoudian, D. Burns, A. Zydney, High-performance tangential flow filtration using charged membranes, Journal of Membrane Science, 159 (1999) 133-142.

[30] V.G.J. Rodgers, R.E. Sparks, Reduction of membrane fouling in the ultrafiltration of binary protein mixtures, AIChE journal, 37 (1991) 1517-1528.

[31] V.G.J. Rodgers, R.E. Sparks, Effect of transmembrane pressure pulsing on concentration polarization, Journal of membrane science, 68 (1992) 149-168.

[32] V.G.J. Rodgers. *Transmembrane pressure pulsing in protein ultrafiltration.* D. Sc. Thesis, 1989.

[33] Z. Cui, K. Wright, Flux enhancements with gas sparging in downwards crossflow ultrafiltration: performance and mechanism, Journal of Membrane Science, 117 (1996) 109-116.

[34] S. Finnigan, J. Howell, The effect of pulsed flow on ultrafiltration fluxes in a baffled tubular membrane system, Desalination, 79 (1990) 181-202.

[35] B. Bellhouse, I. Sobey, S. Alani, B. DeBlois, Enhanced filtration using flat membranes and standing vortex waves, Bioseparation, 4 (1994) 127-138.

[36] T. Kobayashi, X. Chai, N. Fujii, Ultrasound enhanced cross-flow membrane filtration, Separation and Purification Technology, 17 (1999) 31-40.

[37] K.S. Kim, K.H. Lee, K. Cho, C.E. Park, Surface modification of polysulfone ultrafiltration membrane by oxygen plasma treatment, Journal of membrane science, 199 (2002) 135-145.

[38] D.S. Wavhal, E.R. Fisher, Modification of polysulfone ultrafiltration membranes by CO_2 plasma treatment, Desalination, 172 (2005) 189-205.

[39] A.D. Enevoldsen, E.B. Hansen, G. Jonsson, Electro-ultrafiltration of industrial enzyme solutions, Journal of Membrane science, 299 (2007) 28-37.

[40] J.D. Henry, L.F. Lawler, C. Kuo, A solid/liquid separation process based on cross flow and electrofiltration, AIChE Journal, 23 (1977) 851-859.

[41] T. Käppler, C. Posten, Fractionation of proteins with two-sided electro-ultrafiltration, Journal of biotechnology, 128 (2007) 895-907.

[42] B. Sarkar, S. DasGupta, S. De, Electric field enhanced fractionation of protein mixture using ultrafiltration, Journal of Membrane Science, 341 (2009) 11-20.

[43] W. Song, Y. Su, X. Chen, L. Ding, Y. Wan, Rapid concentration of protein solution by a crossflow electro-ultrafiltration process, Separation and Purification Technology, 73 (2010) 310-318.

[44] H. Yukawa, K. Shimura, A. Suda, A. Maniwa, Characteristics of cross flow electro-ultrafiltration for colloidal solution of protein, Journal of Chemical Engineering of Japan, 16 (1983) 246-248.

[45] H. Huotari, G. Trägårdh, I. Huisman, Crossflow membrane filtration enhanced by an external DC electric field: a review, Chemical Engineering Research and Design, 77 (1999) 461-468.

[46] J.M. Radovich, B. Behnam, C. Mullon, Steady-state modeling of electroultrafiltration at constant concentration, Separation Science and Technology, 20 (1985) 315-329.

[47] C. Guizard, F. Legault, N. Idrissi, A. Larbot, L. Cot, C. Gavach, Electronically conductive mineral membranes designed for electro-ultrafiltration, Journal of Membrane Science, 41 (1989) 127-142.

[48] B. Sarkar, S. DasGupta, S. De, Prediction of permeate flux during osmotic pressure-controlled electric field-enhanced cross-flow ultrafiltration, Journal of colloid and interface science, 319 (2008) 236-246.

[49] A.V. Dudchenko, J. Rolf, K. Russell, W. Duan, D. Jassby, Organic fouling inhibition on electrically conducting carbon nanotube–polyvinyl alcohol composite ultrafiltration membranes, Journal of Membrane Science, 468 (2014) 1-10.

[50] G. Brisson, M. Britten, Y. Pouliot, Electrically-enhanced crossflow microfiltration for separation of lactoferrin from whey protein mixtures, Journal of membrane science, 297 (2007) 206-216.

[51] M. Hakimhashemi, A.Y. Gebreyohannes, H. Saveyn, P. Van der Meeren, A. Verliefde, Combined effects of operational parameters on electro-ultrafiltration process characteristics, Journal of membrane science, 403 (2012) 227-235.

[52] U. Balyan, B. Sarkar, Enhanced Separation of Polyethylene Glycol from Bovine Serum Albumin Using Electro-Ultrafiltration, Separation Science and Technology, 50 (2015) 1846-1859.

[53] G. Chen, W. Song, B. Qi, J. Li, R. Ghosh, Y. Wan, Separation of protein mixtures by an integrated electro-ultrafiltration–electrodialysis process, Separation and Purification Technology, 147 (2015) 32-43.

[54] C.-J. Chuang, C.-Y. Wu, C.-C. Wu, Combination of crossflow and electric field for microfiltration of protein/microbial cell suspensions, Desalination, 233 (2008) 295-302.

[55] Y.-H. Weng, L.H. Chaung-Hsieh, H.-H. Lee, K.-C. Li, C. Huang, Removal of arsenic and humic substances (HSs) by electro-ultrafiltration (EUF), Journal of hazardous materials, 122 (2005) 171-176.

[56] L.-H.C. Hsieh, Y.-H. Weng, C.-P. Huang, K.-C. Li, Removal of arsenic from groundwater by electro-ultrafiltration, Desalination, 234 (2008) 402-408.

[57] W. Duan, G. Chen, C. Chen, R. Sanghvi, A. Iddya, S. Walker, H. Liu, A. Ronen, D. Jassby, Electrochemical removal of hexavalent chromium using electrically conducting carbon nanotube/polymer composite ultrafiltration membranes, Journal of Membrane Science, 531 (2017) 160-171.

[58] H. Yukawa, K. Shimura, A. Suda, A. Maniwa, Cross flow electro-ultrafiltration for colloidal solution of protein, Journal of chemical engineering of Japan, 16 (1983) 305-311.

[59] G. Rios, H. Rakotoarisoa, B.T. de La Fuente, Basic transport mechanisms of ultrafiltration in the presence of an electric field, Journal of membrane science, 38 (1988) 147-159.

[60] W.R. Bowen, R.S. Kingdon, H.A. Sabuni, Electrically enhanced separation processes: the basis of in situ intermittent electrolytic membrane cleaning (IIEMC) and in situ electrolytic membrane restoration (IEMR), Journal of Membrane Science, 40 (1989) 219-229.

[61] R.J. Wakeman, E. Tarleton, Experiments using electricity to prevent fouling in membrane filtration, (1986).

[62] R.J. Wakeman, E. Tarleton, Membrane fouling prevention in crossflow microfiltration by the use of electric fields, Chemical engineering science, 42 (1987) 829-842.

[63] C.W. Robinson, M.H. Siegel, A. Condemine, C. Fee, T.Z. Fahidy, B.R. Glick, Pulsed-electric-field crossflow ultrafiltration of bovine serum albumin, Journal of membrane science, 80 (1993) 209-220.

[64] T. Weigert, J. Altmann, S. Ripperger, Crossflow electrofiltration in pilot scale, Journal of membrane science, 159 (1999) 253-262.

[65] S. Oussedik, D. Belhocine, H. Grib, H. Lounici, D. Piron, N. Mameri, Enhanced ultrafiltration of bovine serum albumin with pulsed electric field and fluidized activated alumina, Desalination, 127 (2000) 59-68.

[66] C. De Lannoy, D. Jassby, D. Davis, M. Wiesner, A highly electrically conductive polymer–multiwalled carbon nanotube nanocomposite membrane, Journal of membrane science, 415 (2012) 718-724.

[67] C.-F. de Lannoy, E. Soyer, M.R. Wiesner, Optimizing carbon nanotube-reinforced polysulfone ultrafiltration membranes through carboxylic acid functionalization, Journal of membrane science, 447 (2013) 395-402.

[68] J. Huang, Z. Wang, J. Zhang, X. Zhang, J. Ma, Z. Wu, A novel composite conductive microfiltration membrane and its anti-fouling performance with an external electric field in membrane bioreactors, Scientific reports, 5 (2015).

[69] F. Ahmed, B.S. Lalia, V. Kochkodan, N. Hilal, R. Hashaikeh, Electrically conductive polymeric membranes for fouling prevention and detection: A review, Desalination, 391 (2016) 1-15.

[70] H.M. Huotari, I.H. Huisman, G. Trägårdh, Electrically enhanced crossflow membrane filtration of oily waste water using the membrane as a cathode, Journal of Membrane Science, 156 (1999) 49-60.

[71] H. Liu, G. Zhang, C. Zhao, J. Liu, F. Yang, Hydraulic power and electric field combined antifouling effect of a novel conductive poly (aminoanthraquinone)/reduced graphene oxide nanohybrid blended PVDF ultrafiltration membrane, Journal of Materials Chemistry A, 3 (2015) 20277-20287.

[72] T.E. Creighton, Proteins: structures and molecular properties, Macmillan, 1993.

[73] H.M. Berman, J. Westbrook, Z. Feng, G. Gilliland, T.N. Bhat, H. Weissig, I.N. Shindyalov, P.E. Bourne, The Protein Data Bank, 1999–, in: International Tables for Crystallography Volume F: Crystallography of biological macromolecules, Springer, 2006, pp. 675-684.

[74] G.K. Ackers, Molecular exclusion and restricted diffusion processes in molecular-sieve chromatography, Biochemistry, 3 (1964) 723-730.

[75] J. Killander, Separation of human heme-and hemoglobin-binding plasma proteins, ceruloplasmin and albumin by gel filtration, Biochimica et Biophysica Acta (BBA)-General Subjects, 93 (1964) 1-14.

[76] O. Kedem, A. Katchalsky, Thermodynamic analysis of the permeability of biological membranes to non-electrolytes, Biochimica et biophysica Acta, 27 (1958) 229-246.

[77] R.J. Hunter, Zeta Potential in Colloid Science, Academic Press, London, England, 1981.

[78] J.B. Pilipovich, A. Black, F.A. Eidsness, T. Stearns, Electrophoretic studies of water coagulation, Journal (American Water Works Association), 50 (1958) 1467-1482.

[79] M. Nyström, M. Lindström, E. Matthiasson, Streaming potential as a tool in the characterization of ultrafiltration membranes, Colloids and surfaces, 36 (1989) 297-312.

[80] D.R. Lide, CRC Handbook of Chemistry and Physics, 77 ed., CRC Press, Boca Raton, FL, 1996.

[81] R. van Reis, A. Zydney, Bioprocess membrane technology, Journal of Membrane Science, 297 (2007) 16-50.

[82] M.M. Pendergast, E.M. Hoek, A review of water treatment membrane nanotechnologies, Energy & Environmental Science, 4 (2011) 1946-1971.

[83] S. Wu, Formation of dispersed phase in incompatible polymer blends: Interfacial and rheological effects, Polymer Engineering & Science, 27 (1987) 335-343.

[84] L.E.S. Brink, D.J. Romijn, Reducing the protein fouling of polysulfone surfaces and polysulfone ultrafiltration membranes: Optimization of the type of presorbed layer, Desalination, 78 (1990) 209-233.

[85] N. Ehsani, S. Parkkinen, M. Nyström, Fractionation of natural and model egg-white protein solutions with modified and unmodified polysulfone UF membranes, Journal of membrane science, 123 (1997) 105-119.

[86] E.V. Basiuk, A. Anis, S. Bandyopadhyay, E. Alvarez-Zauco, S.L. Chan, V.A. Basiuk, Poly (vinyl alcohol)/CNT composites: An effect of cross-linking with glutaraldehyde, Superlattices and Microstructures, 46 (2009) 379-383.

[87] B. Bolto, T. Tran, M. Hoang, Z. Xie, Crosslinked poly (vinyl alcohol) membranes, Progress in Polymer Science, 34 (2009) 969-981.

[88] Q. Zheng, A. Javadi, R. Sabo, Z. Cai, S. Gong, Polyvinyl alcohol (PVA)–cellulose nanofibril (CNF)–multiwalled carbon nanotube (MWCNT) hybrid organic aerogels with superior mechanical properties, RSC Advances, 3 (2013) 20816-20823.

[89] W. Duan, A. Ronen, S. Walker, D. Jassby, Polyaniline-Coated Carbon Nanotube Ultrafiltration Membranes: Enhanced Anodic Stability for In Situ Cleaning and Electro-Oxidation Processes, ACS applied materials & interfaces, 8 (2016) 22574-22584.

[90] P. Vandrangi, P. Jreij, T. Rajapaksa, N. Bansal, D. Lo, V. Rodgers, Novel in situ normal streaming potential device for characterizing electrostatic properties of confluent cells, Review of Scientific Instruments, 83 (2012) 074302.

[91] P. Vandrangi. *Vascular Biotransport Considerations in Signaling Cascades.* Ph.D. Thesis, U.C. Riverside, 2012.

[92] Y. Wang. *Electrostatic contributions in binary protein ultrafiltration.* D. Sc. Thesis, U.C. Riverside, 2008.

[93] K.M. Persson, V. Gekas, G. Trägårdh, Study of membrane compaction and its influence on ultrafiltration water permeability, Journal of membrane science, 100 (1995) 155-162.

[94] M. Munoz-Aguado, D. Wiley, A. Fane, Enzymatic and detergent cleaning of a polysulfone ultrafiltration membrane fouled with BSA and whey, Journal of Membrane Science, 117 (1996) 175-187.

[95] S.-T. Hwang, K. Kammermeyer, A. Weissberger, Membranes in separations, Wiley New York, 1975.

[96] V.L. Vilker, C.K. Colton, K.A. Smith, The osmotic pressure of concentrated protein solutions: effect of concentration and pH in saline solutions of bovine serum albumin, Journal of Colloid and Interface Science, 79 (1981) 548-566.

[97] W.R. Krigbaum, F. Kügler, Molecular conformation of egg-white lysozyme and bovine α-lactalbumin in solution, Biochemistry, 9 (1970) 1216-1223.

[98] V. Huxley, F. Curry, R. Adamson, Quantitative fluorescence microscopy on single capillaries: alpha-lactalbumin transport, American Journal of Physiology-Heart and Circulatory Physiology, 252 (1987) H188-H197.

[99] W. Eberstein, Y. Georgalis, W. Saenger, Molecular interactions in crystallizing lysozyme solutions studied by photon correlation spectroscopy, Journal of crystal growth, 143 (1994) 71-78.

[100] L. Palacio, C.-C. Ho, P. Prádanos, A. Hernández, A. Zydney, Fouling with protein mixtures in microfiltration: BSA–lysozyme and BSA–pepsin, Journal of Membrane Science, 222 (2003) 41-51.

[101] F.M. Robbins, R.E. Andreotti, L.G. Holmes, M.J. Kronman, Inter-and intramolecular interactions of α-lactalbumin VII. The hydrogen ion titration curve of α-lactalbumin, Biochimica et Biophysica Acta (BBA)-Protein Structure, 133 (1967) 33-45.
[102] W.S. Opong, A.L. Zydney, Diffusive and convective protein transport through asymmetric membranes, AIChE Journal, 37 (1991) 1497-1510.
[103] J.R. Molek, A.L. Zydney, Separation of PEGylated α-Lactalbumin from Unreacted Precursors and Byproducts Using Ultrafiltration, Biotechnology progress, 23 (2007) 1417-1424.
[104] C. Müller, G. Agarwal, T. Melin, T. Wintgens, Study of ultrafiltration of a single and binary protein solution in a thin spiral channel module, Journal of membrane science, 227 (2003) 51-69.
[105] K. Pillay, E. Cukrowska, N. Coville, Multi-walled carbon nanotubes as adsorbents for the removal of parts per billion levels of hexavalent chromium from aqueous solution, Journal of hazardous materials, 166 (2009) 1067-1075.